UNIVERSITY OF WARMIA AND MAZURY IN OLSZTYN

Technical Sciences

22(1) 2019

OLSZTYN 2019

The Technical Sciences is indexed and abstracted in BazTech (http://baztech.icm.edu.pl) and in IC Journal Master List (http://journals.indexcopernicus.com)

The Journal is available in electronic form on the web sites
http://www.uwm.edu.pl/techsci (subpage Issues)
http://wydawnictwo.uwm.edu.pl (subpage Czytelnia)

The electronic edition is the primary version of the Journal

PL ISSN 1505-4675
e-ISNN 2083-4527

Address
ul. Jana Heweliusza 14
10-718 Olsztyn-Kortowo, Poland
tel.: +48 89 523 36 61
fax: +48 89 523 34 38
e-mail: wydawca@uwm.edu.pl

Ark. wyd. 7,7, ark. druk. 6,5, nakład 85 egz.
Druk – Zakład Poligraficzny UWM, zam. 191

Contents

Technical Sciences, 2019, 22(1), 5–17

UNIWERSYTET WARMIŃSKO-MAZURSKI W OLSZTYNIE

Quarterly peer-reviewed scientific journal
ISSN 1505-4675
e-ISSN 2083-4527
TECHNICAL SCIENCES
Homepage: www.uwm.edu.pl/techsci/

NUMERICAL MODELING OF POROUS CERAMICS MICROSTRUCTURE

Danuta Miedzińska

Department of Mechanics and Applied Computer Science
Faculty of Mechanical Engineering
Military University of Technology in Warsaw

Received 22 May 2018, accepted 13 December 2018, available online 14 January 2019.

K e y w o r d s: porous ceramics, finite element method, microstructure

A b s t r a c t

The presented research is directed to the porous ceramics microstructural behaviour assessment with the use of numerical methods. Such new material can be used for thermal insulation, filters, bio-scaffolds for tissue engineering, and preforms for composite fabrication. One of the newest and most interesting applications, considered in this work, is a usage of those materials for production of proppants for hydraulic fracturing of shale rocks. The hydraulic fracturing is a method of gas recovery from unconventional reservoirs. A large amount of fracturing fluid mixed with proppant (small particles of sand or ceramics) is pumped into the wellbore and its pressure causes the rock cracking and gas release. After fracturing the fluid is removed from the developed cracks leaving the proppant supporting the fracture. In the paper the grain porous ceramics which is used for proppant particles preparation was studied. The influence of grains distribution on the porous ceramics mechanical behaviour during compression was simulated with the use of finite element method.

Introduction – aim of research

Porous ceramics is a group of new and very interesting materials. It can be used for thermal insulation, filters, bio-scaffolds for tissue engineering, and preforms for composite fabrication (HAMMEL et al. 2014).

Correspondence: Danuta Miedzińska, Katedra Mechaniki i Informatyki Stosowanej, Wydział Mechaniczny, Wojskowa Akademia Techniczna, ul. Gen. Witolda Urbanowicza 2, 00-908 Warszawa, phone: +48 261 83 7867, e-mail: danuta.miedzinska@wat.edu.pl

Porous structure of ceramics can be prepared through many processing techniques. One technique is to simply sinter coarse powders or partially sinter a green ceramic to hinder full densification (HAMMEL et al. 2014). Other traditional methods of fabricating porous ceramics can be divided into three basic processing techniques: replica; sacrificial template; and direct foaming as seen in Figure 1 (STUDART et al. 2006). The development process influences the microstructure of the material, what was presented in Figure 2.

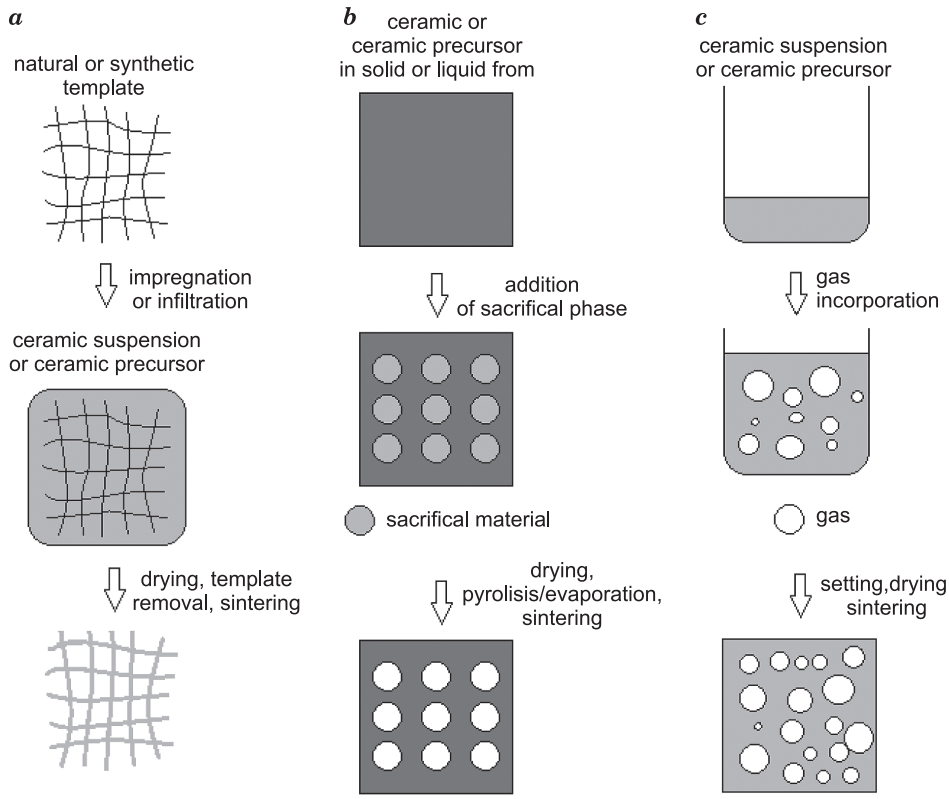

Fig. 1. Typical processing methods for the production of porous ceramics: *a* – replica technique, *b* – sacrificial template technique, *c* – direct foaming technique
Source: after STUDART et al. (2006).

One of the newest and most interesting applications is a usage of those materials for production of proppants for hydraulic fracturing of shale rocks (PETTY 2010, MURPHY 2013). The hydraulic fracturing is a method of gas recovery from unconventional reservoirs. A large amount of fracturing fluid (water or CO_2) (MIEDZIŃSKA et al. 2013) mixed with proppant (small particles

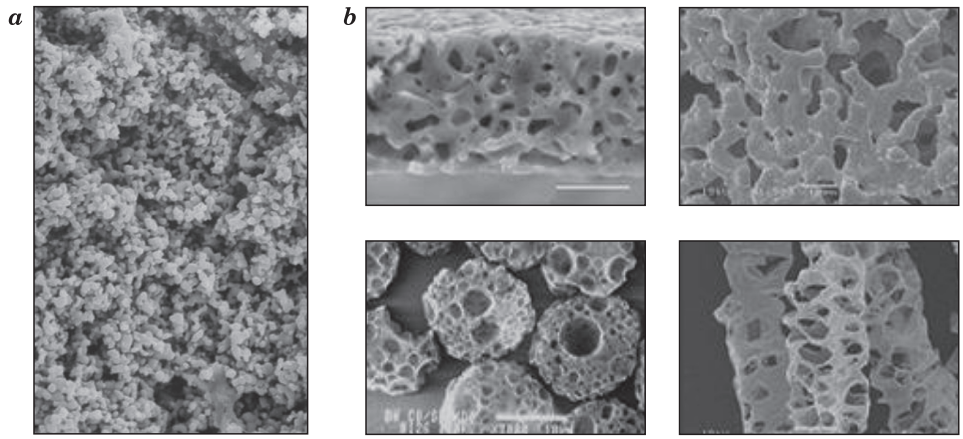

Fig. 2. Porous ceramics microstructure: *a* – grain structure made by sintering, *b* – structure made by replication
Source: *a* – after KALITA at al. (2003), *b* – after WALSH at al. (2005).

of natural sand or ceramics) is pumped into the wellbore and its pressure causes the rock cracking and gas release. After fracturing the fluid is removed from the developed cracks leaving the proppant supporting the fracture (LO et al. 2002), what was shown in Figure 3.

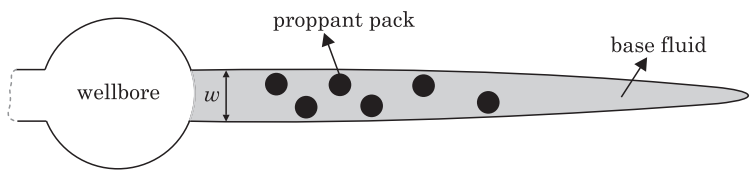

Fig. 3. Crack developed with hydraulic fracturing filled with fluid mixed with proppant

So it is obvious that the proppant should be characterized with high compressive strength but must achieve the highest permeability of the crack. The most often used proppants are natural sands and solid ceramic spheres (KNEZ et al. 2013). The newest solution is the proppant made of cellular ceramics (WEAVER et al. 2007). The example of such structure was shown in Figure 4. Such solution can improve the frack permeability but only in case of assuring the proper strength.

In the paper the main interest is directed to the grain porous ceramics which is used for proppant particles preparation. The numerical modelling of idealized microstructure of such material was presented to study the influence of grains distribution on the porous ceramics mechanical behaviour.

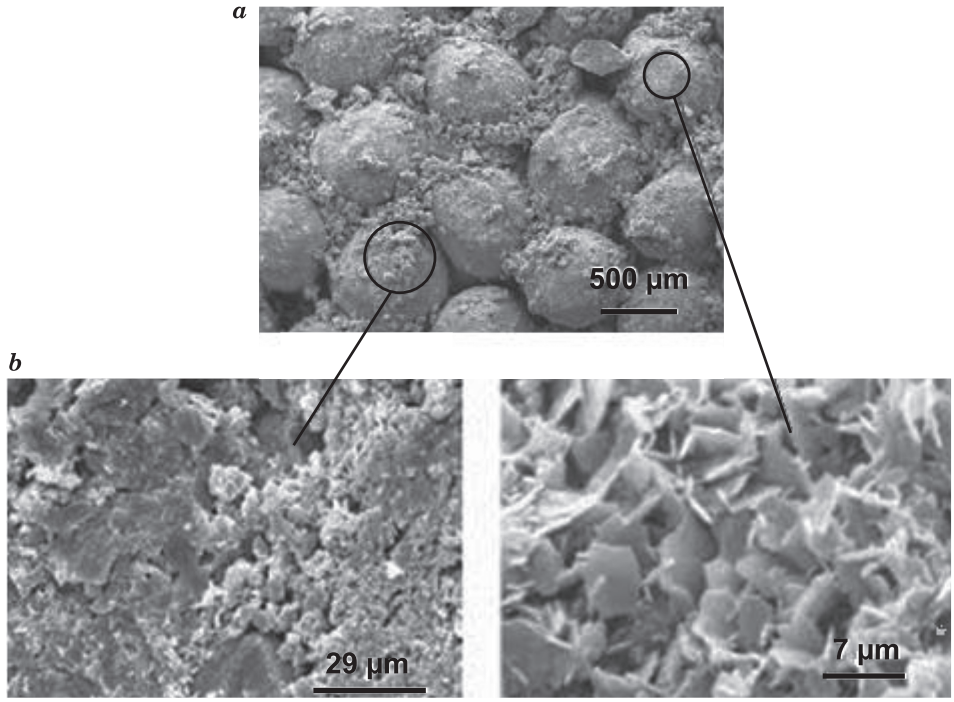

Fig. 4. Porous ceramic proppant: *a* – proppant spheres, *b* – magnitude of porous structure of proppant sphere

Source: after WEAVER et al. (2007).

Research methodology – numerical models and analyses description

The research was carried out using finite element method. LS Dyna computer code for dynamic analyses were used. Explicit time integration – central difference scheme was applied. This method assesses the linear change in acceleration. It was developed on the base of the single degree of freedom damped system, where forces acting on mass m are: f_s – elastic force, f_I – inertia force, f_D – damping forces, $p(t)$ – external forces (HALLQUIST 2016).

The equations of equilibrium are obtained from d'Alambert's principle:

$$f_I + f_D + f_{\text{int}} = p(t) \tag{1}$$

where:

$$f_I = m\ddot{u}; \qquad \ddot{u} = \frac{d^2u}{dt^2} \qquad \text{– acceleration,}$$

$$f_D = c\dot{u}; \quad \dot{u} = \frac{du}{dt} \quad \text{– velocity}$$
$$f_{\text{int}} = ku; \quad u \quad \text{– displacement.}$$

In the above equations c is the damping coefficient, and k is the linear stiffness.

The equations of motion for linear behaviour lead to linear ordinary differential equation:

$$m\ddot{u} + c\dot{u} + ku = p(t) \tag{3}$$

but for the nonlinear case the internal force varies as a nonlinear function of the displacement, leading to the nonlinear formula:

$$m\ddot{u} + c\dot{u} + f_{\text{int}}(u) = p(t) \tag{4}$$

Analytical solutions of linear ordinary differential equations are available, so instead one consider the dynamic response of linear system subjected to harmonic loading. Some commonly used terms can be defined as follows:

$$\begin{aligned}
p(t) &= p_0 \sin \omega t && \text{– harmonic loading,}\\
\omega &= \sqrt{\frac{k}{m}} && \text{– circular frequency for single degree of freedom,}\\
f &= \frac{\omega}{2\pi} = \frac{1}{T} && \text{– natural frequency, } T \text{ – period,}\\
\xi &= \frac{c}{c_{cr}} = \frac{c}{2m\omega} && \text{– damping ratio,}\\
\omega_0 &= \omega\sqrt{1-\xi^2} && \text{– damped vibration frequency,}\\
\beta &= \frac{\bar{\omega}}{\omega} && \text{– applied load frequency.}
\end{aligned} \tag{5}$$

The closed form solution can be defined as:

$$u(t) = u_0 \cos \omega t + \frac{\dot{u}_0}{\omega} \sin \omega t + \frac{p_0}{k} \frac{1}{1-\beta^2} (\sin \bar{\omega} t - \beta \sin \omega t) \tag{6}$$

with the initial conditions: initial displacement u_0, initial velocity $\dot{u}_0$ and static displacement $\frac{p_0}{k}$.

For nonlinear problems, only numerical solutions are possible. In the problem described in the paper the explicit central difference scheme, built in LS Dyna, were applied to integrate the equations of motions.

To describe the central difference method the semi-discrete equations of motion at time n are defined as:

$$Ma^n = P^n - F^n + H^n \tag{7}$$

where M is the diagonal mass matrix, P^n accounts for external and body force loads, F^n is the stress divergence vector and H^n is the hourglass resistance. To advance to time t^{n+1}, the central difference time integration is used in the following form:

$$a^n = M^{-1}(P^n - F^n + H^n) \tag{8}$$

$$v^{n+\frac{1}{2}} = v^{n-\frac{1}{2}} + a^n \Delta t^n \tag{9}$$

$$u^{n+1} = u^n + v^{n+\frac{1}{2}} \Delta t^{n+\frac{1}{2}} \tag{10)}$$

where:

$$\Delta t^{n+\frac{1}{2}} = \frac{\Delta t^n + \Delta t^{n+1}}{2} \tag{11}$$

and v and u are the global nodal velocity and displacement vectors, respectively. The geometry can be updated by adding the displacement increments to the initial geometry:

$$x^{n+1} = x^0 + u^{n+1} \tag{12}$$

The modelling of porous ceramics can be found in literature. In DOLTINIS and DATTKE (2001) a numerical model for microcrack formation and damage evolution in brittle porous solids under internal fluid pressure was presented. In SHCHUROVA (2016), for the purpose of universality, ceramics grains and pores were modelled as six-sided subareas. In SADOWSKI and SAMBORSKI (2003) a mesomechanical modelling of porous polycrystalline ceramics subjected to different kinds of loading was presented.

Four types of geometry were used to simulate the grains distribution in porous ceramics microstructure, called **u1**, **u2**, **u3** and **u4**. The proposed models were designed to consider the various types of dense packing of sphere shaped grains in idealistic structure. Model **u1** and **u2** were built of 9 spheres packed regularly and hexagonally respectively (like in crystallographic net). Model **u3** was a coupling of model **u1** and **u2**, in which spheres in two bottom rows were distributed regularly and in two top rows – hexagonally. Model **u4** was a modification of model **u1** based on addition of smaller spheres in free spaces between existing ones, such as they are tangent to each other and allow to fill the space in more dense way. Those applied distributions resulted in different porosities and dimensions of the models what influenced the results presentation in relative manner. The models were presented in Figure 5.

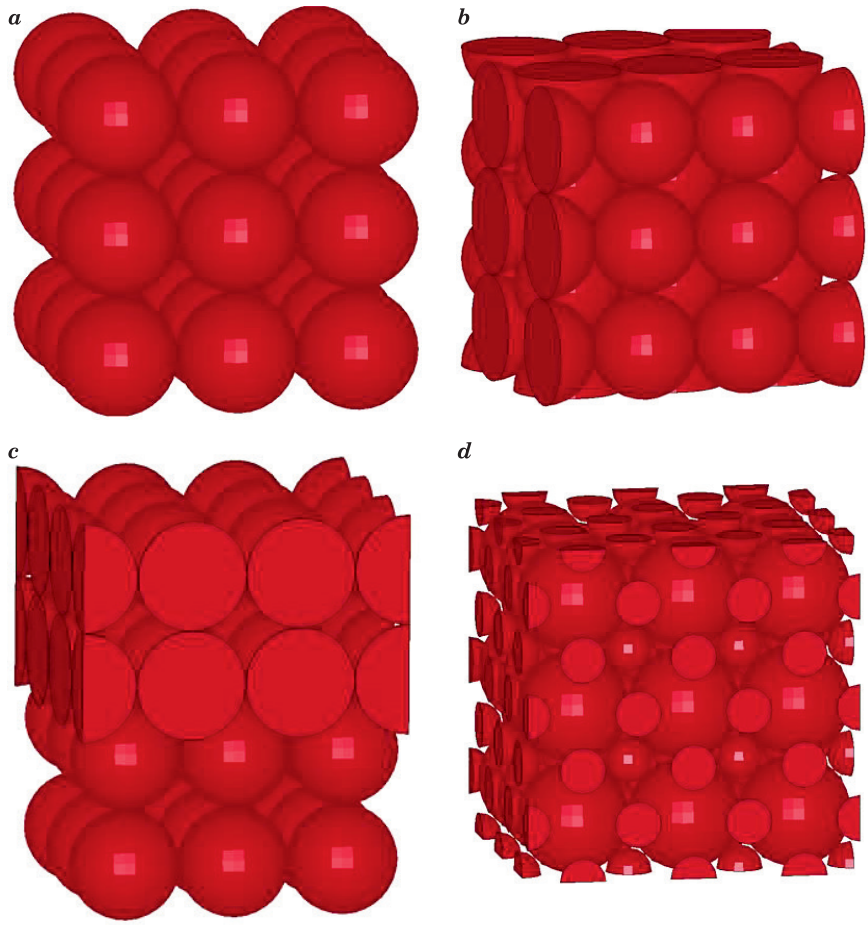

Fig. 5. Numerical models of porous ceramics microstructure: *a* – **u1**, *b* – **u2**, *c* – **u3**, *d* – **u4**

Solid hexagonal 4-nodal elements were used to developed the finite element mesh. The applied material model was *MAT_JOHNSON_HOLMQUIST_CERAMICS which is useful when modeling brittle materials, such as ceramics, subjected to large pressures, shear strain and high strain rates. The model attempts to include the phenomena encountered when brittle materials are subjected to load and damage. The equivalent stress for a ceramic-type material is given by HALLQUIST (2016):

$$\sigma^* = \sigma_i^* - D\left(\sigma_i^* - \sigma_f^*\right) \tag{13}$$

where:

$$\sigma_i^* = a(p^* + t^*)^n(1 + c\ \ln\dot{\varepsilon}^*) \tag{14}$$

represents the intact, undamaged behavior,

$$D = \sum \Delta\varepsilon^p / \varepsilon_f^p \tag{15}$$

represents the accumulated damage based upon the increase in plastic strain per computational cycle and the plastic strain to fracture:

$$\varepsilon_f^p = d_1(p^* + t^*)^{d_2} \tag{16}$$

and

$$\sigma_f^* = b(p^*)^m(1 + c\ln\dot{\varepsilon}) \leq \text{SFMAX} \tag{17}$$

represents the damaged behavior. In each case, the '*' indicates a normalized quantity, the stresses being normalized by the equivalent stress at the Hugoniot elastic limit, the pressures by the pressure at the Hugoniot elastic limit and the strain rate by the reference strain rate (HALLQUIST 2016).

The material constants for Al_2O_3 were shown in Table 1.

Table 1

Material constants for Al_2O_3 (CRONIN at al., 2003)

Parameter	Value
Density [kg/m^3]	3,226
Shear Modulus [GPa]	90.16
Strength Constants	
A	0.93
B	0.31
C	0.0
M	0.6
N	0.6
Ref Strain Rate (EPSI)	1.0
Tensile Strength [GPa]	0.2
Normalized Fracture Strength	NA
HEL [GPa]	2.79
HEL Pressure [GPa]	1.46
HEL Vol. Strain	0.01117
HEL Strength [GPa]	2.0
Damage Constants	
D1	0.005
D2	1.0
Equation of State	
K1 [GPa] (Bulk Modulus)	130.95
K2 [GPa]	0
K3 [GPa]	0
Beta	1.0

The boundary conditions were as follows: the model was stated on the rigid wall, compression was carried out with the displacing rigid wall (velocity $v = 1$ mm/ms), rigid walls also blocked the rest of walls of the model to simulate

the influence of the surrounding structure. The surface to surface contact with penalty function was applied. The static friction coefficient between ceramic faces and rigid wall and ceramic was 0.3 and dynamic one – 0.2.

Results and discussion

The results were shown as deformations in time step of 0, 0.5 and 1 ms (Fig. 6) and stress-strain curves (Fig. 7). It must be mentioned that stress was calculated on the base of initial cross-section of the polyhedron escribed on each model and reaction force in the base rigid wall. Strain was calculated on the base of initial height of the sample and displacement of the moving rigid wall.

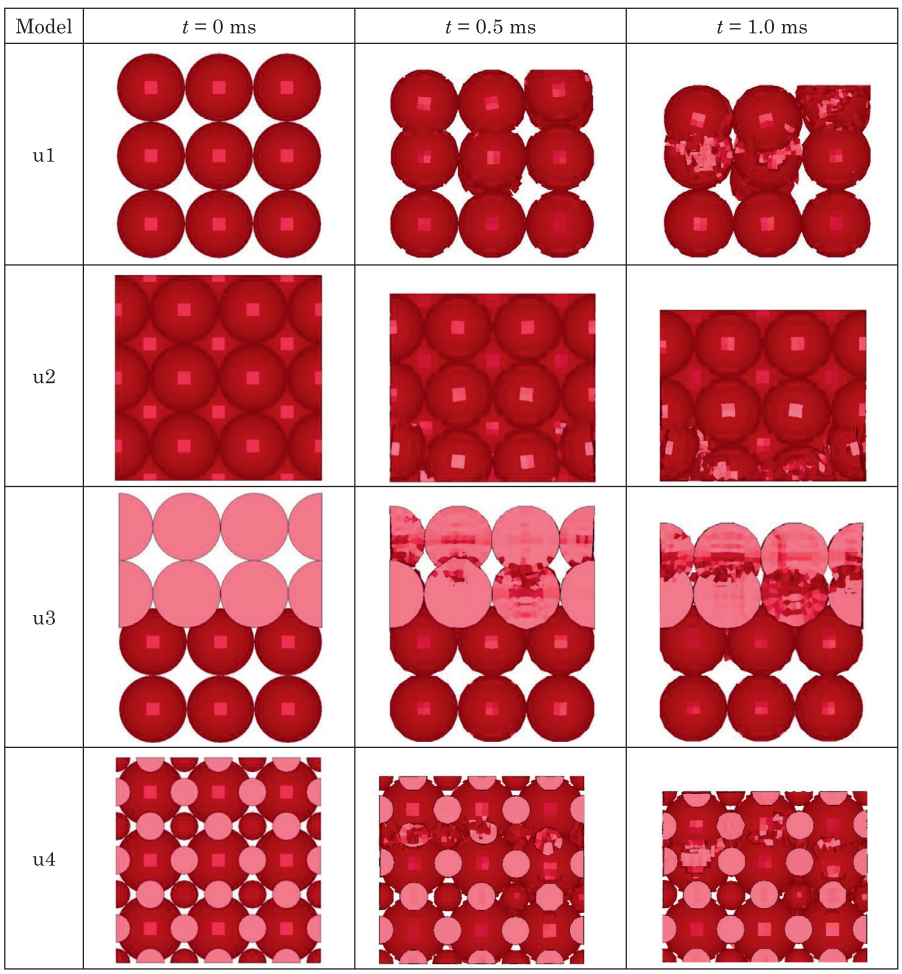

Fig. 6. Deformations of porous ceramics microstructure numerical models during compression

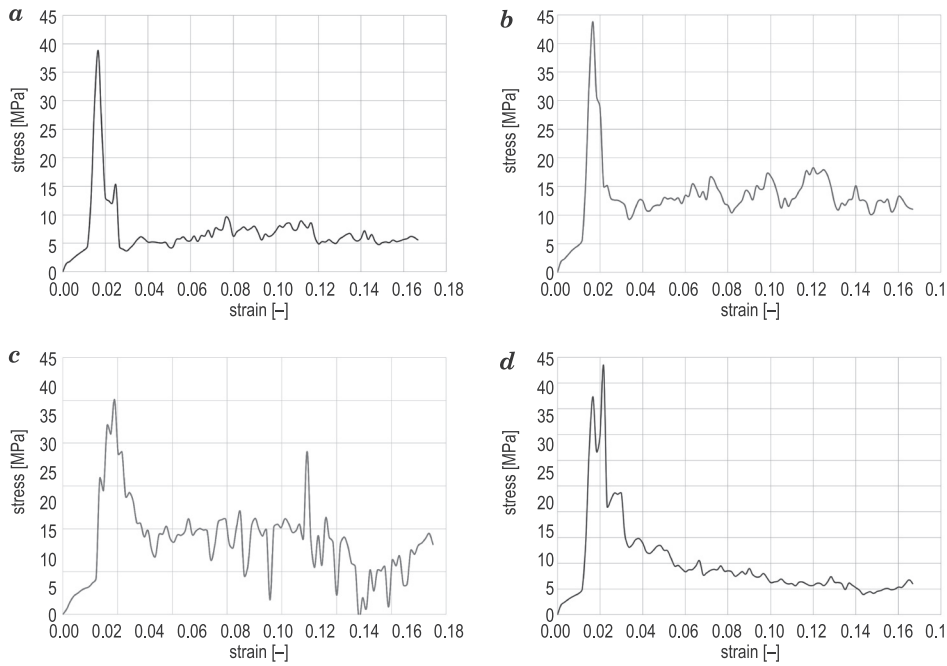

Fig. 7. Stress – strain charts for porous ceramics microstructure numerical models during compression test: *a* – **u1**, *b* – **u2**, *c* – **u3**, *d* – **u4**

To assess the differences between models the comparison stress – strain chart was prepared (Fig. 8). Also values of mass, porosity and maximum stress were compared in Figure 9.

Firstly, the differences in deformations between models were observed. They depended on the spheres distribution. For **u1** model the damage begins in the middle of the sample, in **u2** and **u4** models – at the top and in **u3** – at the bottom.

Also the stress-strain charts differed from each other. Even though the maximum stress appeared for the same strain for all samples (0.2), it must be noticed that the charts shape after that point reflected the microstructural specific behaviour for each spheres distribution. The most interesting example of this phenomenon can be seen for **u4** chart, where two "peaks" of stress appeared – what was the result of small and big spheres damage.

Comparing the maximum stress values it was visible that the biggest one was for **u4** distribution, when the smallest one – for **u3**. The biggest porosity value was for **u1** sample, the smallest one – for **u2**. Considering mass – the biggest one was for **u2** sample, the smallest one for **u1**.

However, the most important factors for assessing the porous ceramics for implementation as proppant material were maximum stress vs. porosity and maximum stress vs. mass ratios (marked as MS/P and MS/M accordingly) – shown

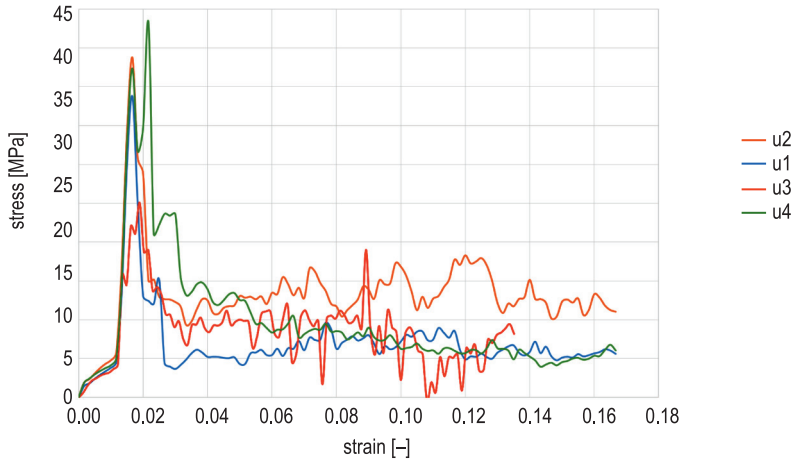

Fig. 8. Comparison of stress – strain characteristics for porous ceramics microstructure numerical models during compression test

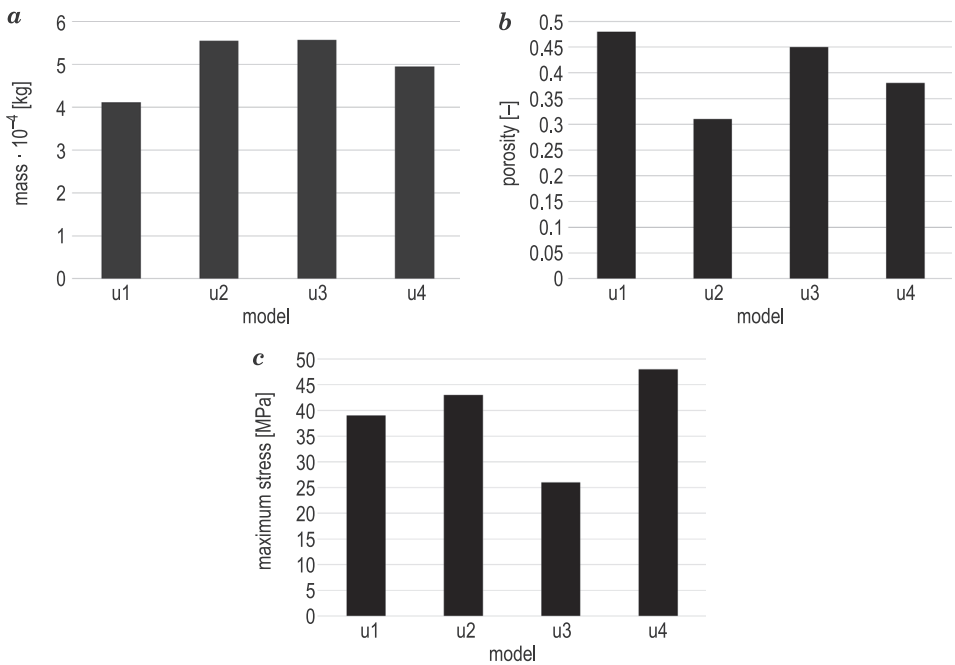

Fig. 9. Comparison of mass, porosity and maximum stress values for porous ceramics microstructure numerical models during compression test: *a* – mass – comparison, *b* – porosity – comparison, *c* – maximum stress – comparison

in Table 2. The MS/P ratio is very important considering the fracture supporting ability of proppant (should be as big as possible) and gas flow through fracture (also as big as possible). The MS/M ratio reflected the ability of proppant to support the fracture versus its mass, which can be very important for the phenomenon of carrying the proppant by the fracking fluid to the fracture (the lightest proppant is, the further it can be placed in the crack supporting the larger area of open fracture). In this case the best value of MS/P ratio (the smallest one) was observed for **u3** sample, also acceptable for **u1** one. But in the same time the **u3** and **u1** samples were characterized by the worse MS/M ratio.

Table 2

Maximum stress vs. porosity and maximum stress vs. mass ratios (marked as MS/P and MS/M accordingly) for tested models

Model	MS/P	MS/M
u1	79.9	9.42
u2	139.6	7.98
u3	55.6	4.57
u4	126.8	9.75

Conclusions

The research presented in the paper was dedicated to study the influence of the grains distribution in porous ceramics on such material global mechanical properties with mass and porosity consideration. The study was carried out using finite element method and idealistic models of described structures.

On the base of achieved results it can be concluded that the selection of the porous ceramics microstructure for the implementation as proppant material should be based on the needs of the fracturing process design, which depend on e.g. shale reservoir geological properties and the depth on which it is situated. Finally, it must be mentioned that the solid ceramics has two or three times bigger compression strength but does not allow to increase the gas flow in the wellbore. So the proppant selection also should be based on the strength requirements for a fractured reservoir.

Acknowledgements

The paper supported by a grant No BG2/DIOX4SHELL/14 financed in the years 2014-2018 by The National Centre for Research and Development, Poland.

References

CRONIN D.S., BUI K., KAUFMANN C., MCINTOSH G., BERSTAD T., CRONIN D. 2003. *Implementation and validation of the Johnson–Holmquist ceramic material model*. In Proceedings of LS-DYNA 4th European LS-DYNA Users Conference, UIM, Germany.

DOLTSINIS I., DATTKE R. 2001. *Modelling the damage of porous ceramics under internal pressure*. Computer Methods in Applied Mechanics and Engineering, 191(1-2): 29-46.

HALLQUIST J. 2006. *LS-DYNA theory manual*. LSTC, Livermore.

HAMMEL E.C., IGHODARO O.L.-R., OKOLI O.I. 2014. *Processing and properties of advanced porous ceramics: An application based review*. Ceramics International, 40(10): 15351-15370.

KALITA S.J., BOSE S., HOSICK H.L., BANDYOPADHYAY A. 2003. *Development of controlled porosity polymer – ceramic composite scaffolds via fused deposition modelling*. Materials Science and Engineering, C, 23: 611-620.

KNEZ D., ZIAJA J., PIWOŃSKA M. 2017. *Computer simulation of the influence of proppant high diameter grains damage on hydraulic fracturing efficiency*. AGH Drilling, Oil, Gas, 34(2): 411-418.

LO S.-W., MILLER M.J., LI J. 2002. *Encapsulated breaker release rate at hydrostatic pressure at elevated temperatures*. In Proceedings of SPE Annual Technical Conference and Exhibition, San Antonio, Texas, SPE-77744.

MIEDZIŃSKA D., NIEZGODA T., MAŁEK E., ZASADA Z. 2013. *Study on coal microstructure for porosity levels assessment*. Bulletin of the Polish Academy of Sciences — Technical Sciences, 61(2): 499-505.

MURPHY B. 2013. *CARBO Ceramics is Sitting in the Fracking Catbird Seat: CRR, UPL, CHK*. SmallCap Network, 1: 13-15.

PETTY N.A., XU G. 2010. *The Effects of Proppant Concentration on the Rheology of Slurries for Hydraulic Fracturing - A review*. UCR Undergraduate Research Journal, 1: 45-50.

SADOWSKI T., SAMBORSKI S. 2003. *Prediction of the mechanical behaviour of porous ceramics using mesomechanical modelling*. Computational Materials Science, 28(3-4): 512-517.

SHCHUROVA E.I. 2016. *Modeling of the Ceramics Structure for the Finite Element Analysis*. Procedia Engineering, 150: 179-184.

STUDART A.R., GONZENBACH U.T., TERVOORT E., GAUCKLER L.J. 2006. *Processing routes to macroporous ceramics: a review*. Journal of the American Ceramic Society, 89: 1771-1789.

WALSH D., BOANINI E., TANAKA J., MANN S. 2005. *Synthesis of tri-calcium phosphate sponges by interfacial deposition and thermal transformation of self-supporting calcium phosphate films*. Journal of Materials Chemistry, 15: 1043-1048.

WEAVER J.D., BATENBURG D.W., NGUYEN P.D. 2007. *Fracture-Related Diagenesis May Impact Conductivity*. Petroleum Engineers Source SPE, 12(3): 155-163.

Technical Sciences, 2019, 22(1), 19–34

UNIWERSYTET WARMIŃSKO-MAZURSKI W OLSZTYNIE

Quarterly peer-reviewed scientific journal
ISSN 1505-4675
e-ISSN 2083-4527
TECHNICAL SCIENCES
Homepage: www.uwm.edu.pl/techsci/

DIFFUSION OF Cd(II), Pb(II) AND Zn(II) ON CALCIUM ALGINATE BEADS

Sylwia Kwiatkowska-Marks, Justyna Miłek, Ilona Trawczyńska

Department of Chemical and Bioprocess Engineering
Faculty of Chemical Technology and Engineering
University of Technology and Life Sciences in Bydgoszcz

Received 29 March 2018, accepted 20 December 2018, available online 14 January 2019.

Key words: effective diffusion, alginate beads, cadmium, lead, zinc.

Abstract

Effective diffusion coefficients (D_e) for different heavy-metal salts: Cd, Pb, Zn in calcium alginate beads were determined. Their values depend on the metal type, anion from the metal salt, and the alginate content in the beads. The results of calculations indicate a decrease in the values of D_e, caused by an increase in the alginate content in the alginate sorbent beads. This is in agreement with the mechanism of the diffusion process taking place in porous carriers. Experimental data were found to be in good agreement with the mathematical model, as indicated by high values of the correlation coefficient.

Nomenclature

A_s – biosorbent bead area [m^2],
C_i – initial sorbate concentration in solution [$g \cdot L^{-1}$],
C_L – sorbate concentration in solution at time t [$g \cdot L^{-1}$],
C_S – sorbate concentration in sorbent pores at time t [$g \cdot L^{-1}$],
C_{S0} – sorbate concentration in sorbent pores for $t=0$ [$g \cdot L^{-1}$],
C_∞ – equilibrium concentration of sorbate in solution [$g \cdot L^{-1}$],
D_e – effective coefficient of sorbate diffusion in sorbent pores [m^2/s],
D_{aq} – coefficient of diffusion in dilute aqueous solution [m^2/s],
K – partition ratio [–],
N – number of sorbent bead,
P_t – conductivity of solution after time t [μS],

Correspondence: Sylwia Kwiatkowska-Marks, Zakład Inżynierii Chemicznej i Bioprocesowej, Wydział Technologii i Inżynierii Chemicznej, Uniwersytet Technologiczno-Przyrodniczy im. Jana i Jędrzeja Śniadeckich, ul. Seminaryjna 3, 85-326 Bydgoszcz, phone +48 52 374 90 49, e-mail: sylwia.kwiatkowska@utp.edu.pl

P_∞ – conductivity of solution after time ∞ [μS],
q_n – a parameter, defined by Equation (5) [–],
r – bead radial coefficient,
R – sorbent bead radius [m],
t – time [s],
V_L – volume of the solution which contains the sorbate [ml],
α – a parameter, defined by Equation (6) [–],
β – porosity [–],
φ – diffusion retardation coefficient [–],
τ – tortuosity factor [–].

Introduction

Heavy metals have a proven harmful effect on many forms of life. Lead and cadmium are known to be especially harmful to man and the environment (MEENA et al. 2008). Wastewater that contains zinc is harmful for both irrigational and industrial applications (LAI et al. 2008). Lead, copper and zinc are generally present in water as a result of industrial pollution of rivers and reservoirs, and/or by dissolution of natural sources. The World Health Organization in the guidelines for drinking water has recommended a desirable limit concentration of 0.01 $mg \cdot L^{-1}$ for lead and 3 $mg \cdot L^{-1}$ for zinc. Cadmium compounds are potentially carcinogenic to humans, being the recommended levels of 0.003 $mg \cdot L^{-1}$. The European Union Council Directive on water quality set the permissible levels in drinking water for Pb to 10 $\mu mol \cdot L^{-1}$ (2 $mg \cdot L^{-1}$) and for Cd to 5 $\mu mol \cdot L^{-1}$ (0.56 $mg \cdot L^{-1}$).

Various methods have been suggested and applied for the removal of toxic heavy metals from aqueous solutions, such as chemical precipitation, evaporation, ion-exchange, adsorption, solvent extraction, electrolysis and reverse osmosis (DHAKAL et al. 2005, LAI et al. 2008, CHAND et al. 2009). These conventional processes face several constraints and have certain disadvantages like high cost, environmental impact, technical efficiency (WANG et al. 2016), generation of large volumes of sediment, problems with recycling and with the reuse of adsorbents or ion exchangers (GHIMIRE et al. 2003, DHAKAL et al. 2005, CHAND et al. 2009), that limit their use. Therefore, there is a growing interest in the search for low cost, easily available and environmentally friendly biologically-derived materials suitable for the efficient removal of these toxic substances (LAI et al. 2008, IQBAL, SAEED 2002). Biosorption, an alternative technology, is based on the properties of inactive and dead biomass, which can bind and concentrate hazardous ions from aqueous solutions (RUIZ et al. 2013). Biosorption on materials of natural origin seems to provide the most prospective results: in addition to being highly efficient, it enables elimination of the entire content of metal ions, even if they are present at very low concentrations in the liquid waste. Biosorption is based on sorbents in the form of readily available materials of natural origin or on

waste products arising in industry or agriculture: such sorbents have a high sorption capacity and are rather inexpensive, in comparison with high-priced synthetic sorbents.

The process of sorption with biomass can be linked to various organic species, e.g. chitosan (DEMEY et al. 2017, DEMEY et al. 2018 b) or alginate.

Pollutants do not only include toxic, cancerogenic and mutagenic metals (such as cadmium, lead) but also metals of economic value (such as silver, gold, platinum), therefore, possibilities of their recovery have become another important issue. Once again, biosorption has appeared to be efficacious though low-cost solution for the recovery of heavy metals. For the above reasons, sorption on materials of natural origin has become the subject of extensive studies (described, for instance, in: VOLESKY, HOLAN 1995, HU et al. 1996, VEGLIO, BEOLCHI 1997, KRATOCHVIL, VOLESKY 1998, ECLES 1999, FIGUEIRA et al. 2000, VOLESKY 2001, JEON et al. 2002, VOLESKY 2003, RINCON et al. 2005, PAPAGEORGIOU et al. 2006, 2008, CHOJNACKA 2010). The studies have demonstrated that marine algae, which are acquired at a rather low cost, have a considerable sorption capacity.

Alginate as one of the major components of brown algae (KAWAI, MURATA 2016), whose high affinity for heavy metals has been confirmed by many studies. The sorption properties of alginates have been investigated since 1990's (PAPAGEORGIOU et al. 2006, 2008, JANG et al. 1990, 1991, DEANS, DIXON 1992, CHEN et al. 1993, JANG 1994, LEWANDOWSKI, ROE 1994, JANG et al. 1995a, 1995b, CHEN et al. 1997, KONISHI et al. 1998, AKSU et al. 1992, IBANEZ, UMETSU 1999, 2000, VEGLIO et al. 2002, LAI et al. 2008, DEZE et al. 2012, PLAZINSKI 2012, NASTAJ et al. 2016). Alginates are linear copolymers of β-D-mannuronate (M) and α-L-guluronate (G) residues in (1→4)-linkage, arranged in a block-wise pattern along the linear chain (DAVIS et al. 2003). Alginates are biopolymers with high sorption capacity for heavy metals, even at low concentrations of the metals in solutions. Their sorption capacities are much higher than those of commonly used metal sorbents, such as active carbon (PAPAGEORGIOU et al. 2006). A very simple technology provides a biosorbent in the form of beads, which are easily separated from the sorbate solution. Moreover, alginate sorbents have the added advantage of being reusable after regeneration (typically, by means of a dilute acid solution) (KWIATKOWSKA-MARKS et al. 2011a) with a simultaneous recovery of metals. Their other advantages also include: biodegradability, hydrophilicity and the presence of carboxylic groups (ARICA et al. 2004). Owing to all these advantages, alginates are regarded as the most-promising category of biosorbents of heavy metals (APEL, TORMA 1993, NESTLE, KIMMICH 1996, PAPAGEORGIOU et al. 2006, 2008).

The alginate biosorbents are typically prepared in the form of spherical beads of calcium alginate. In aqueous solutions, heavy metal ions show higher affinity and displace calcium ions, and are combined with the alginates. Sorption of metals takes place throughout the structure of the alginate beads,

therefore, they can be regarded as a porous ion exchanger of high permeability and capacity (IBANEZ, UMETSU 1999, 2000). Moreover, they can be applied in identical process and equipment solutions as ion exchangers.

The sorption of metal ions on alginates takes place at a very fast rate and is only limited by diffusion phenomena. Therefore, according to the commonly accepted belief, the rate of sorption with this type of sorbent is limited by internal diffusion. In order to use the quantitative approach to the diffusive-mass movement within the porous beads having a complicated geometrical structure, the notion of effective diffusion coefficient, D_e, has been introduced. Since the rate of sorption on alginate beads is determined by the rate of diffusion in the sorbent pores, it is essential to know the effective diffusion coefficient to design the equipment.

The effective diffusion coefficient, D_e, is connected with the diffusion coefficient for highly dilute aqueous solution, D_{aq}, by the following relationship:

$$D_e = \frac{D_{aq} \cdot \beta}{\tau} \tag{1}$$

The tortuosity factor (τ) in the relationship takes into account the irregular shape, tortuosities, and variable bead pore sizes. Its values are typically in the range from 1 to 3 and can be found if porosity, β, is known. Formulas for calculating the tortuosity are presented in the paper SOBIESKI and LIPIŃSKI (2017).

In the case of alginate gels, it is convenient to use the diffusion retardation coefficient, φ:

$$\phi = \frac{D_e}{D_{aq}} = \frac{\beta}{\tau} \tag{2}$$

The value of the diffusion retardation coefficient is preferably not higher than 1 ($\varphi = 1$ means that $D_e = D_{aq}$; and $\varphi > 1$ means that $D_e > D_{aq}$).

The rate of diffusion has hitherto been determined based on changes in sorbate concentration in the solution during the sorption process. Measurements of the diffusion coefficient can be made in either an open or a closed system. The closed system is used more often because of its simplicity and a much greater abundance of reference material for the diffusion coefficients, found for that system previously. Measurements of D_e can be performed regardless of the sorption process, by measuring the rate of diffusion from the beads into the solution. If, during the experiments, diffusion is accompanied by sorption, then the effective coefficient of diffusion in carriers is usually found using the shrinking core model (SCM) (JANG et al. 1991, LEWANDOWSKI, ROE 1994, ARAUJO, TEIXEIRA 1997) or the linear absorption model (LAM) (CHEN et al. 1993, ARAUJO, TEIXEIRA 1997, PAPAGEORGIOU et al. 2006).

It should be noted that the effective diffusion coefficient calculating by SCM or by LAM method will provide different values of D_e. Moreover, LAM will fail in

the case of low concentrations of metals in solution (PAPAGEORGIOU et al. 2006). The SCM and LAM methods often provide unsatisfactory results (for instance, the calculated value of D_e is higher than the effective diffusion coefficient of the same metal in water), moreover, they are connected with the use of labor-consuming procedures in measuring the metal concentrations.

The known calculation models have had numerous disadvantages, therefore, a new method of determination of the effective diffusion coefficient was proposed (KWIATKOWSKA-MARKS et al. 2011b). Known as the conductometric method, it is based on measuring changes in the metal-salt solution conductivity (which depends on the solution's concentration) and correlating them with the effective diffusion coefficient.

The main objectives of this research work are:

– preparation of calcium alginate beads from sodium alginate solution;

– to determine by the conductometric method the effective diffusion coefficient for different heavy-metal salts: Cd, Zn and Pb in calcium alginate beads;

– to determine the effect of the metal type, anion from the metal salt and the alginate content in the beads on the D_e value.

Materials and Methods

Reagents

The alginate beads were made of the sodium alginate from KELCO. Six different heavy-metal salts were examined: $CdCl_2$, $CdSO_4$, $ZnCl_2$, $ZnSO_4$, $Zn(NO_3)_2$, $Pb(NO_3)_2$.

Preparation of the alginate beads

Calcium alginate beads were prepared by dropwise addition of a viscous, aqueous sodium alginate solution to 0.05 mol·L^{-1} of $CaCl_2$ solution. All the beads were prepared in the same way, only the concentration of the aqueous solution of sodium alginate was varied. During the gelation process, the sodium alginate reacted with the Ca ion from the $CaCl_2$ solution and a cross-linked Ca-alginate was formed. The gelation process was continued for 0.5 hr. The beads were then placed in a new 0.05 mol·L^{-1} portion of $CaCl_2$ for 24 hours to establish an equilibrium between the calcium ions that remained in the solution and those adsorbed by the beads. The resultant beads differed in their alginate gel contents (from 1.3 to 6.1 wt.%). The beads were kept in the refrigerator.

The beads were washed with distilled water prior to the analysis to ensure the bead pores contained no calcium ions, otherwise, the solution's conductivity

could be affected. The beads were then saturated with a selected heavy-metal salt for 24 hours. A 0.1 mol·L^{-1} solution of the selected heavy-metal salt solution was prepared and a suitable amount of calcium alginate beads was immersed in it. The solution was stirred with a magnetic stirrer. Conductivity of metal salts was determined using the microcomputer conductometer model CPC-551 from ELMETRON. All the experiments were performed at a constant pH of the solution (5.0) into which the heavy-metal salts diffused, and at a constant temperature of 25°C± 0.5°C.

The conductometric method for determination of effective diffusion coefficient

The LAM and SCM methods are based on the diffusion of metal ions from the solution into the beads and their sorption therein; therefore, the coefficient calculated according to LAM and SCM relates to the diffusion of the given metal ions. Conversely, a reversed situation takes place in the conductometric method: the biosorbent beads are saturated with the test metal salt and dropped into distilled water, where diffusion of the metal salt molecules from the bead pores into the solution containing the beads takes place. An increase in the metal salt content of the solution leads to an increase in the solution's conductivity. In the conductometric method, conductivity of the solution into which the test metal salts diffuse is measured. The conductivity varies with the effective diffusion coefficient. The experiment is carried out for a diffusion in the closed system.

In modeling diffusion of the metal salts from the alginate bead pores into the solution, it was assumed that:

1. The alginate beads are spheres with a radius, R.
2. The total volume of the beads is a sum of the solid volume and the pore volume.
3. During the diffusion, the pores are entirely filled with the aqueous solution of the metal salt.
4. Mass transport takes place only due to diffusion within the pores.
5. The metal salt concentration in water is uniform (the solution is homogeneous).
6. The liquid volume does not change.
7. Desorption of the metal ions from the alginate beads does not take place.

The metal salt diffusion in the alginate beads is a non-stationary process and, assuming that the effective diffusion coefficient is a constant value, it can be described with Fick's second equation. When the homogeneous alginate beads are spherical, the general mass balance for the diffusion of substances in the spherical beads (for non-stationary state) takes the following form:

$$\frac{\partial C_S}{\partial t} = D_e\left(\frac{\partial^2 C_S}{\partial r^2} + \frac{2}{r}\frac{\partial C_S}{\partial r}\right) \tag{3}$$

If N beads which contain the dissolved substance are immersed in a well stirred solution containing no sorbate and has a strictly defined volume, then the following initial and boundary conditions apply:

$t=0$	$0<r<R$	$C_S=$ const.
$t=0$	$r>R$	$C_L=0$
$t>0$	$r=0$	$\frac{\partial C_s}{\partial r} = 0$
$t>0$	$r=R$	$V_L\frac{\partial C_L}{\partial t} = KA_sD_e\frac{\partial C_S}{\partial r}\quad\vert_{r=R}$

Assuming that the sorbate is uniformly distributed within the bead and the beads are in equilibrium with the liquid phase, the rate of the sorbate's diffusion from the sorbent beads into the solution is expressed by the following equation, describing the substrates' diffusion outside the sphere in the closed system (ARNAUD et al. 1992, SOMERS et al. 1989):

$$C_L = \left(\frac{C_{S_0}}{1+\alpha}\right)\left\{1 - \sum_{n=1}^{\infty}\frac{6\alpha(\alpha+1)}{9+9\alpha+q_n^2\alpha^2}\exp\left(-q_n^2\frac{D_e t}{R^2}\right)\right\} \tag{4}$$

Where q_n represents positive, non-zero roots of Equation (5):

$$\mathrm{tg}q_n = \frac{3q_n}{3+\alpha q_n^2} \tag{5}$$

and parameter α is defined by Equation (6):

$$\alpha = \frac{3V_L}{4N\pi R^3 K} \tag{6}$$

C_∞ (the sorbate's equilibrium concentration in the solution) is linked with C_{S0} (sorbate's concentration in the beads for $t=0$) as follows:

$$C_\infty = \frac{C_{S_0}}{(1+\alpha)} \tag{7}$$

therefore, Equation (4) can be described as follows:

$$\frac{C_L}{C_\infty} = 1 - \sum_{n=1}^{\infty}\frac{6\alpha(1+\alpha)}{9+9\alpha+\alpha^2 q_n^2}\cdot\exp\left(-q_n^2\frac{D_e t}{R^2}\right) \tag{8}$$

By selecting suitable experimental conditions ($\alpha \geq 100$, which means that the sorbent sample volume is at least 100 times smaller than that of distilled water), it is possible to simplify Equation (8) into the form which was derived for

the open system (thus avoiding the troublesome calculation of the consecutive values of q_n):

$$\frac{C_L}{C_\infty} = 1 - \frac{6}{\pi^2}\sum_{n=1}^{\infty}\frac{1}{n^2}\cdot\exp\left(-\frac{D_e n^2\pi^2 t}{R^2}\right) \tag{9}$$

In the new, conductometric method, determination of the effective diffusion coefficient is based on measurements of conductivity of the solution into which the sorbate diffuses; therefore, assuming that dependence of conductivity on concentration is linear, the following equation is obtained (by transforming the non-stationary diffusion equation):

$$\frac{P_t}{P_\infty} = 1 - \frac{6}{\pi^2}\sum_{n=1}^{\infty}\frac{1}{n^2}\exp\left(\frac{-D_e n^2\pi^2 t}{R^2}\right) \tag{10}$$

where:

P_t – conductivity of the solution after the time t,
P_∞ – conductivity of the solution after the time ∞.

A strictly defined sample of alginate beads, saturated with the test metal salt was placed in a beaker filled with distilled water. The content of the beaker was thermostated and stirred vigorously to eliminate external diffusion resistance and provide an ideal mixing in the system. The metal salt molecules in the sorbent pores diffused into distilled water and the process rate was determined by the effective diffusion coefficient. An increase in the metal ion concentration in the solution was observed to lead to an increase in conductivity, as measured with the conductometer. The sorbent sample volume was more than 100 times smaller than that of distilled water and conductivity was in linear dependence on concentration, therefore, the effective diffusion coefficient was calculated using Equation (10). The amount of the beads, to be used for the test, depended on their diameter. After being saturated with the metal salt, the beads, of which the

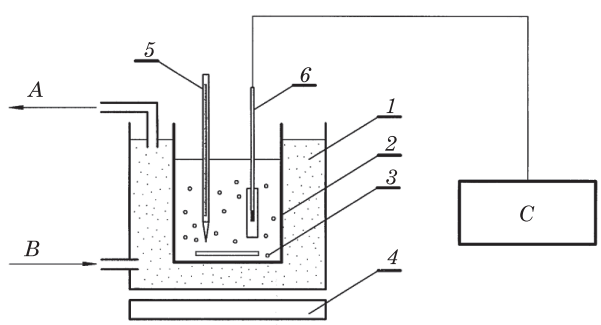

Fig. 1. Setup for determination of effective diffusion coefficient:
A – to thermostat, B – from thermostat, C – conductometer; description in the text

total volume was not higher than 1 ml, were dropped in 100 ml of distilled water while the magnetic stirrer and a stopper were started. A constant temperature of 25°C ± 0.5°C was maintained throughout the experiment. After a defined time (1, 2, 3, 4, 5, 10, 15, 20, 30, 40, 50, 60 min., etc., until the value of conductivity was constant), the solution's conductivity was measured.

The setup for determination of the effective diffusion coefficient is shown in Figure 1. It was composed of a 120 ml beaker (*2*) containing distilled water and alginate beads (*3*), saturated with the test metal salt. A thermostated water jacket (*1*), magnetic stirrer (*4*), thermometer (*5*), and conductometer with electrode (*6*).

Results and Discussion

Conducted experiments confirmed that dependence of the solution's conductivity on the given test-metal salt concentration is linear, and performed analysis enabled the authors to find that satisfactory accuracy of the results is obtained by using the initial 6 terms of Equation (10) for determination of the effective diffusion coefficient for the metal salt diffusion in the calcium alginate beads.

After measuring conductivity of the solution into which the test metal salt ions diffused from the beads, the measurement data were used for determination of the effective diffusion coefficient. The coefficient was calculated from Equation (10), using the Levenberg-Marquardt non-linear regression optimization procedure, incorporated in the SLIDE WRITE Plus software.

A typical dependence P_t/P_∞ on the process duration is shown in Figure 2.

The value of effective diffusion coefficient depends on temperature and the alginate content in the biosorbent beads. According to the mechanism of diffusion in porous carriers, an increase in the alginate content in the beads leads to lower

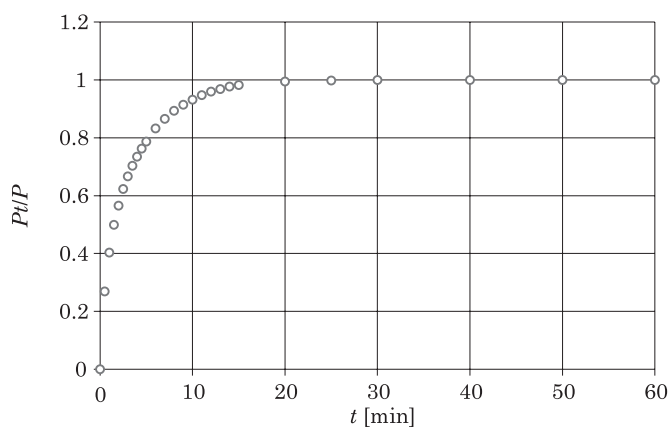

Fig. 2. Dependence of P_t/P_∞ on the process duration for diffusion of cadmium sulfate from alginate beads with a dry weight of 1.5%

values of D_e. Conversely, an increase in the process temperature contributes to an increase in the values of the effective diffusion coefficient.

Sulfates, chlorides and nitrates of 3 heavy metals: Cd, Zn and Pb, were examined. The diffusion coefficients of all the heavy-metal salts for a highly dilute aqueous solution (D_{aq}) for a temperature of 25°C were calculated using the Nernst equation.

Cadmium(II) salt diffusion

Table 1 and Figure 3 show the results of calculation for cadmium chloride and cadmium sulfate. The effect of alginate content in the biosorbent beads on the effective diffusion coefficient D_e and retardation coefficient φ is shown.

Table 1

Dependence of effective diffusion coefficient on alginate content in beads for cadmium salts

Alginate content in beads [wt %]	Effective diffusion coefficient $D_e \cdot 10^{-9}$ [m^2/s]	Correlation coefficient r^2	Retardation coefficient $\phi = \frac{D_e}{D_{aq}}$
$CdCl_2$ (D_{aq}=1.26·10^{-9} m^2/s)			
1.5	0.73	0.978	0.58
3.7	0.67	0.989	0.53
5.7	0.59	0.987	0.47
$CdSO_4$ (D_{aq}=0.86·10^{-9} m^2/s)			
1.5	0.47	0.996	0.55
3.7	0.40	0.995	0.46
5.7	0.37	0.994	0.43

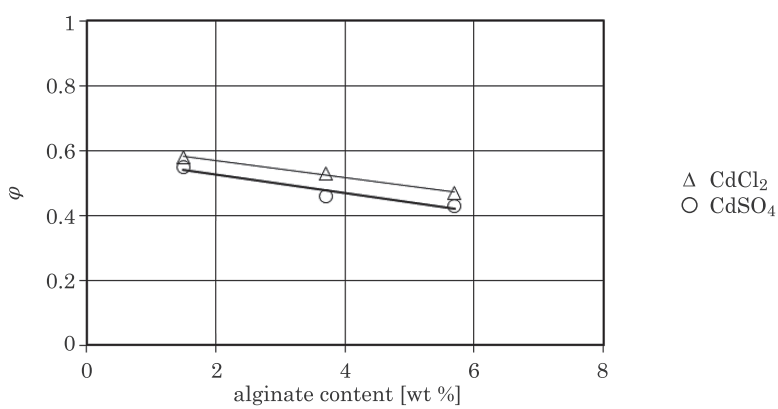

Fig. 3. Dependence of retardation coefficient on alginate content in beads for cadmium salts

All the values of D_e, obtained by the conductometric method, are lower than the calculated diffusion coefficients in a highly dilute aqueous solution of the given this salt, D_{aq}. As in the case of copper salts, the values of D_e were observed to decrease for increased alginate contents in the sorbent beads. The effective diffusion coefficients, as calculated for cadmium chloride, were higher than those for cadmium sulfate but, when compared with copper salts, the differences were slightly less pronounced (for instance, $D_{e,}$, calculated for 1.5% calcium alginate in the case of $CdSO_4$, was 35% lower in comparison with the value obtained for 1.5% alginate and the diffusion of $CdCl_2$).

Both the retardation coefficient φ and the effective diffusion coefficient also depended on the alginate content in the beads; when the alginate content in the beads increased from 1.5% to 5.7%, the value of φ decreased by 19% and 22% for $CdCl_2$ and $CdSO_4$, respectively.

Also in this case, literature data (Tab. 2) indicated significant differences between the values of D_e, as obtained by the SCM (KLIMIUK, KUCZAJOWSKA-ZADROŻNA 2002) and LAM (PAPAGEORGIOU et al. 2006) methods.

Table 2

Values of effective diffusion coefficient for Cd(II) ions in the alginate beads according to literature

$D_e \cdot 10^{-9}$ [m^2/s]	φ^b	Environmental conditions				Source
		pH	temperature [°C]	C_i [$mg \cdot L^{-1}$]	other	
0.30	0.42	no data	no data	100	as calculated according to SCM sorbate: $CdSO_4$ sorbent: 2% alginate beads	KLIMIUK, KUCZAJOWSKA-ZADROŻNA (2002)
0.6	0.83	4.0	no data	no data	no data	VOLESKY (2003)
1.9	2.64	4.5	25°C	100	as calculated according to LAM, sorbate: $CdSO_4$ sorbent: 2% alginate beads	PAPAGEORGIOU et al. (2006)
4.5	6.26	4.5	25°C	100	sorbate: $CdSO_4$ sorbent: 2% alginate beads	PAPAGEORGIOU et al. (2008)
0.0134	0.02	5.0	23°C	51	sorbate: $Cd(NO_3)_2$	APEL, TORMA (1993)
0.208	0.29	4.0	20°C	33.7	as calculated according to LAM, sorbate: $CdCl_2 \cdot H_2O$ sorbent: alginate with polyethylenimine	DEMEY et al. (2018a)

[b] for Cd(II) ions at a temperature of 298 K: $D_{aq} = 0.719 \cdot 10^{-9} m^2/s$ VOLESKY (2003).

Zinc(II) salt diffusion

Diffusion was tested for 3 zinc salts: chloride, sulfate and nitrate. Tables 3 shows the calculated values of the effective diffusion coefficient and the retardation coefficient for all of the zinc(II) salts tested.

No information has been found in the literature on the effective coefficient of diffusion of zinc ions in the alginate beads.

Also in this instance, all of the values of De, as obtained by the conductometric method, are lower than the diffusion coefficients in a given, highly dilute aqueous solution this salts (D_{aq}). The retardation coefficient (Fig. 4) and

Table 3

Dependence of effective diffusion coefficient on alginate content in beads for zinc salts

Alginate content in beads [wt %]	Effective diffusion coefficient $D_e \cdot 10^{-9}$ [m^2/s]	Correlation coefficient r^2	Retardation coefficient $\phi = \frac{D_e}{D_{aq}}$
$ZnCl_2$ (D_{aq}=1.25·10^{-9} m^2/s)			
1.5	0.77	0.977	0.62
3.7	0.73	0.982	0.59
5.7	0.66	0.982	0.53
$ZnSO_4$ (D_{aq}=0.85·10^{-9} m^2/s)			
1.5	0.44	0.962	0.52
3.7	0.37	0.988	0.43
5.7	0.24	0.967	0.28
$Zn(NO_3)_2$ (D_{aq}=1.22·10^{-9} m^2/s)			
1.5	0.84	0.985	0.69
3.7	0.63	0.981	0.52
5.7	0.50	0.966	0.41

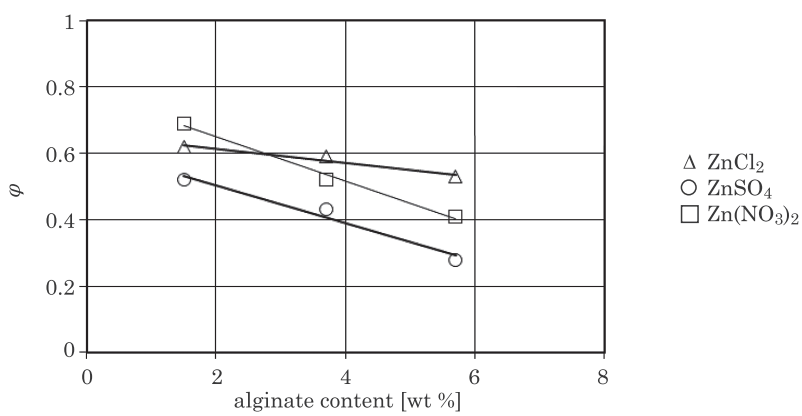

Fig. 4. Dependence of retardation coefficient on alginate content in beads for zinc salts

the effective diffusion coefficient were found to decrease with an increase in the alginate content in the beads. The lowest diffusion coefficients and the lowest retardation coefficients were obtained for zinc sulfate; the highest were obtained for zinc chloride.

Diffusion of lead nitrate

Lead nitrate was used for the tests because both lead sulfate and lead chloride are difficult dissolve in water. The results of calculation are shown in Table 4.

For lead nitrate, the retardation coefficient decreases with an increase in the alginate content in the beads, however, its decrease is not very pronounced because the alginate beads, of which the alginate content is nearly four times as high, have a retardation coefficient of just more than 13% lower (down from 0.52 to 0.45).

No information has been found in the literature on the effective diffusion coefficient for lead ions in the alginate beads.

Table 4

Dependence of the effective retardation coefficient on alginate content in the beads for lead salt

Alginate content in beads [wt %]	Effective diffusion coefficient $D_e \cdot 10^{-9}$ [m^2/s]	Correlation coefficient r^2	Retardation coefficient $\phi = \frac{D_e}{D_{aq}}$
$Pb(NO_3)_2$ (D_{aq} =1.41·10^{-9} m^2/s)			
1.5	0.74	0.980	0.52
3.7	0.70	0.994	0.49
5.7	0.64	0.991	0.45

For all tested metal salts the value of the effective diffusion coefficient is affected by the metal salt anion. In the case of sulfates, the highest values of D_e were obtained for the Cu salts, the lowest – for the Zn sulfate. For the chlorides, the highest values of D_e were obtained also for Cu, and the lowest – for Cd; the values of D_e for Zn were not much higher than those calculated for Cd. For the nitrate salts, the lowest diffusion coefficients were those for chromium. Significantly higher values of D_e were recorded for zinc nitrate and the highest, with the exception of the 1.5% alginate beads, were those for lead nitrate.

Conclusions

The experimental results clearly indicate a decrease in the values of D_e, caused by an increase in the alginate content in the sorbent beads. This is in agreement with the mechanism of the diffusion process taking place in porous

carriers. Good agreement between the experimental data and the mathematical model was obtained, as shown by the high values of correlation coefficients.

The value of the effective diffusion coefficient is affected by the metal salt anion, therefore, it should also be taken into account in the calculations.

All the values of D_e, obtained by the conductometric method, are lower than the calculated diffusion coefficients in highly dilute aqueous solution of the given this salt, D_{aq}. More often than not, the condition is not satisfied in literature reports, especially in calculations by conventional methods (SCM, LAM).

The conductometric method is simple and it provides good results in calculating the effective diffusion coefficients for heavy metals in alginate sorbents.

References

Aksu Z., Sag Y., Kutsal T. 1992. *The Biosorption of copper(II) by C. vulgaris and Z. ramigera*. Environmental Technology, 13: 579-586, doi: 10.1080/09593339209385186.

Apel M.L., Torma A.E. 1993. *Determination of kinetics and diffusion coefficients of metal sorption on Ca-alginate beads*. The Canadian Journal of Chemical Engineering,71: 652-656, doi:10.1002/cjce.5450710419.

Araujo M.M., Teixeira J.A. 1997. *Trivalent chromium sorption on alginate beads*. International Biodeterioration and Biodegradation, 40: 63-74, doi:10.1016/s0964-8305(97)00064-4.

Arnaud J.-P., Lacroix C., Castaigne F. 1992. *Counterdiffusion of lactose and lactic acid in κ-carrageenan/locust bean gum gel beads with or without entrapped lactic acid bacteria.* Enzyme and Microbial Technology, 14: 715–724, doi: 10.1016/0141-0229(92)90111-Z.

Arica M.Y., Bayramoglu G., Yilmaz M., Bektas S., Genc O. 2004. *Biosorption of Hg^{2+}, Cd^{2+}, and Zn^{2+} by ca-alginate and immobilized wood-rotting fungus Funalia Trogii*. Journal of Hazardous Materials, B109: 191-199.

Chand R., Narimura K., Kawakita H., Ohto K., Watari T., Inoue K. 2009. *Grape waste as a biosorbents for removing Cr(VI) from aqueous solution*. Journal of Hazardous Materials, 163: 245-250, doi: 10.1016/j.jhazmat.2008.06.084.

Chen D., Lewandowski Z., Roe F., Surapaneni P. 1993. *Diffusivity of Cu^{2+} in calcium alginate gel beads*. Biotechnology and Bioengineering, 41: 755-760, doi: 10.1002/bit.260430212.

Chen J., Tendeyong F., Yiacoumi S. 1997. *Equilibrium and kinetic studies of copper ion uptake by calcium alginate*. Enviromental Science and Technology, 31: 1433-1439, doi: 10.1021/es9606790.

Chojnacka K. 2010. *Biosorption and Bioaccumulation – The prospects for practical applications*. Environment International, 36: 299-307, doi: 10.1016/j.envint.2009.12.001.

Davis T.A., Volesky B., Mucci A. 2003. *A review of the biochemistry of heavy metal biosorption by brown algae*. Water Res, 37: 4311– 4330.

Deans J.R., Dixon B.G. 1992. *Uptake of Pb^{2+} and Cu^{2+} by novel biopolymers*. Water Research, 26: 469-472, doi:10.1016/0043-1354(92)90047-8.

Deze E.G., Papageorgiou S.K., Favvas E.P., Katsaros F.K. 2012. *Porous alginate aerogel beads for effective and rapid heavy metal sorption from aqueous solutions: Effect of porosity in Cu2+ and Cd2+ ion sorption*. Chemical Engineering Journal, 209: 537–546.

Dhakal R.P., Ghimire K.N., Inoue K. 2005. *Adsorptive separation of heavy metals from an aquatic environment using orange waste*. Hydrometallurgy, 79: 182-190, doi: 10.1016/j.hydromet.2005.06.007.

Demey H., Tria S.A., Soleri R., Guiseppi-Elie A., Bazin I. 2017. *Sorption of his-tagged Protein G and Protein G onto chitosan/divalent metal ion sorbent used for detection of microcystin-LR*. Environmental Science and Pollution Research, 24(1): 15-24, doi: 10.1007/s11356-015-5758-y.

DEMEY H., VINCENT T., GUIBAL E. 2018a. *A novel algal-based sorbent for heavy metal removal*. Chemical Engineering Journal, 332: 582-595. DOI:10.1016/j.cej.2017.09.083.

DEMEY H., LAPO B., RUIZ M., FORTUNY A., MARCHAND M., SASTRE A.M. 2018b. *Neodymium Recovery by Chitosan/Iron(III) Hydroxide [ChiFer(III)] Sorbent Material: Batch and Column Systems*. Polymers 10(2): 204, doi: 10.3390/polym10020204.

ECLES H. 1999. *Treatment of metal-contaminated wastes: why select a biological process?* Trends in Biotechnology, 17: 462-465, doi: 10.1016/S0167-7799(99)01381-5.

Council Directive 98/83/EC of 3 November 1998 on the quality of water intended for human consumption. 1998. In Document N◦ 01998L0083-20151027. European Commission, European Union, Brussels, Belgium.

FIGUEIRA M.M., VOLESKY B., CIMINELLI V.S.T. 2000. *Biosorption of metals in brown seaweed biomass*. Water Research, 34: 196-204, doi: 10.1016/S0043-1354(99)00120-7.

GHIMIRE K.N., INOUE K., YAMAGUCHI H., MAKINO K., MIYAJIMA T. 2003. *Adsorptive separation of arsenate and aresnite anions from aqueous medium by using orange waste*. Water Research, 37: 4945-4953, doi: 10.1016/j.watres.2003.08.029.

HU M.Z.C, NORMAN M.J., FAISON B.D., REEVES M.E. 1996. *Biosorption of uranium by pseudomonas aeruginosa strain csu: characterization and comparison studies*. Biotechnology and Bioengineering, 51: 237-247, doi: 10.1002/(SICI)1097-0290(19960720)51:2<237::AID-BIT14>3.0.CO;2-J.

IBANEZ J.P., UMETSU Y. 1999. *Uptake of copper from extremely dilute solutions by alginate sorbent material: an alternative for enviromental control*. Proceedings Of Copper 99-Cobre 99 International Environment Conference, p. 387-397.

IBANEZ J.P., UMETSU Y. 2000. *Removal of heavy metal ions by using alginate beads*. Proceedings V International Conference On Clean Technologies For The Mining Industry, Santiago, Chile, p. 49-58.

IQBAL M., SAEED A. 2002. *Removal of heavy metals from contaminated water by petiolar felt-sheath of palm*. Environmental Technology, 23: 1091–1098.

JANG K.L., GEESEY G.G., LOPEZ S.L., EASTMAN S.L., WICHLACZ P.L. 1990. *Sorption equilibrium of copper by partially-coagulated calcium alginate gel*. Chemical Engineering Communication, 96: 63-77.

JANG K.L., LOPEZ S.L., EASTMAN S.L., PRYFOGLE P. 1991 *Recovery of copper and cobalt by biopolymer gels*. Biotechnology and Bioengineering, 37: 266-273.

JANG K.L. 1994. *Diffusivity of Cu^{2+} in calcium alginate gel beads*. Biotechnology and Bioengineering, 43: 183-185, doi:10.1002/bit.260410710.

JANG L.K., NGUYEN D., GEESEY G.G. 1995. *Selectivity of alginate gel for Cu vs Co*. Water Research, 29: 307-313, doi:10.1016/0043-1354(94)E0090-S.

JANG L.K., NGUYEN D., GEESEY G.G. 1995. *Effect of pH on the absorption of Cu(II) by alginate gel*. Water Research, 29: 315-321, doi:10.1016/0043-1354(94)E0091-J.

JEON C., PARK J.Y., YOO Y.J. 2002. *Characteristics of metal removal using carboxylated alginic acid*. Water Research, 36: 1814-1824, doi:10.1016/S0043-1354(01)00389-X.

KAWAI S., MURATA K. 2016. *Biofuel production based on carbohydrates from both brown and red macroalgae: Recent developments in key biotechnologies*. International Journal of Molecular Sciences, 17: 145.

KLIMIUK E., KUCZAJOWSKA-ZADROŻNA M. 2002. *The effect of poly(vinyl alcohol) on cadmium adsorption and desorption from alginate adsorbents*. Polish Journal of Environmental Studies, 11(4): 375-384.

KONISHI Y., SHIMAOKA J., ASAI S. 1998. *Sorption of rare-earth ions on biopolymer gel beads of alginic acid*. Reactive and Functional Polymers, 36: 197-206.

KRATOCHVIL D., VOLESKY B. 1998. *Advances in the biosorption of heavy metals*. Trends in Biotechnology, 16: 291-300, doi: 10.1016/S0167-7799(98)01218-9.

KWIATKOWSKA-MARKS S., WÓJCIK M., KOPIŃSKI L. 2011. *Biosorption of heavy metals on alginate beads*. Przemysł Chemiczny, 90(10): 1924-1930.

KWIATKOWSKA-MARKS S., KOPIŃSKI L., WÓJCIK M. 2011. *Konduktometryczne wyznaczanie efektywnego współczynnika dyfuzji jonów miedzi w granulkach alginianowych*. Inżynieria i Aparatura Chemiczna, 50(6): 9-11.

LAI Y.-L., ANNADURAI G.Y, HUANG F.-C., LEE J.-F. 2008. *Biosorption of Zn(II) on the different Ca-alginate beads from aqueous solution*. Bioresource Technology, 99: 6480-6487, doi: 10.1016/j.biortech.2007.11.041.

LEWANDOWSKI Z., ROE F. 1994. *Communication to the editor. Diffusivity of Cu^{2+} in calcium alginate gel beads: recalculation*. Biotechnology and Bioengineering, 43: 186-187, doi:10.1002/bit.260430213.

MEENA A.K., KADIRVELU K., MISHRA G..K, RAJAGOPAL C., NAGAR P.N. 2008. *Adsorption of Pb(II) and Cd(II) metal ions from aqueous solutions by mustard husk*. Journal of Hazardous Materials, 150: 619-625, doi: 10.1016/j.jhazmat.2007.05.011.

NASTAJ J., PRZEWŁOCKA A., RAJKOWSKA-MYŚLIWIEC M. 2016. *Biosorption of Ni(II), Pb(II) and Zn(II) on calcium alginate beads: equilibrium, kinetic and mechanism studies*. Polish Journal of Chemical Technology, 18: 81-87, doi: 10.1515/pjct-2016-0052.

NESTLE N.F.E.I., KIMMICH R. 1996. *NMR imaging of heavy metal absorption in alginate, immobilized cells and kombu algal biosorbents*. Biotechnology and Bioengineering, 51: 538-543, doi:10.1002/(SICI)1097-0290(19960905)51:5<538::AID-BIT5>3.3.CO;2-R.

PAPAGEORGIOU S.K., KATSAROS F.K., KOUVELOS E.P., NOLAN J.W., LE DEIT H., KANELLOPOULOS N.K. 2006. *Heavy metal sorption by calcium alginate beads from Laminaria Digitata*. Journal of Hazardous Materials, B137: 1765-1772, doi:10.1016/j.jhazmat.2006.05.017.

PAPAGEORGIOU S.K., KOUVELOS E.P., KATSAROS F.K. 2008. *Calcium alginate beads from Laminaria digitata for the removal of Cu^{2+} and Cd^{2+} from dilute aqueous metal solutions*. Desalination, 224: 293-306, doi:10.1016/j.desal.2007.06.011.

PLAZINSKI W. 2012. *Sorption of lead, copper, and cadmium by calcium alginate. Metal binding stoichiometry and the pH effect*. Environmental Science and Pollution Research, 19: 3516–3524, doi:10.1007/s11356-012-0913-1.

RINCON J., GONZALEZ F., BALLESTER A., BLAZQUEZ M.L., MUNOZ J.A. 2005. *Biosorption of heavy metals by chemically activated alga Fucus Vesiculosus*. Journal of Chemical Technology and Biotechnology, 80: 1403-1407, doi:10.1002/jctb.1342.

RUIZ M., TOBALINA C., DEMEY-CEDEÑO H., BARRON-ZAMBRANO J.A., SASTRE A.M. 2013. *Sorption of boron on calcium alginate gel beads*. Reactive & Functional Polymers, 73: 653–657, doi:10.1016/j.reactfunctpolym.2013.01.014.

SOBIESKI W., LIPIŃSKI S. 2017. *The analysis of the relations between porosity and tortuosity in granular beds*. Technical Sciences, 20(1): 75–85.

SOMERS W., VAN'T REIT K., ROZIE H., ROMBOUTS F.M., VISSER J. 1989. *Isolation and purification of endo-polygalacturonase by affinity chromatography in a fluidized bed reactor*. The Chemical Engineering Journal, 40: B7-19, doi:10.1016/0300-9467(89)80046-2.

WANG S., VINCENT T., FAUR C., GUIBAL E. 2016. *Alginate and Algal-Based Beads for the Sorption of Metal Cations: Cu(II) and Pb(II)*. International Journal of Molecular Sciences, 17: 1453, doi:10.3390/ijms17091453.

Guidelines for drinking – Water quality. 2011. Fourth ed. World Health Organization, Geneva.

VEGLIO F., BEOLCHI F. 1997. *Removal of metals by biosorption: a review*. Hydrometallurgy, 44: 301-316.

VEGLIO F., ESPOSITO A., REVERBERI A.P. 2002. *Copper adsorption on calcium alginate beads: equilibrium pH-related models*. Hydrometallurgy, 65: 43-57, doi:10.1016/S0304-386X(02)00064-6.

VOLESKY B., HOLAN Z.R. 1995. *Biosorption of heavy metals*. Biotechnology Progress, 11: 235-250, doi: 10.1021/bp00033a001.

VOLESKY B. 2001. *Detoxification of metal-bearing effluents: biosorption for the next century*. Hydrometallurgy, 59: 203-216, doi:10.1016/S0304-386X(00)00160-2.

VOLESKY B. 2003. *Sorption and Biosorption*. Bv-Sorbex, Inc., St.Lambert, Quebec.

VOLESKY B. 2003. *Biosorption process simulation tools*. Hydrometallurgy, 71: 179-190, doi:10.1016/S0304-386X(03)00155-5.

Technical Sciences, 2019, 22(1), 35–43

UNIWERSYTET WARMIŃSKO-MAZURSKI W OLSZTYNIE

Quarterly peer-reviewed scientific journal
ISSN 1505-4675
e-ISSN 2083-4527
TECHNICAL SCIENCES
Homepage: www.uwm.edu.pl/techsci/

APPLICATION OF MODIFIED SILICA GEL IN THE PROCESS OF TRYPSIN IMMOBILIZATION

Justyna Miłek, Sylwia Kwiatkowska-Marks, Ilona Trawczyńska

Department of Chemical and Bioprocess Engineering
Faculty of Chemical Technology and Engineering
University of Technology and Life Sciences

Received 27 February 2018, accepted 8 January 2019, available online 14 January 2019.

Key words: trypsin, immobilization, silica gel, biocatalyst.

Abstract

The paper presents the use of modified silica gel for the production of immobilized trypsin from bovine pancreas. Silica gel was modified with 3-aminopropyltriethoxysilane, followed by glutaraldehyde. The influence of stirring time on activity of the prepared biocatalyst was determined for individual stages of the modification. Activity of both native and immobilized trypsin was measured using Kunitz method. At the temperature of 55°C and pH 7.6 native and immobilized trypsin onto modified silica gel indicate optimum activity. The influence of multiple recycling and storage time on activity of immobilized trypsin was tested. After fourteen days of storage at the temperature of 4°C immobilized trypsin exhibits 75% of its initial activity.

Correspondence: Justyna Miłek, Zakład Inżynierii Chemicznej i Bioprocesowej, Wydział Technologii i Inżynierii Chemicznej, Uniwersytet Technologiczno-Przyrodniczy im. Jana i Jędrzeja Śniadeckich, ul. Seminaryjna 3, 85-326 Bydgoszcz, phone: 52 374 90 49, e-mail: jmilek@utp.edu.pl

Introduction

Trypsin (EC 3.4.21.4) is one of the most important digestive enzymes. Optimal pH for enzyme activity ranges between 7 and 9. The role of trypsin is hydrolysis of proteins. It causes certain peptide bonds to break, decreasing the number of allergenic proteins in hypoallergenic food production (MOHAMAD et al. 2015). Trypsin is also used to improve texture of fish products and tenderness of meat; to stabilize meat; for tissue culture (cleavage of proteins); for extraction of seasonings and flavorings from vegetable and animal proteins (GOMEZ, ROMERO 2009)

Application of native enzymes has following disadvantages: influence of environmental conditions on enzyme deactivation; difficulty in removing a substrate from solution which may lead to contamination of the product. For this reason, enzyme immobilization on carriers may significantly contribute to cost reduction and improvement of the process, due to the reusability of the same portion (*Endopeptidases: Advances in Research…* 2012).

Silica gel is among carriers used for immobilization enzymes (GOMEZ, ROMERO 2009, SUN et al. 2015). It is characterized by high mechanical strength, low cost and modifiability. Additionally, techniques of trypsin immobilization onto a carrier with the use of covalent bonds become increasingly common. Such method consists of forming a covalent bond between functional groups of the carrier and protein. This ensures that enzyme is rigidly attached to the surface of a carrier. Immobilization using such method involves several stages. Firstly, activation of the carrier is conducted by attaching a reactive group, then the enzyme attaches (YANG et al. 2010). Cross-linking agents can be glutaraldehyde and 3-aminopropyltriethoxysilane (SHEN et al. 2011).

Cellulose was also used as a trypsin immobilization carrier (*Methods of Enzymatic Analysis* 2012). However, cellulose tends to be washed away in aqueous solutions during hydrolysis. Thus, silica gel was found to be a more effective carrier. Silica gel does not swell in aqueous environment, exhibits a decent mechanical strength, and is able to undergo a heat treatment. SHEN et al. (2011) presented that surface modification of silica nanoparticle by aminopropyl groups (3-aminopropyltriethoxysilane) causes an increase in adsorption ability of bovine serum albumin (BSA), in comparison to unmodified silica nanoparticles. YANG et al. (2010) proved that activity of immobilized lipase on aminosilica gel activated by glutaraldehyde is greater compared to immobilized lipase without being activated by glutaraldehyde. Thus, modification of the gel has been carried out, using 3-aminopropyltriethoxysilane (3-APTES) and glutaraldehyde solutions. Figure 1 illustrates the process of trypsin immobilization on silica gel with the use of 3-aminopropyltriethoxysilane (3-APTES) and glutaraldehyde.

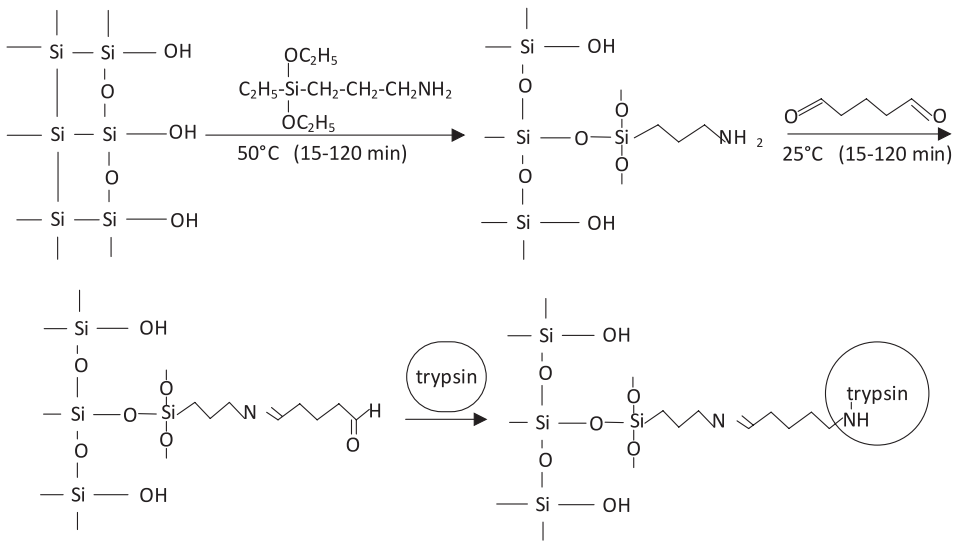

Fig. 1. The process scheme of trypsin immobilization with the use of 3-APTES and glutaraldehyde

Major and most important source of protein in milk is casein (2.4-2.6%). Hydrolysis of proteins with the use of enzymes occurs in significantly milder temperature conditions. Due to selectivity of enzymes, the number of by products produced in hydrolyzed proteins is limited.

The aim of the study was to produce immobilized trypsin from bovine pancreas on modified silica gel in optimal conditions. Modification of silica gel by 3-aminopropyltriethoxysilane (3-APTES) and glutaraldehyde in immobilization process was applied for the first time. Activity of native and immobilized enzyme was measured using Kunitz's method (ZHOU et al. 2011, SALAR et al. 2017). Effects of temperature within the range of 35-75℃ and pH between 3 and 9 on activity of native and immobilized trypsin on modified silica gel were determined. Reusability of the biocatalyst was also tested.

Materials and Methods

For the enzyme assays, native enzymes or immobilized trypsin carrying the same amount of enzyme were used. In this study, all experiments were done triplicate, and the results are expressed as mean ± SD.

Activity of native and immobilized trypsin

Trypsin enzyme activity was measured using modified Kunitz method. The reaction mixture was prepared as 0.2 ml enzyme solution or three biocatalyst (0.9-1 g) and 2 ml 1% casein in 0.1 M phosphate buffer (pH 7.6). After incubation at 55°C for 20 min, 3 ml trichloroacetic acid solution was added to terminate the reaction. After that, the mixture was incubated at room temperature for 10 min. Samples were centrifuged at 12,000 rpm for 10 min. The absorbance values were measured spectrophotometrically at 280 nm. One unit of enzyme activity was defined as the amount of enzyme that produced 1 µmol tyrosine per minute under the assay conditions. Activity retention for the immobilized trypsin was determined by the ratio between the activity of the immobilized trypsin and the activity of a similar amount of the free enzyme. Relative activity trypsin was determined according to equation 1:

$$\text{Relative activity} = (A/A_{\text{max.}})\cdot 100\% \quad (1)$$

where:

A – the measured activity trypsin,

$A_{\text{max.}}$ – the activity of trypsin in optimum conditions.

Relative activity was also presented by CARAMORI et al. (2010), MONTEIRO and SILVA (2007), SUN et al. (2015), YANG et al. (2010) for activity immobilized and native trypsin.

Process of trypsin immobilization

10 g of silica gel was weighed and added to 50 ml 10% 3-aminopropyltriethoxysilane solution. Mixture was being stirred at temperature of 50°C for specified time. The influence of stirring time (15 min, 30 min, 60 min, 120 min) on immobilized trypsin activity was tested. Modified 3-APTES silica gel was washed by 0.1 M phosphate buffer (pH 7.6). Then, silica gel was stirred with 25 ml 2.5% glutaraldehyde solution at 25°C. The influence of stirring time with glutaraldehyde within the range of 15–120 min on activity of immobilized enzyme was tested. Such modified silica gel was added to 20 ml of native trypsin solution with a concentration of 0.3 mg/ml. The effects of stirring time within the range of 15–120 min at temperature of 25°C of activated silica gel with native trypsin solution on immobilized trypsin activity were tested.

The effect of temperature and pH on activity of native and immobilized trypsin

The optimum temperature was determined by incubating native and immobilized trypsin 0.1 M phosphate buffer pH 7.6 at temperatures in the range 35–75°C for 20 min. At the end of the time, 3 ml trichloroacetic acid solution was added to terminate the reaction and the enzyme activity of each sample was determined.

The effect of pH on trypsin activity was measured at 55°C over a range of pH 3.0–9.0. For pH 3.0 a citric acid-sodium dihydrogen phosphate buffer was used, and between pH 6.0 and 9.0, the activity was determined in 0.1 M phosphate buffer. To analyze the effect of pH on trypsin stability, the enzyme solutions were incubated in buffers (0.2 ml enzyme solution or three biocatalyst) of varying pH values (3.0–9.0) for 20 min at 55°C. Residual activity was determined under optimum conditions (phosphate buffer, pH 7.6, 55°C).

Repeated uses and storage stability of immobilized trypsin

Hydrolysis of casein by immobilized trypsin was carried out at temperature of 55℃ and pH equal to 7.6. After incubation at 55℃ for 20 min, activity was determined, and immobilized trypsin on silica gel was placed into 1% casein solution.

The storage stability at the temperature of 4℃ on activity of immobilized trypsin was tested. Biocatalyst was stored for 14 days. Measurements were taken at temperature of 55℃ and pH equal to 7.6. Hydrolysis of casein was carried out on the day of immobilized trypsin production as well as after 1, 3, 7, 10 and 14 days of storage.

Results and discussion

This study aimed to optimize production of immobilized trypsin from bovine pancreas on silica gel. Table 1 presents the effect of activation time of silica gel by 10% 3-APTES solution on immobilized trypsin activity. Extension of stirring time from 15 min to 120 min causes a 40% increase in enzyme activity.

The effect of activation time of silica gel by 2.5% glutaraldehyde solution on immobilized trypsin activity is presented in Table 1. Extension of stirring time to 120 min causes a 20% increase in enzyme activity.

The effect of activation time by trypsin solution on activity was also tested (Tab. 1), in order to optimize the production of immobilized trypsin.

Table 1

Relative activity of immobilization trypsin at different activation time

Activity of immobilization trypsin [%]				
Activation time	15 min	30 min	60 min	120 min
I step – 10% 3-APTES				
	62	70	87	100
II step – 2.5% glutaraldehyde				
	81	85	88	100
III step – solution of trypsin				
	81	83	88	100

The temperature profile of free and immobilized trypsin was determined by incubating trypsin with casein solution at different temperatures (35–70°C). Figure 2 presents the effect of temperature on activity of tested native and immobilized trypsin. The optimal temperatures for both native and immobilized trypsin were similar (55°C for both).

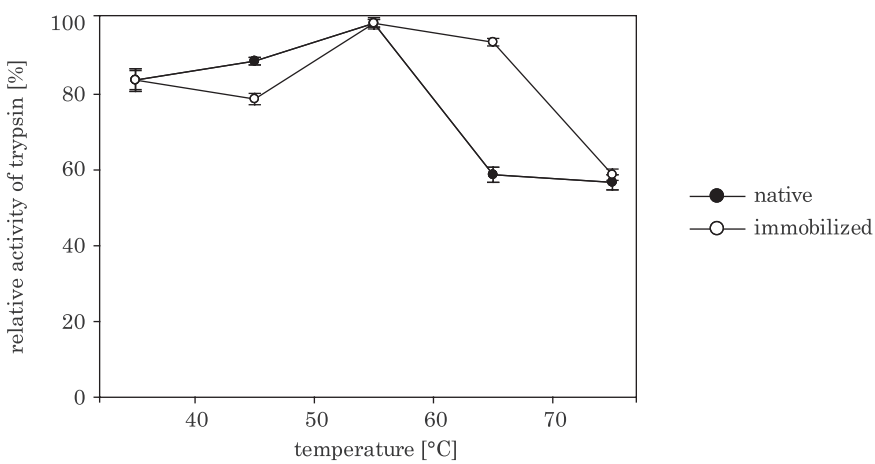

Fig. 2. The effect of temperature on activity of native and immobilized trypsin (t=20 min, pH 7.6)

The relative activities of free and immobilized enzyme at different temperatures were normalized to that of 55°C. At the temperature of 65°C immobilized trypsin activity is more than 35% greater that activity of native trypsin, suggesting that biocatalyst is more tolerant to inactivation at high temperature. Studies influence of temperature on immobilized trypsin activity are comparable to the results achieved by MONTEIRO and SILVA (2007). Those experimentals for

temperature within the range of 25°C to 65°C indicate that immobilized trypsin on silica at 65°C possesses higher activity values, compared to the activity of native trypsin. This proves that biocatalyst obtained through the immobilization process is more resistant to temperature conditions.

The variation of pH in the reaction medium can affect the stability of the enzyme and, consequently, its activity. The effects of reaction pH on the activities of immobilized trypsin were studied and compared with those for the free trypsin. Activity of immobilized and native trypsin for pH between 3 and 9 during hydrolysis of milk proteins was assayed. As can be seen, both free and immobilized trypsin had their highest activities at pH 7.6, which is the "optimum pH" value of trypsin (Fig. 3). In the whole of the pH range studied the immobilized trypsin maintained its activity better than the native trypsin. Immobilized trypsin at pH 3 and 9 exhibited greater activity compared to native trypsin, by 30% and over 20% respectively. Possibly, the covalent interaction between the silica gel-(3-APTES)-glutaraldehyde nanoparticles and trypsin increased the rigidity of the trypsin molecules, inhibiting the extensional distortion and nonspecific aggregation of the trypsin molecules, thus allowing them to better resist the effect of pH change.

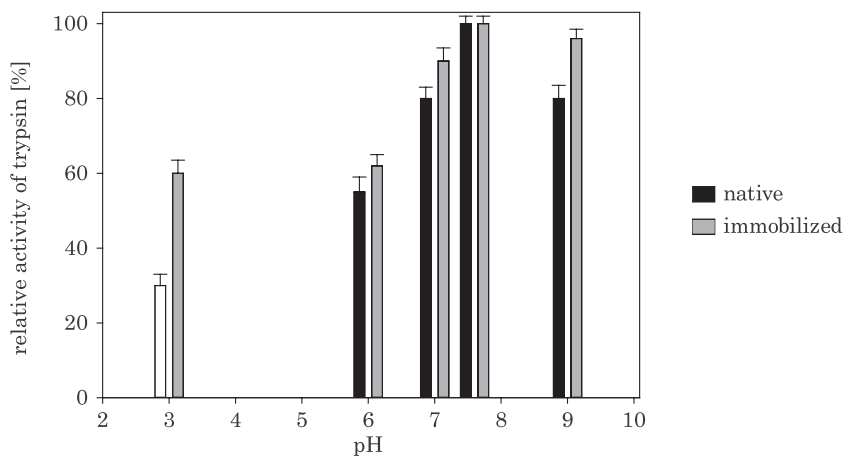

Fig. 3. The effect of pH on activity of native and immobilized trypsin

Moreover, the reusability of immobilized trypsin for hydrolysis of milk proteins was assayed. Reusability is one of the best advantages of enzyme immobilization. The reusability of immobilized trypsin was shown (Fig. 4).

Three different samples of immobilized trypsin were repeatedly used at least 8 times, and they all kept similarly high activity during such use. All of the results suggest that the immobilized trypsin displayed very good reusability.

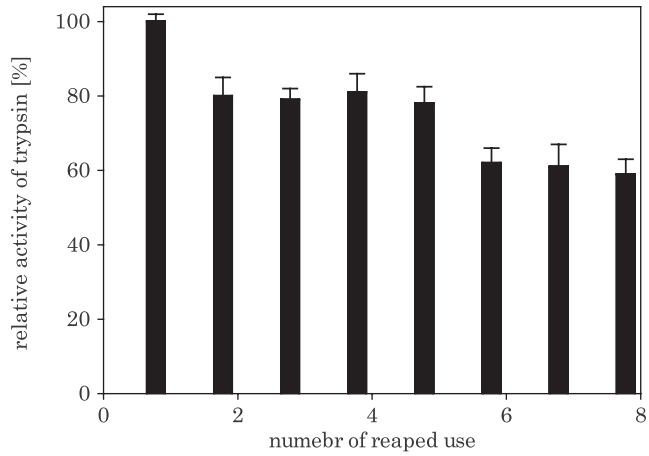

Fig. 4. Repeated uses of immobilized trypsin

During the test eight cycles were performed. In the cycles 2-5, activity of immobilized trypsin was 80%. In the cycles 6-8 it was equal to approximetly 60%.

The effect of storage time at 4℃ of immobilized trypsin on silica gel on activity was tested (Fig. 5). After 1, 3 and 14 days the activity decreased by approximetely 2%, 20% and 25% respectively.

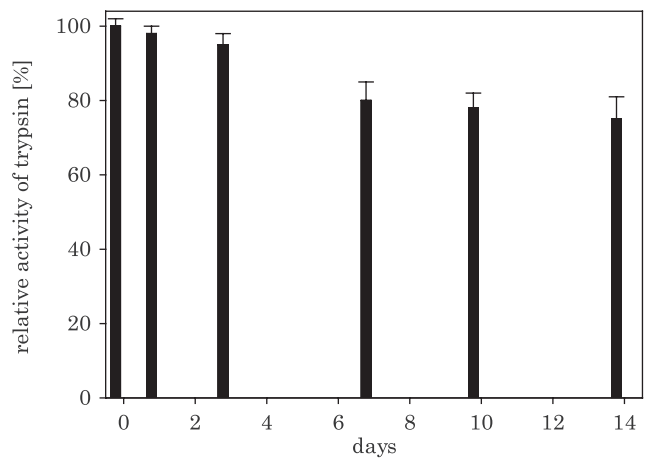

Fig. 5. The storage stability at the temperature of 4℃ on activity of immobilized trypsin

Conclusions

The aim of the study was to produce immobilized trypsin from bovine pancreas on modified silica gel in optimal conditions. Optimal conditions for production of immobilized trypsin on modified silica gel are as follows: activation time of 10% 3-aminopropyltriethoxysilane solution, 2.5% glutaraldehyde solution and trypsin solution is 120 minutes for each of the solutions. The trypsin immobilization on modified silica gel coating obtained higher thermal stability in temperature 65°C than native trypsin. Also, excellent reusability and long time storage in temperature of 4°C the immobilized trypsin illustrate the potential of this system of trypsin immobilized on silica gel for enzyme hydrolysis.

References

Endopeptidases: Advances in Research and Application: 2011. 2012. Ed. Q.A. Acton. A Scholarly Editions eBook, Atlanta, Georgia, p. 159-160.

Methods of Enzymatic Analysis. 2012. Volume 2. Ed. H.-U. Bergmeyer. Elsevier, Science, Academic Press, p. 1020.

Caramori S.S., de Faria F.N., Viana M.P., Fernandes K.F., Carvalho L.B. Jr. 2011. *Trypsin immobilization on discs of polyvinyl alcohol glutaraldehyde/polyaniline composite*. Materials Science and Engineering, C, 31: 252–257.

Gomez J., Romero M. 2009. *Adsorption of trypsin on commercial silica gel. Life* Sciences, 9(4): 336-341.

Mohamad N.R., Marzuki N.H.C., Buang N.A., Huyop F., Waha R.A. 2015. *Review. Agriculture and environmental biotechnology. An overview of technologies for immobilization of enzymes and surface analysis techniques for immobilized enzymes.* Biotechnology and Biotechnological Equipment, 29(2): 205-220.

Monteiro F.M.F., Silva G.M.M. 2007. *Immobilization of trypsin on polysaccharide film from Anacardium occidentale L. and its application as cutaneous dressing*. Process Biochemistry, 42: 884-888.

Salar S., Mehrnejad F., Sajedi R.H., Arough J.M. 2017. *Chitosan nanoparticles-trypsin interactions: Bio-physicochemical and molecular dynamics simulation studies*. International Journal of Biological Macromolecules, 103: 902–909.

Shen S.-C., Ng W.K., Chia L., Dong Y.-C., Tan R.B.H. 2011. *Sonochemical synthesis of (3-aminopropyl) triethoxysilane-modified monodispersed silica nanoparticles for protein immobilization*. Materials Research Bulletin, 46: 1665–1669.

Sun X., Cai X., Wang R.-Q., Xiao J. 2015. *Immobilized trypsin on hydrophobic cellulose decorated nanoparticles shows good stability and reusability for protein digestion*. Analytical Biochemistry, 477: 21–27.

Yang G., Wu J., Xu G., Yang L. 2010. *Comparative study of properties of immobilized lipase onto glutaraldehyde-activated amino-silica gel via different methods*. Colloids and Surfaces B: Biointerfaces, 78: 351–356.

Zhou C., Wu X., Jiang B., Shen S. 2011. *Immobilization strategy of accessible transmission for trypsin to catalyze synthesis of dipeptide in mesoporous suport*. Korean Journal of Chemical Engineering, 28(12): 2300-2305.

Zhao Q., Hou Y., Gong G.-H., Yu M.-A., Jiang L., Liao F. 2010. *Characterization of alcohol dehydrogenase from permeabilized brewer's yeast cells immobilized on the derived attapulgite nanofibers*. Applied Biochemistry and Biotechnology, 160(8): 2287–2299.

Technical Sciences, 2019, 22(1), 45–59

UNIWERSYTET WARMIŃSKO-MAZURSKI W OLSZTYNIE

Quarterly peer-reviewed scientific journal
ISSN 1505-4675
e-ISSN 2083-4527
TECHNICAL SCIENCES
Homepage: www.uwm.edu.pl/techsci/

LIE GROUP ANALYSIS OF HEAT FLUX EFFECT ON MHD SECOND SLIP FLOW FOR A SLIGHTLY RAREFIED GAS PAST A STRETCHING SHEET WITH HEAT GENERATION

Ahmed M. Megahed, Reda G. Abdel-Rahman

Department of Mathematics
Faculty of Science
Benha University, Benha, Egypt

Received 29 September 2017, accepted 4 February 2019, available online 7 February 2019.

K e y w o r d s: Lie group analysis, second order slip, slightly rarefied gas, MHD, heat flux.

A b s t r a c t

The present paper discusses steady MHD second order slip flow and heat transfer for a slightly rarefied gas due to an impermeable stretching sheet with heat flux and internal heat generation. By using the Lie group analysis, new similarity transformations are obtained. Employing these transformations, allows the partial differential equations governing the problem to transform into a system of ordinary differential equations which are later treated numerically using shooting method. Effects of the governing parameters on the dimensionless velocity and dimensionless temperature profiles are outlined graphically. Furthermore, results for the local skin-friction coefficient and the local Nusselt number are presented for some different values of the governing parameters in a tabular form. Also, results show that there is a strong dependency of the dimensionless temperature on the heat flux.

Correspondence: Ahmed M. Megahed, Department of Mathematics, Faculty of Science, Benha University, Benha, Egypt, e-mail: ah_mg_sh@yahoo.com; Reda G. Abdel-Rahman, e-mail: redakhaled2004@yahoo.com

Introduction

Of late, there has been a significant interest on the study of rarefied gas flows over a stretching sheet to obtain a thorough cognition for their behaviors and their various applications. Motivated by (FANG, AZIZ 2010), we are interested in acquiring the knowledge of heat transfer characteristics for the rarified MHD gas flow over a stretching sheet with heat flux and internal heat generation. The micro-electro-mechanical systems (MEMS) have an immense interest because in these systems, the slip flow regime and its behavior must be treated as a rarefied gas flow (FANG, AZIZ 2010). Also, for problems with low density, the fluid can be also treated as a rarefied gas flow, for example, in outer space applications (SHIDLOVSKIY 1967). The behavior of a rarefied gas flow can be determined by the Knudsen number K_n which defined as ($K_n = \frac{\lambda_e}{D_e}$) the mean free path ($\lambda_e$) divided by a characteristic length (D_e) for the flow. When Knudsen number is very small, no slip is observed between the surface and the fluid. Also, when Knudsen number lies in the range 0.001 to 0.1, slip occurs at the surface fluid interaction and the Navier-Stokes equations with the slip boundary conditions become applicable. But, for large values of Knudsen number, the Navier-stokes equations are not applicable and the kinetic theory of gases must be employed (MAHMOUD 2012). For the accurate prediction of gas flow and heat transfer in many applications second order slip boundary condition is critical. So, a significant amount of research on the fluid flow and heat transfer caused by stretched surfaces with second order slip under different conditions and in the presence of various physical effects has been reported (FANG et al. 2010, KHADER, MEGAHED 2014).

In our study, we will use the Lie-group method to derive the similarity solutions for our proposed problem. Lie group method is one of the most powerful methods in order to determine particular solutions of partial differential equations. It reduces the number of the independent variables of the partial differential equations under consideration and keeps the system of equations and associated initial and boundary condition invariant. The basic concepts of Lie group method can be found in Books (OLVER 1986, IBRAGIMOV 1994). In the field of viscous fluids there are many papers dealing with aspect of Lie group method. In 2001, YÜRÜSOY et al. presented exact solution of boundary layer equations for non-Newtonian fluids by using Lie group method. Lie group method used to study both problems of natural convection heat and mass transfer flow past an inclined plate for various parameters by (SIVASANKARAN et al. 2006). LIKEWISE, in 2010, MEKHEIMER et al. (2010) studied the Lie group analysis and similarity solutions for a couple stress fluids with heat transfer. The similarity reductions for the problem of heat and mass transfer over a moving porous plate with hydrodynamic slip and thermal convective boundary conditions were investigated

by (HAMAD et al. 2012). By using the Lie group method (MINA, AMIN 2014) studied the nonlinear inviscid flows with a free surface under gravity. Also (HOSSAN 2015) applied lie group method to study the boundary layer flow and heat transfer of an electrically conducting viscous fluid over a stretching sheet. Thus, the main aim of the present work is to study the effects of heat flux and internal heat generation on the MHD flow and heat transfer for a rarefied gas over a stretching sheet with second order slip velocity.

Mathematical formulation

Let us consider a two-dimensional laminar MHD flow of slightly rarefied gas over a stretching sheet which exposed to a heat flux and internal heat generation in the presence of second order slip effect. The origin is located at a slit, through which the sheet is drawn through the fluid medium. The *x*-axis is chosen along the plane of the sheet and the *y*-axis is taken normal to the plane. We assume that the surface starts stretching from rest with the velocity u_w and temperature distribution T_w and the temperature of the fluid at the ambient is T_∞. On the other hand, the gas fluid is assumed to be an electrically conducting in the presence of a uniform magnetic field applied normal to the sheet, and the induced magnetic field is neglected under the approximation of small Reynolds number.

So, the governing equations of steady boundary layer flow are based on the continuity, momentum and the energy equations taking into account the effect of heat generation and magnetic field, which are given as :

$$\frac{\partial \bar{u}}{\partial \bar{x}} + \frac{\partial \bar{v}}{\partial \bar{y}} = 0 \tag{1}$$

$$\bar{u}\frac{\partial \bar{u}}{\partial \bar{x}} + \bar{v}\frac{\partial \bar{u}}{\partial \bar{y}} = \frac{\mu}{\rho}\frac{\partial^2 \bar{u}}{\partial \bar{y}^2} - \frac{\sigma \bar{B}_0{}^2(\bar{x})}{\rho}\bar{u} \tag{2}$$

$$\bar{u}\frac{\partial T}{\partial \bar{x}} + \bar{v}\frac{\partial T}{\partial \bar{y}} = \frac{\kappa}{\rho c_p}\frac{\partial^2 T}{\partial \bar{y}^2} + \frac{Q(\bar{x})}{\rho c_p}(T - T_\infty) \tag{3}$$

with boundary conditions

$$\bar{y} = 0 : \bar{u} = \bar{u}_w(\bar{x}) + a(\bar{x})\frac{\partial \bar{u}}{\partial \bar{y}} + b(\bar{x})\frac{\partial^2 \bar{u}}{\partial \bar{y}^2}, \bar{v} = 0, -\kappa\frac{\partial T}{\partial \bar{y}} = \bar{q}_s(\bar{x}) \tag{4}$$

$$\bar{y} \to \infty : \bar{u} \to 0, T \to T_\infty \tag{5}$$

Introducing the non-dimensional parameters:

$$x=\frac{\bar{x}}{L},\quad y=\frac{\bar{y}}{L}\sqrt{\mathrm{Re}},\quad u=\frac{\bar{u}}{U_0},\quad v=\frac{\bar{v}}{U_0}\sqrt{\mathrm{Re}},\quad q_s=\frac{L\bar{q}_s}{\kappa\sqrt{\mathrm{Re}}},$$
$$Q(x)=\frac{\bar{Q}(\bar{x})}{Q_0}\sqrt{\mathrm{Re}},\quad \theta=\frac{(T-T_\infty)}{q_s(x)}\quad,\quad u_w=\frac{\bar{u}_w(x)}{U_0} \tag{6}$$

where $\mathrm{Re}=\frac{LU_0}{\nu}$ is the Reynolds number, U_0, L are the characteristic velocity and the characteristic length.

Use $u=\frac{\partial\psi}{\partial y}$, $v=-\frac{\partial\psi}{\partial x}$ we get

$$H_1=\frac{\partial\psi}{\partial y}\frac{\partial^2\psi}{\partial y\,\partial x}-\frac{\partial\psi}{\partial x}\frac{\partial^2\psi}{\partial y^2}-\frac{\partial^3\psi}{\partial y^3}+M^*{B_0}^2(x)\frac{\partial\psi}{\partial y}=0 \tag{7}$$

$$H_2=\frac{1}{q_s(x)}\frac{dq_s}{dx}\frac{\partial\psi}{\partial y}\theta+\frac{\partial\psi}{\partial y}\frac{\partial\theta}{\partial x}-\frac{\partial\psi}{\partial x}\frac{\partial\theta}{\partial y}-\frac{1}{Pr}\frac{\partial^2\theta}{\partial y^2}+\gamma^*Q(x)\theta=0 \tag{8}$$

The boundary conditions (4) and (5) will be

$$y=0;\quad \frac{\partial\psi}{\partial y}=u_w(x)+a^*(x)\frac{\partial^2\psi}{\partial y^2}+b^*(x)\frac{\partial^3\psi}{\partial y^3},\quad \frac{\partial\psi}{\partial x}=0,\ \frac{\partial\theta}{\partial y}=-1 \tag{9}$$

$$y\to\infty;\quad \frac{\partial\psi}{\partial y}\to 0,\quad \theta\to 0 \tag{10}$$

where $M^*=\frac{\sigma L}{\rho U}$, $\gamma^*=\frac{L}{\rho c_p U}$, $a^*(x)=\frac{\sqrt{\mathrm{Re}}}{L}a(x)$, $b^*(x)=\frac{\mathrm{Re}}{L}b(x)$.

Symmetry analysis and infinitesimal generators

In this section, we apply the techniques of Lie group theory to the equations (7) and (8). Details of the theory can be found in (Olver 1986, Ibragimov 1994). To perform this task, we consider the one-parameter (ε) Lie group of infinitesimal transformation in (x, y, ψ, θ) which given by :

$$\bar{x}=x+\varepsilon\xi_1(x,y,\psi,\theta)+o(\varepsilon^2)$$
$$\bar{y}=y+\varepsilon\xi_2(x,y,\psi,\theta)+o(\varepsilon^2)$$
$$\bar{\psi}=\psi+\varepsilon\eta_1(x,y,\psi,\theta)+o(\varepsilon^2)$$
$$\bar{\theta}=\theta+\varepsilon\eta_2(x,y,\psi,\theta)+o(\varepsilon^2) \tag{11}$$

here (ξ_1, ξ_2, η_1, η_2) are the infinitesimal transformation of the variables x, y, ψ, θ.

The corresponding infinitesimal generator of Lie group is

$$V = \xi_1 \frac{\partial}{\partial x} + \xi_2 \frac{\partial}{\partial y} + \eta_1 \frac{\partial}{\partial \psi} + \eta_2 \frac{\partial}{\partial \theta}. \tag{12}$$

Now, the infinitesimal transformations ξ_1, ξ_2, η_1 and η_2 can be determined from the following invariance conditions:

$$V^{(3)} \, |H_i|_{H_i=0} = 0, \quad i = 1,2 \tag{13}$$

here: $H_i = 0$, $i = 1, 2$ represent the equations (7) and (8) , $V^{(3)}$ is the third prolongation of infinitesimal generator V and $V^{(3)}$ is given by

$$V^{(3)} = V + \eta_{1x} \frac{\partial}{\partial \psi_x} + \eta_{1y} \frac{\partial}{\partial \psi_y} + \eta_{2x} \frac{\partial}{\partial \theta_x} + \eta_{2y} \frac{\partial}{\partial \theta_y} + \eta_{1xx} \frac{\partial}{\partial \psi_{xx}} +$$
$$\eta_{1yy} \frac{\partial}{\partial \psi_{yy}} + \eta_{2xx} \frac{\partial}{\partial \theta_{xx}} + \eta_{2yy} \frac{\partial}{\partial \theta_{yy}} + \eta_{1yyy} \frac{\partial}{\partial \psi_{yyy}}, \tag{14}$$

where η_{1x}, η_{1y}, η_{1xx}, η_{1yy}, η_{2x}, η_{2y}, η_{2yy} and η_{1yyy}, can be calculated from the following equations:

$$\eta_{1_x} = D_x(\eta_1) - \psi_x D_x(\xi_1) - \psi_y D_x(\xi_2), \quad \eta_{1_y} = D_y(\eta_1) - \psi_x D_y(\xi_1) - \psi_y D_y(\xi_2),$$

$$\eta_{2_x} = D_x(\eta_2) - \theta_x D_x(\xi_1) - \theta_y D_x(\xi_2), \quad \eta_{2_y} = D_y(\eta_2) - \theta_x D_y(\xi_1) - \theta_y D_y(\xi_2),$$

$$\eta_{1_{xx}} = D_x(\eta_{1_x}) - \psi_{xx} D_x(\xi_1) - \psi_{yx} D_x(\xi_2), \quad \eta_{1_{yy}} = D_y(\eta_{1_y}) - \psi_{xy} D_y(\xi_1) - \psi_{yy} D_y(\xi_2),$$

$$\eta_{2_{xx}} = D_x(\eta_{2_x}) - \theta_{xx} D_x(\xi_1) - \theta_{yx} D_x(\xi_2), \quad \eta_{2_{yy}} = D_y(\eta_{2_y}) - \theta_{xy} D_y(\xi_1) - \theta_{yy} D_y(\xi_2),$$

$$\eta_{1_{xy}} = D_x(\eta_{1_{xy}}) - \psi_{yx} D_x(\xi_1) - \psi_{yy} D_x(\xi_2),$$

$$\eta_{1_{yyy}} = D_y(\eta_{1_{yy}}) - \psi_{xyy} D_y(\xi_1) - \psi_{yyy} D_y(\xi_2) \tag{15}$$

where D_x, D_y are the operators of total differentiation with respect to x and y, respectively. By applying the third prolongation (14) to the original equations (7) and (8), we get

$$\eta_{1_y}\psi_{xy} + \eta_{1_{xy}}\psi_y - \eta_{1_x}\psi_{yy} - \eta_{1_{yy}}\psi_x - \eta_{1_{yyy}} + M^* B^2(x)\eta_{1_y} + 2M^*\xi_1 \frac{dB(x)}{dx} = 0, \tag{16}$$

$$\left(\frac{d}{dx}\left(\frac{1}{q_w(x)}\frac{dq_w}{dx}\right)\right)\xi_1\psi_y\theta + \frac{1}{q_w(x)}\frac{dq_w}{dx}\eta_2\psi_y + \frac{1}{q_w(x)}\frac{dq_w}{dx}\eta_{1_y}\theta + \eta_{1_y}\theta_x +$$
$$\eta_{2_x}\psi_y - \eta_{1_x}\theta_y - \eta_{2_y}\psi_x - \frac{1}{\mathrm{Pr}}\eta_{2_{yy}} - \gamma^*\xi_1\frac{dQ(x)}{dx}\theta - \gamma^* Q(x)\eta_2 = 0 \tag{17}$$

Substituting about η_{1x}, η_{1y}, η_{2x}, η_{2y}, η_{1xy}, η_{1yy}, η_{2yy} and η_{1yyy} from equations (15) into equations (16), (17) and setting the coefficients involving ψ_x, ψ_y, ψ_{xx}, ψ_{yy}, ψ_{xy}, ψ_{xyy}, ψ_{yyy}, θ_x, θ_y, θ_{xy}, θ_{xx}, θ_{xy}, θ_{yy}, and various products to zero which may be leads to a system of coupled partial differential equations. So, we have:

$$\xi_1 = d_1 + d_2 x, \quad \xi_2 = d_3 y + F(x), \quad \eta_1 = (d_2 - d_3)\psi, \quad \eta_2 = d_3\theta \tag{18}$$

where $\mathbf{d_1}$, $\mathbf{d_2}$ and $\mathbf{d_3}$ are arbitrary constants and $\boldsymbol{F(x)}$ is an arbitrary functions depends on x. The functions $B(x)$, $q_w(x)$ and $Q_w(x)$ are to be determined from the following equations:

$$\frac{dB(x)}{dx} + \left(\frac{d_3}{d_1 - d_2 x}\right) B(x) = 0, \quad \frac{dQ(x)}{dx} + \left(\frac{2d_3}{d_1 - d_2 x}\right) Q(x) = 0,$$
$$\frac{dq_s(x)}{dx} - \left(\frac{d_3}{d_1 + d_2 x}\right) q_w(x) = 0. \tag{19}$$

This implies that, the system of nonlinear equations (7) and (8) has the four-parameter Lie group of point symmetries generated by generators

$$V_1 = \frac{\partial}{\partial x}, \quad V_2 = x\frac{\partial}{\partial x} + \psi\frac{\partial}{\partial \psi}, \quad V_3 = y\frac{\partial}{\partial y} - \psi\frac{\partial}{\partial \psi} + \theta\frac{\partial}{\partial \theta}, \quad V_4 = F(x)\frac{\partial}{\partial y} \tag{20}$$

From the invariance of the boundary conditions, we get $F(x) = 0$ and the functions $u_w(x)$, $a(x)$ and $b(x)$ should satisfy the following equations

$$\frac{du_w(x)}{dx} - \left(\frac{d_2 - 2d_3}{d_1 - d_2 x}\right) u_w(x) = 0, \quad \frac{da^*(x)}{dx} - \left(\frac{d_3}{d_1 - d_2 x}\right) a^*(x) = 0,$$
$$\frac{db^*(x)}{dx} - \left(\frac{2d_3}{d_1 + d_2 x}\right) b^*(x) = 0 \tag{21}$$

From equations (19) and (20) can be obtained on different forms for the functions $B(x)$, $Q(x)$, $u_w(x)$, $a^*(x)$, $q_s(x)$ and $b^*(x)$ via choosing the constants d_1, d_2 and d_3 as follows.

Setting $d_1 = 1$, $d_2 = 1$ and $d_3 \neq 1$ we get:

$$u_w = A_1 e^{-2d_3 x}, \; a^*(x) = \lambda_1 e^{d_3 x}, \quad b^*(x) = \lambda_2 e^{2d_3 x}, \; B(x) = B_0 e^{-d_3 x},$$
$$q_s(x) = A_2 e^{d_3 x}, \quad Q(x) = Q_0 e^{-2d_3 x} \tag{22}$$

Considered the general case in which both constants are involved

$$u_w(x) = A_1(d_1 + d_2 x)^{\frac{d_2 - 2d_3}{d_2}}, a^*(x) = \lambda_1(d_1 + d_2 x)^{\frac{d_3}{d_2}}, \quad b^*(x) = \lambda_2(d_1 + d_2 x)^{\frac{2d_3}{d_2}},$$
$$Q_0(x) = Q_0(d_1 + d_2 x)^{\frac{-d_3}{d_2}}, q_w(x) = A_4(d_1 + d_2 x)^{\frac{-d_3}{d_2}}, \quad B(x) = B_0(d_1 + d_2 x)^{\frac{-d_3}{d_2}} \tag{23}$$

Choosing d_1, $d_2 \neq 0$ and $d_3 = 0$ we have:

$$u_w = A_1(d_1 + d_2 x), \quad a(x) = \lambda_1, \quad b(x) = \lambda_2, q_w(x) = q_{0s}, \quad B(x) = B_0, \quad Q(x) = Q_0 \tag{24}$$

where A_1, A_2, A_3, q_{0s}, A_4, λ_1, λ_2, B_0 and Q_0 are arbitrary constants.

The solutions of equations (7) and (8) are invariant under infinitesimal transformations (11) if $V(\psi - \psi(x, y)) = 0$ when $\psi = \psi(x, y)$ and $V(\theta - \theta(x, y)) = 0$ when $\theta = \theta(x, y)$.

These conditions can be rewritten as

$$\xi_1 \frac{\partial \psi}{\partial x} + \xi_2 \frac{\partial \psi}{\partial y} = 0, \qquad \xi_1 \frac{\partial \theta}{\partial x} + \xi_2 \frac{\partial \theta}{\partial y} = 0 \tag{25}$$

Equation (25) is called the invariant surface conditions, which are quasi-linear equations. The subsidiary equations can be expressed as:

$$\frac{dx}{\xi_1(x, y, \psi, \theta)} = \frac{dy}{\xi_2(x, y, \psi, \theta)} = \frac{d\psi}{\eta_1(x, y, \psi, \theta)} = \frac{d\theta}{\eta_2(x, y, \psi, \theta)} \tag{26}$$

From the solution of characteristic equation (26), we get on three constants one of them is called similarity variable and other called similarity functions.

Reduction to ordinary differential equations

Here, we will consider the various reductions of the partial differential equations (7) and (8).

1. We consider the combination $V_1 + d_3 V_3$, then the characteristic equations would be

$$\frac{dx}{1} = \frac{dy}{d_3 y} = \frac{d\psi}{-d_3 \psi} = \frac{d\theta}{d_3 \theta} \tag{27}$$

Solving equation (27), we have the following similarity variable and functions

$$\eta = y e^{-d_3 x}, \qquad \psi = e^{-d_3 x} f(\eta), \quad \theta = e^{d_3 x} G(\eta). \tag{28}$$

Inserting the similarity variable $\boldsymbol{\eta}$ and functions into equations (7) and (8) yields the following ordinary differential system:

$$f''' - d_3 f f'' + 2 d_3 f'^2 - M f' = 0, \tag{29}$$

$$G'' - \Pr(d_3 f G' + 2 d_3 f' G - \gamma G) = 0 \tag{30}$$

and boundary conditions are transformed to

$$f'(0) = 1 + \lambda_1 f''(0) + \lambda_2 f'''(0), \quad f(0) = 0, \quad G'(0) = -1, \text{ at } \eta = 0 \tag{31}$$

$$f'(\infty) = 0, \quad G(\infty) = 0, \text{ at } \eta \to 0 \tag{32}$$

where the functions $\underline{u}_w(x)$, $a(x)$, $b(x)$, $B(x)$, $Q(x)$ are defined in equation (22) and $A_1 = 1$, $M = M^* B_0^2$, $\gamma = \gamma^* Q_0$.

2. Consider the general case $d_1V_1 + d_2V_2 + d_3V_3$, then equation (26) take the form

$$\frac{dx}{d_1 + d_2 x} = \frac{dy}{d_3 y} = \frac{d\psi}{(d_2 - d_3)\psi} = \frac{d\theta}{d_3 \theta} \tag{33}$$

from equation (33), we get

$$\eta = y(d_1 + d_2 x)^{-\frac{d_3}{d_2}}, \quad \psi = (d_1 + d_2 x)\frac{d_2 - d_3}{d_2} f(\eta), \quad \theta = (d_1 + d_2 x)^{\frac{d_3}{d_2}} G(\eta) \tag{34}$$

Consequently, substituting equation (34) into equations (7) and (8) and boundary conditions (9) and (10), we obtain the following similarity equations

$$f''' + (d_2 - d_3) f f'' - (d_2 - 2d_3) f'^2 - M f' = 0 \tag{35}$$

$$G'' + \Pr((d_2 - d_3) f G' - (A_4 + 1) d_3 f' G + \gamma G) = 0 \tag{36}$$

and boundary conditions take the form

$$f'(0) = 1 + \lambda_1 f''(0) + \lambda_2 f'''(0), \quad f(0) = 0, \quad G'(0) = -1, \text{ at } \eta = 0 \tag{37}$$

$$f'(\infty) = 0, \quad G(\infty) = 0, \text{ at } \eta \to 0 \tag{38}$$

where the functions $\underline{u}_w(x)$, $a(x)$, $b(x)$, $B(x)$, $Q(x)$ are defined in equation (23) and $A_1 = 1$, $M = M^* B_0^2$, $\gamma = \gamma^* Q_0$.

3. Consider $d_1V_1 + d_2V_2$, from equation (26) we have

$$\eta = y, \qquad \psi = (d_1 + d_2 x) f(\eta), \quad \theta = G(\eta) \tag{39}$$

Substituting from equation (39) into equations (7) to (10) we get the following system of ordinary differential equations:

$$f''' + d_2 f f'' - d_2 f'^2 - M f' = 0 \tag{40}$$

$$G'' + \Pr(d_2 f G' + \gamma G) = 0 \tag{41}$$

and boundary conditions will be

$$f'(0) = 1 + \lambda_1 f''(0) + \lambda_2 f'''(0), \quad f(0) = 0, \quad G'(0) = -1, \text{ at } \eta = 0 \tag{42}$$

$$f'(\infty) = 0, \quad G(\infty) = 0, \text{ at } \eta \to 0 \tag{43}$$

where the functions $\underline{u}_w(x)$, $a(x)$, $b(x)$, $B(x)$, $Q(x)$ and $\underline{q}_w(x)$ are defined in equation (24) $A_1 = 1$, $M = M^* B_0^2$, $\gamma = \gamma^* Q_0$.

The physical quantities of interest are the local skin-friction coefficient C_f and the local Nusselt number Nu_x which are defined as:

$$C_f = \frac{2\tau_w}{\rho u_w{}^2}, \quad Nu_x = \frac{xq_s}{\kappa(T_w - T_\infty)} \tag{44}$$

Further, τ_w is the shear stress which given by :

$$\tau_w = -\mu(\frac{\partial u}{\partial y})_{y=0} \tag{45}$$

Using Eqs. (39) (The third case), we obtain:

$$\frac{1}{2}\mathrm{Re}_x{}^{\frac{1}{2}} C_f = -f''(0), \qquad Nu_x \,\mathrm{Re}_x{}^{-\frac{1}{2}} = \frac{1}{\theta(0)} \tag{46}$$

where $\mathrm{Re}_x = \frac{xu_w(x)}{\nu}$ is the local Reynolds number.

Results and discussion

In this section, to get clear insight of the physical problem, numerical results for the second order slip flow and heat transfer for a slightly rarefied gas within a boundary layer in the presence of heat generation/absorption, magnetic field and heat flux effects was performed with the purpose of identifying the characteristics of the gas flow over a stretching sheet (third case). Figures 1-7 depict the graphical illustrations of the various controlling parameters on the velocity and temperature profiles. The dimensionless velocity profiles for some selected values of magnetic parameter M are plotted in Figure 1. It is apparent that the velocity decreases along the surface with an increase in the magnetic parameter. Physically, it is well known that the magnetic field presents a damping effect on the velocity field by creating linear magnetic drag force in the form of $(-Mf')$ which appear in the non-dimensional momentum boundary layer equation (40), is directly proportional to M. Therefore greater retarding effect is generated in the flow with greater M values which causes a decrease for the velocity distribution inside the momentum boundary layer.

Figure 2, shows the effect of magnetic parameter M on the temperature profiles above the surface. It is noticed that, an increase in the parameter M has the effect of increasing the temperature distribution, the wall temperature $\theta(0)$ and the thermal boundary layer thickness.

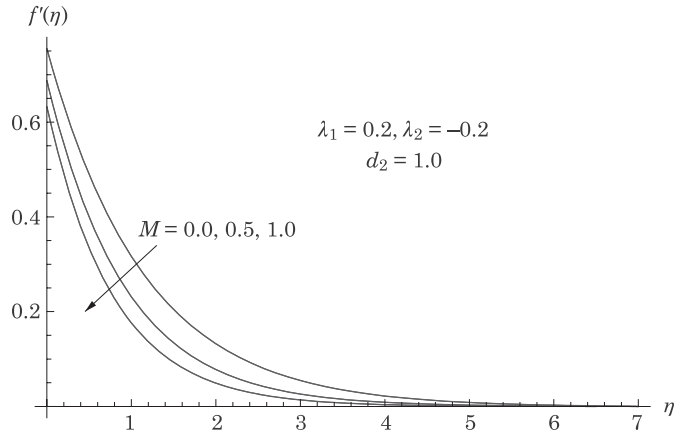

Fig. 1. The velocity distribution for various values of M

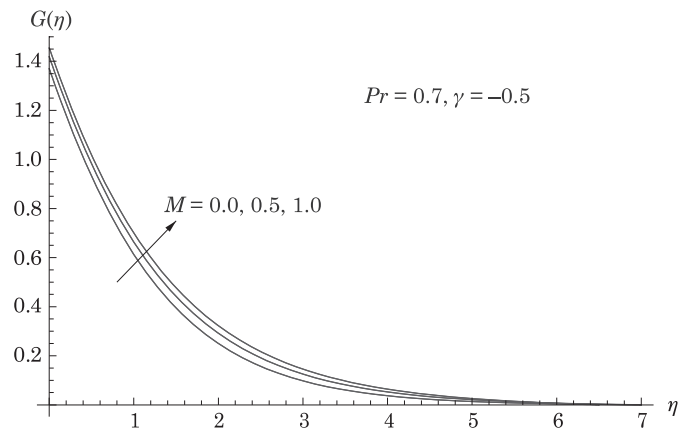

Fig. 2. The temperature distribution for various values of M

The effects of the first order velocity slip parameter on the dimensionless velocity and temperature profiles are depicted in Figures 3 and 4, respectively. It is clear from these figures that the velocity decreases with the increase of the first order velocity slip parameter, while the temperature distribution and the wall temperature $\theta(0)$ are increased with the increase of the same parameter. Physically, as the slip parameter increases in magnitude, causes a creation for the friction force which permit more fluid to slip past the sheet, the flow slows down for distances close to the sheet and the temperature rise due to the presence for this force.

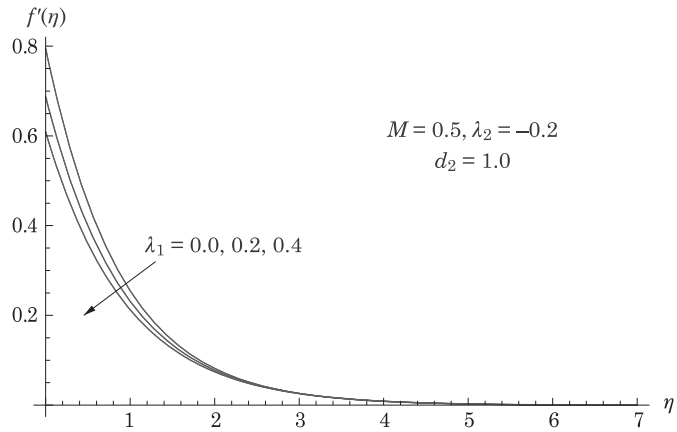

Fig. 3. The velocity distribution for various values of λ_1

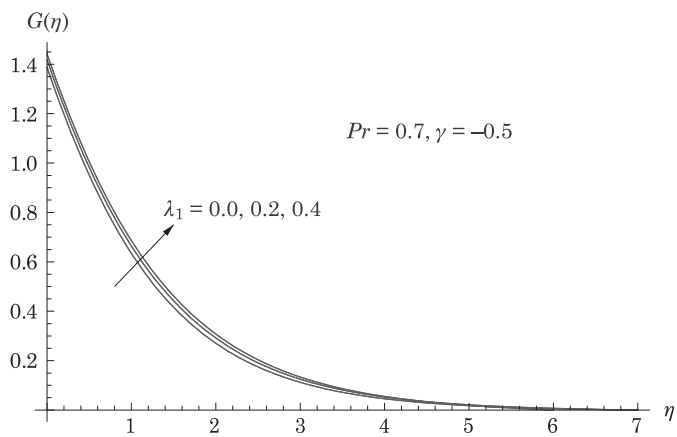

Fig. 4. The temperature distribution for various values of λ_1

Figures 5 and 6, illustrate the effects of the second velocity slip parameter on the dimensionless velocity and temperature profiles, respectively. It can be seen that the dimensionless velocity is gradually reduced with increasing the amount of the absolute value of second velocity slip parameter but the reverse is true for the temperature distribution along the thermal boundary layer and the wall temperature $\theta(0)$.

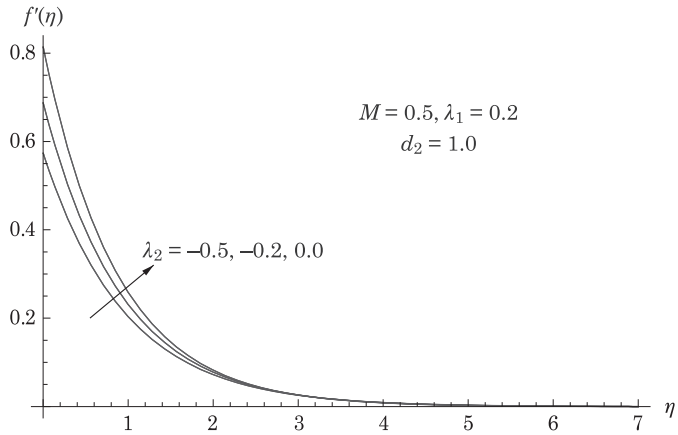

Fig. 5. The velocity distribution for various values of λ_2

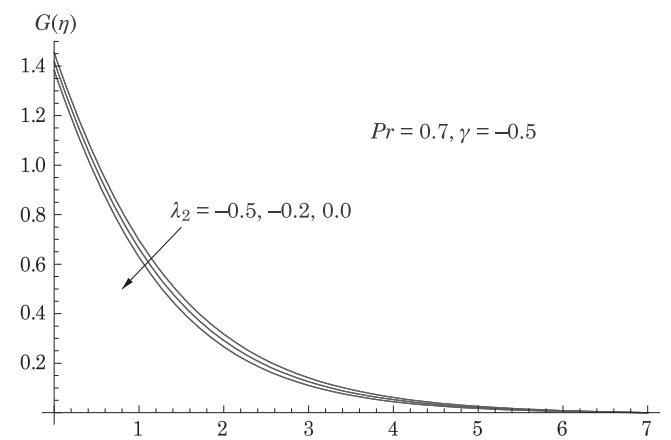

Fig. 6. The temperature distribution for various values of λ_2

Figure 7 shows the temperature profile against the similarity variable η for various values of heat generation/absorption parameter γ. This figure shows that the heat generation or absorption has a profound effect on the thermal boundary layer thickness in which the absorption parameter $\gamma < 0$ reduces the thermal boundary layer thickness and the wall temperature $\theta(0)$, whereas heat

generation parameter $\gamma > 0$ thickens the thermal boundary layer and increases the wall temperature $\theta(0)$. However, the net effect for the absorption parameter is to slow down the temperature distribution but the reverse is true for the heat generation parameter.

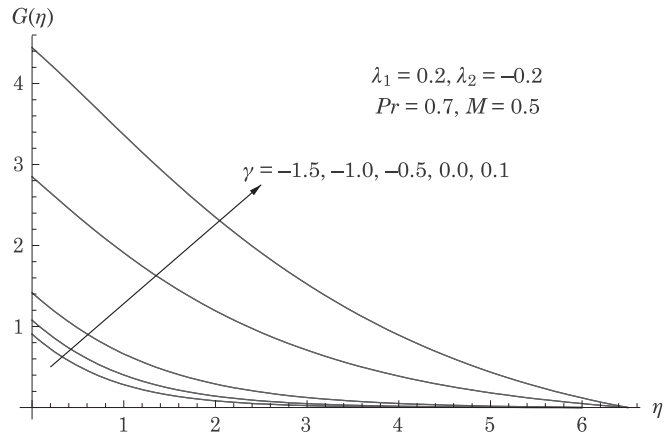

Fig. 7. The temperature distribution for various values of γ

Finally, to show the behavior of the quantities of relevant physical interest like the local skin-friction coefficient $\frac{1}{2}\mathrm{Re}_x^{\frac{1}{2}} C_f$ and the local Nusselt number $Nu_x \mathrm{Re}_x^{-\frac{1}{2}}$ with changes in the first order slip velocity parameter λ_1, the second order slip velocity parameter λ_2, the magnetic parameter M and the heat generation/absorption parameter γ. One can then see from Table 1 that, increases in the first order slip velocity parameter or the absolute value of the second order slip velocity parameter leads to a decrease in both the local skin-friction coefficient and the local Nusselt number. Physically, when the slip velocity on the surface rises, friction between the fluid and the surface is reduced. With decreasing friction, the heat generated on the surface which transferred to the flow is reduced. This leads to a decrease in the rate of heat transfer. Also, it is observed from the same table that, an increase in the magnetic parameter causes an increase in the local skin-friction coefficient but the reverse trend is noted for the local Nusselt number. On the other hand, increases in the heat absorption parameter leads to an enhancement in the local Nusselt number. Likewise, an increase in the heat generation parameter causes a decrease in the local Nusselt number.

Table 1

Values of the local skin-friction coefficient $\frac{1}{2}\mathrm{Re}_x^{\frac{1}{2}}C_f$ and the local Nusselt number $Nu_x\mathrm{Re}_x^{-\frac{1}{2}}$ for various values of M, λ_1, λ_2 and γ with Pr = 0.7

$Nu_x\mathrm{Re}_x^{-\frac{1}{2}}$	$\frac{1}{2}\mathrm{Re}_x^{\frac{1}{2}}C_f$	γ	λ_2	λ_1	M
0.730256	0.656093	-0.5	-0.2	0.2	0.0
0.705121	0.748668	-0.5	-0.2	0.2	0.5
0.687691	0.807587	-0.5	-0.2	0.2	1.0
0.720946	0.903753	-0.5	-0.2	0.0	0.5
0.705121	0.748668	-0.5	-0.2	0.2	0.5
0.693715	0.640927	-0.5	-0.2	0.4	0.5
0.687897	0.594106	-0.5	-0.5	0.2	0.5
0.705121	0.748668	-0.5	-0.2	0.2	0.5
0.723733	0.93238	-0.5	0.0	0.2	0.5
1.103830	0.748668	-1.5	-0.2	0.2	0.5
0.927601	0.748668	-1.0	-0.2	0.2	0.5
0.705121	0.748668	-0.5	-0.2	0.2	0.5
0.350826	0.748668	0.0	-0.2	0.2	0.5
0.225079	0.748668	0.1	-0.2	0.2	0.5

Conclusion

This article deals with the effects of MHD second order slip on a slightly rarefied gas flow and heat transfer over a stretching surface in the presence of internal heat generation and heat flux. The governing partial differential equations for the flow and temperature fields are reduced to a system of coupled nonlinear ordinary differential equations by deducing suitable similarity transformations via Lie group analysis. These nonlinear differential equations are then solved numerically by the shooting method coupled with the fourth-order Runge Kutta scheme. As here it clearly brings out, the rate of heat transfer decreases with an increase in the heat generation parameter, magnetic parameter, the first order slip parameter and the absolute value of the second order slip velocity parameter. Also, it was observed that the local Nusselt number increases as the heat absorption parameter increases. Thus fast cooling of the stretching sheet can be achieved by implementing this effect. Finally, a large value of the first order slip velocity parameter and the absolute value of the second order slip velocity parameter lead to a decrease in the value of the skin-friction coefficient.

References

FANG T., AZIZ A. 2010. *Viscous flow with second-order slip velocity over a stretching sheet*. Zeitschrift für Naturforschung A, 65a: 1087-1092.

FANG T., YAO S., ZHANG J., AZIZ A. 2010. *Viscous flow over a shrinking sheet with second order slip flow model*. Communications in Nonlinear Science and Numerical Simulation, 15: 1831-1842.

HAMAD M.A.A., UDDIN M.J., ISMAIL A.I.M. 2012. *Investigation of combined heat and mass transfer by Lie group analysis with variable diffusivity taking into account hydrodynamic slip and thermal convective boundary conditions*. International Journal of Heat and Mass Transfer, 55: 1355-1362.

HOSSAM S.H. 2015. *Symmetry analysis for MHD viscous flow and heat transfer over a stretching sheet*. Applied Mathematics, 6: article ID: 53062,16 pages.

IBRAGIMOV N.C.R.C. 1994. *Handbook of Lie group analysis of differential equations*. Vol 1: *Symmetries, exact solutions and conservation laws*. CRC Press, Boca Raton, FL.

KHADER M.M., MEGAHED A.M. 2014. *Differential transformation method for the flow and heat transfer due to a permeable stretching surface embedded in a porous medium with a second order slip and viscous dissipation*. ASME Journal of Heat Transfer, 136(7): 072602– 072607.

KHADER M.M., MEGAHED A.M. 2014. *Numerical solution for the flow and heat transfer due to a permeable stretching surface embedded in a porous medium with a second order slip and viscous dissipation*. European Physical Journal Plus, 129: 10.

KHADER M.M., MEGAHED A.M. 2014. *Effect of viscous dissipation on the boundary layer flow and heat transfer past a permeable stretching surface embedded in a porous medium with a second-order slip using Chebyshev finite difference method*. Transport in Porous Media, 105: 487–501.

MAHMOUD M.A.A. 2012. *MHD flow and heat transfer in a viscous fluid over a non-isothermal stretching surface with thermal radiation in slip-flow regime*. Chemical Engineering Communications, 199: 925-942.

MEKHEIMER K.S., HUSSENY S.Z.A., ALI A.T., ABO-ELKHAIR R.E. 2010. *Lie Group Analysis and Similarity Solutions for a Couple Stress Fluid with Heat Transfer*. Journal of Advanced Research in Applied Mathematics, 2: 1-17.

MINA B.M., AMIN A.M. 2014. *Lie group analysis of nonlinear inviscid flows with a free surface under gravity*. Journal of Computational and Applied Mathematics, 258: 17-29.

NANDEPPANAVAR M.M, VAJRAVELU K., ABEL M.S., SIDDALINGAPPA, M.N. 2012. *Second order slip flow and heat transfer over a stretching sheet with non-linear Navier boundary condition*. International Journal of Thermal Science, 58: 143-150.

OLVER P. 1986. *Applications of Lie groups to differential equations*. Springer-Verlag, New York.

RAMASAMI E.K. 2006. *Lie group analysis of natural convection heat and mass transfer in an inclined porous surface with heat generation*. International Journal of Applied Mathematics and Mechanics, 2: 34–40.

RAMASAMI E.K. 2006. *Lie group analysis of natural convection heat and mass transfer in an inclined surface*. Nonlinear Analysis: Modelling and Control, 11: 201–212.

SHIDLOVSKIY V.P. 1967. *Introduction to the Dynamics of Rarefied Gases*. American Elsevier Publishing Company Inc., New York.

SIVASANKARAN S., BHUVANESWARI M., KANDASWAMY P., STEPHANI H. 1989. *Differential Equations: Their Solution Using Symmetries*. Cambridge University Press, New York.

WU L. 2008. *A slip model for rarefied gas flows at arbitrary Kundsen Number*. Applied Physics Letters, 93: 253103.

YÜRÜSOY M., PAKDEMIRLI M., NOYAN O.F. 2001. *Lie group analysis of creeping flow of a second grade fluid*. International Journal of Non-Linear Mechanics, 36: 955–960.

Technical Sciences, 2019, 22(1), 61–74

UNIWERSYTET WARMIŃSKO-MAZURSKI W OLSZTYNIE

Quarterly peer-reviewed scientific journal
ISSN 1505-4675
e-ISSN 2083-4527
TECHNICAL SCIENCES
Homepage: www.uwm.edu.pl/techsci/

PARTICLE SWARM OPTIMIZATION AND DISCRETE ARTIFICIAL BEE COLONY ALGORITHMS FOR SOLVING PRODUCTION SCHEDULING PROBLEMS

Tadeusz Witkowski

Faculty of Production Engineering
Warsaw University of Technology in Warsaw

Received 13 December 2018, accepted 6 February 2019, available online 7 February 2019.

Key words: Discrete Artificial Bee Colony, Particle Swarm Optimization, production scheduling problem, makespan.

Abstract

This paper shows the use of Discrete Artificial Bee Colony (DABC) and Particle Swarm Optimization (PSO) algorithm for solving the job shop scheduling problem (JSSP) with the objective of minimizing makespan. The Job Shop Scheduling Problem is one of the most difficult problems, as it is classified as an NP-complete one. Stochastic search techniques such as swarm and evolutionary algorithms are used to find a good solution. Our objective is to evaluate the efficiency of DABC and PSO swarm algorithms on many tests of JSSP problems. DABC and PSO algorithms have been developed for solving real production scheduling problem too. The experiment results indicate that this problem can be effectively solved by PSO and DABC algorithms.

Introduction

The job shop scheduling problem has become a classic scheduling problem. Although it is mainly associated with industrial engineering, it is required in other sectors, too. The study of the scheduling problem is carried out taking inputs from various sources, such as computer science, operations research, management and manufacturing.

Correspondence: Tadeusz Witkowski, Instytut Organizacji Systemów Produkcyjnych, Wydział Inżynierii Produkcji, Politechnika Warszawska, ul. Narbutta 85, 02-524 Warszawa, e-mail: tawit@poczta.onet.pl

Scheduling involves assigning a set of tasks on resources in a time period, taking into account the time, capability and capacity constraints. Many studies have been done to solve this problem or to determine the closest approach to the solution. Commonly used scheduling techniques include the following (BŁAŻEWICZ et al. 2007):

– Exact Algorithms (e.g. Branch and Bounds Methods, Linear Programming, Dynamic Programming);

– Approximation Algorithms [Artificial Intelligence Algorithms (e.g. Artificial Neural Network), Local Search Algorithms (e.g. Greedy Randomized Adaptive Search Procedure, Taboo Search, Simulated Annealing), Evolutionary Algorithms (e.g. Genetic Algorithm), Swarm Optimization Algorithms (e.g. Ant Colony Optimization, Bee Colony Algorithm, Particle Swarm Optimization)].

WITKOWSKI (2016) presents a research study of state-of-the-art algorithms for FJSP. Therefore, these algorithms can be called swarm-intelligence-based, bio-inspired, physics-based and chemistry-based, depending on the sources of inspiration.

Swarm-intelligence-based algorithms include: Accelerated PSO, Ant colony optimization, Artificial bee colony, Bacterial foraging, Bacterial-GA Foraging, Bat algorithm, Bee colony optimization, Bee system, BeeHive, Wolf search, Bees algorithms, Bees swarm optimization, Bumblebees, Cat swarm, Consultant-guided search, Cuckoo search, Eagle strategy, Fast bacterial swarming algorithm, Firefly algorithm, Fish swarm/school, Good lattice swarm optimization, Glowworm swarm optimization, Hierarchical swarm model, Krill Herd, Monkey search, Particle swarm algorithm, Virtual ant algorithm, Virtual bees, Weightless Swarm Algorithm and other algorithms Anarchic society optimization, Artificial cooperative search, Backtracking optimization search, Differential search algorithm, Grammatical evolution, Imperialist competitive algorithm, League championship algorithm, Social emotional optimization.

Bio-Inspired (not swarm-intelligence-based) algorithms include: Atmosphere clouds model, Biogeography-based optimization, Brain Storm Optimization, Differential evolution, Dolphin echolocation, Japanese tree frogs calling, Eco-inspired evolutionary algorithm, Egyptian Vulture, Fish-school Search, Flower pollination algorithm, Gene expression, Great salmon run, Group search optimizer, Human-Inspired Algorithm, Invasive weed optimization, Marriage in honey bees, OptBees, Paddy Field Algorithm, Roach infestation algorithm, Queen-bee evolution, Shuffled frog leaping algorithm, Termite colony optimization.

Physics- and chemistry-based algorithms include: Big bang-big Crunch, Black hole, Central force optimization, Charged system search, Electro-magnetism optimization, Galaxy-based search algorithm, Gravitational search, Harmony search, Intelligent water drop, River formation dynamics, Self-propelled particles, Simulated annealing, Stochastic diffusion search, Spiral optimization, Water cycle algorithm.

Other algorithms used for job scheduling problem are the following: Raven roosting optimization algorithm, Camel herds algorithm, artificial flora algorithm, Rhinoceros search algorithm, Beer froth artificial bee colony.

Hence, a variety of heuristics and metaheuristics procedures such as taboo search, simulated annealing and genetic algorithm have been applied to solve these problems and find an optimal or near-optimal schedule in a reasonable time (WITKOWSKI et al. 2010) Swarm intelligence systems are typically made up of a population of simple agents interacting locally with one another and with their environment. Particle Swarm, Ant Colony, Bee Colony are examples of swarm intelligence. A survey (KRAUSE et al. 2013) shows that PSO was the most frequently found algorithm, representing 25% of all papers analyzed, and scheduling problems are the most frequently analyzed. The ABC algorithm came second, representing 13% of the total.

Production Scheduling Problem

The structure of the production scheduling problem can be described as follows (MESGHOUNI et al. 2004).

Consider a set of N jobs $\{J_j\}_{i\,j\,N}$, where these jobs are independent of one another; each job J_j has an operating sequence, called G_j; each operating sequence G_j is an ordered series of operations, G_{ij} indicating the position of the operation in the technological sequence of the job; the realization of each operation O_{ij} requires a resource or a machine selected from a set of machines, $\{M_k\}_{i\,j\,M}$ (for FJSSP problem); M is the total number of machines existing in the shop, this implying the existence of an assignment problem; there is a predefined set of processing times; for a given machine, and a given operation O_{ij}, the processing time is denoted by P_{ijMk}; an operation which has started runs to completion (non-preemption condition); each machine can perform operations one after another (resource constraints). Our objective is to determine the minimal makespan ($C_{\max}$ value), where $C_{\max} = \max\{C_j\}$, and C_j is the completion time of job J_j.

To evaluate schedules different performance measures or optimality criteria have been used (BŁAŻEWICZ et al. 2007): schedule length (makespan), mean flow time, mean weighted flow time, maximum lateness, mean tardiness, mean weighted tardiness, mean earliness, mean weighted earliness, number tardy task and weighted number of tardy tasks.

The flexible job shop scheduling problem (FJSSP) is an extended traditional JSSP problem. It discards the restriction of unique resources and allows each operation to be processed by several different machines, and so makes the JSSP problem more similar to the actual production situation.

PSO and ABC algorithms for Solving the Scheduling Problem

The issues of production scheduling cover a wide range of models and algorithms as well as optimization criteria. Papers on JSSP problems with basic PSO and ABC algorithms (non-hybrid) were presented, among others, in SUREKHA and SUMATHI (2010) and ABU-SRHAHN and AL-HASAN (2015). In SUREKHA and SUMATHI (2010), we find a knowledge – based approach to JSSP using Particle Swarm Optimization and Ant Colony Optimization. The well known FISHER and THOMPSON (1963) 10×10 instance (FT10) and ADAMS et al. (1988) 10×10 instance (ABZ10) problem are selected as the experimental benchmark problems. Based on simulation and evaluation results, it is concluded that PSO is the superior computational intelligence algorithm for solving the JSSP problem.

A. ABU-SRHAHN and M. AL-HASAN (2015) present a hybrid algorithm (Cuckoo Search Optimizer is used along with a GA) to minimize $C_{\max}$ value for JSSP. The algorithms were tested using well known datasets in order to verify the validity of the proposed algorithm. The instances FT06, FT10, and FT20 are designed by FISHER and THOMPSON (1963), and instances LA01 to LA16 are designed by LAWRENCE (1984). The results have been compared with GA algorithm and Ant Colony Optimization Algorithm (ACO) to show the importance of the proposed algorithm. The results show that the hybrid algorithm yields the best solutions as measured by $C_{\max}$ value, and GA algorithm is better then ACO.

In this paper, Discrete Artificial Bee Colony (DABC) algorithm and Particle Swarm Optimization (PSO) algorithm are proposed for solving the job shop scheduling problem with the objective of minimizing makespan (which is the total length of the schedule, that is, when all the jobs have finished processing – $C_{\max}$ value).

PSO Algorithm

Particle swarm optimization (PSO) is a population-based optimization algorithm. Each particle is an individual and the swarm is composed of particles. The problem solution space is formulated as a search space. Each position in the search space is a correlated solution of the problem. Particles cooperate to find out the best position (best solution) in the search space (solution space). Particles move toward the pbest position and gbest position with each iteration. The pbest position is the best position found by each particle so far. Each particle has its own pbest position. The gbest position is the best position found by the swarm so far. The particle moves according to its velocity. The velocities are randomly generated toward pbest and gbest positions. For each particle k and dimension j, the velocity and position of particles can be updated by the following equations:

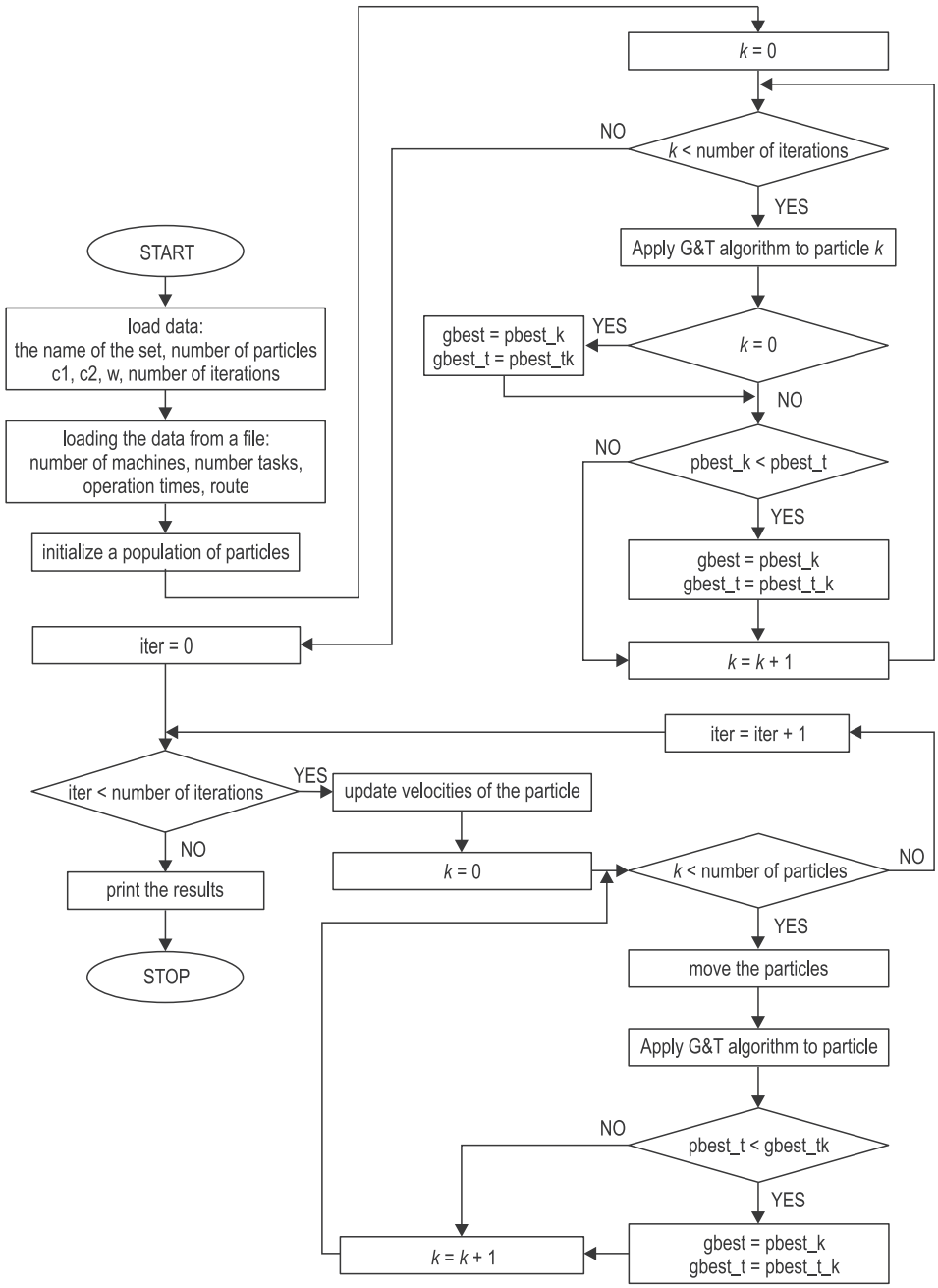

Fig. 1. The detailed flow chart of PSO algorithm to solve JSSP
Source: based on SHUA and HSU (2006).

$$V_{kj} \leftarrow w\, v_{kj} + c_1\, \mathrm{rand}_1\, (\mathrm{pbest}_{kj} - x_{kj}) + c_2\, \mathrm{rand}_2\, (\mathrm{gbest}_j - x_{kj}) \quad (1)$$

$$x_{kj} \leftarrow x_{kj} + v_{kj} \quad (2)$$

In Equations (1) and (2), v_{kj} is the velocity of particle k on dimension j, and x_{kj} is the position of particle k on dimension j. The pbest_{kj} is the pbest position of particle k on dimension j, and gbest_j is the gbest position of the swarm on dimension j. The inertia weight w is used to control exploration and exploitation. The particles maintain high velocities with a larger w, and low velocities with a smaller w. A larger w can prevent particles from becoming trapped in local optima, and a smaller w encourages particles exploiting the same search space area. The constants c_1 and c_2 are used to decide whether particles prefer moving toward a pbest position or gbest position. The rand_1 and rand_2 are random variables between 0 and 1. The process for PSO is as follows (SHUA, HSU 2006):

Step 1: Initialize a population of particles with random positions and velocities on d dimensions in the search space.

Step 2: Update the velocity of each particle, according to Equation (1).

Step 3: Update the position of each particle, according to Equation (2).

Step 4: Map the position of each particle into solution space and evaluate its fitness value according to the desired optimization fitness function. At the same time, update pbest and gbest position if necessary.

Step 5: Loop to step 2 until a criterion is met, usually a sufficiently good fitness or a maximum number of iterations.

Figure 1 shows the detailed flow chart of PSO algorithm to solve JSSP.

DABC Algorithm

The classical artificial bee colony (ABC) algorithm proposed by D. Karaboga (KARABOGA, BASTURK 2007) is a population algorithm often used for constrained optimization problems. As the basic ABC algorithm was originally designed for continuous function optimization, in order to make it applicable for solving the problem considered, a discrete version of the ABC algorithm (DABC). Composite mutation strategies are proposed to enable the DABC to explore the new search space and solve the permutation flow shop scheduling problem. We consider each discrete job permutation as a food source (FS) and apply discrete operations to generate a new neighborhood food source for different bees to make artificial bee colony algorithm suitable for JSP. Each FS is a permutation of operations. In order to generate good diversity neighboring solutions several mutation strategies are proposed to enable the DABC to solve the JSP. Initial population consists of schedule generated based on a random permutation of operations (priority rule). Whenever during employed or onlooker bee phase a new food source (schedule) is produced, for each bee new neighboring solutions are generated using proposed mutations strategies. Figure 2 shows the flow chart of DABC algorithm to solve JSSP.

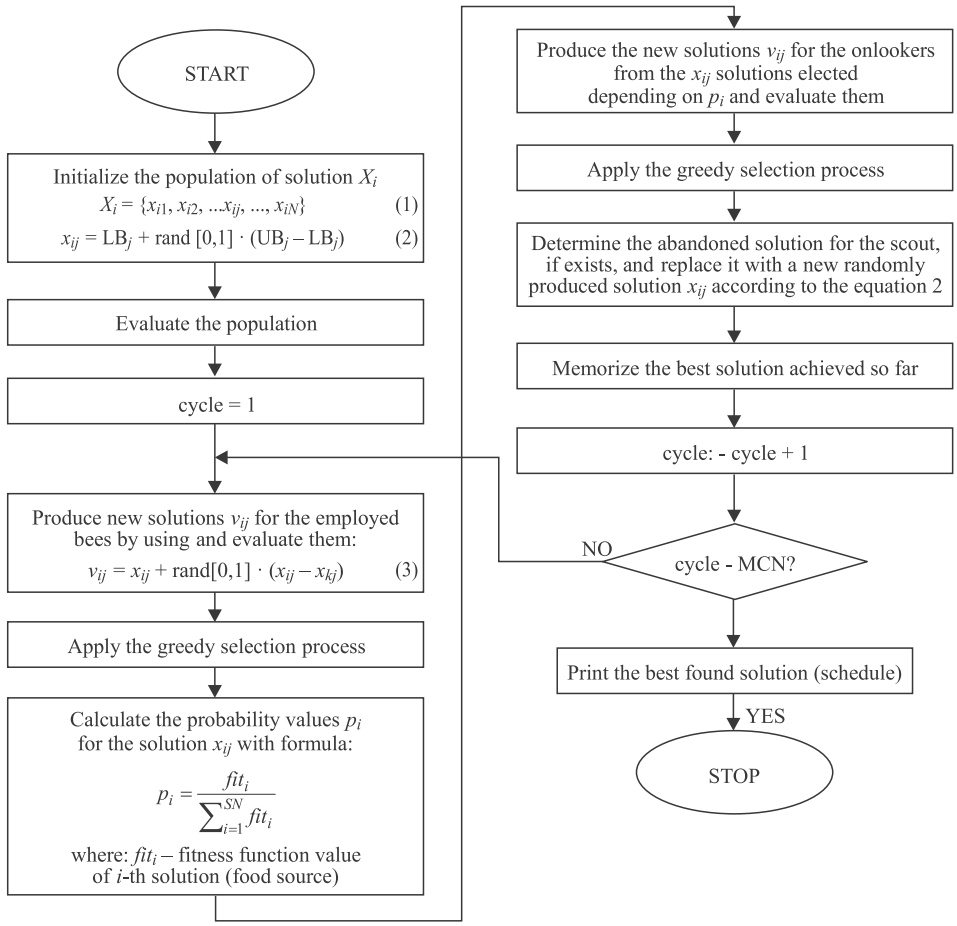

Fig. 2. The flow chart of DABC algorithm to solve JSSP
Source: based on KARABOGA and BASTRUK (2007).

Experiment Results

This section describes the computational experiments to evaluate the performance of the proposed algorithms. The experiments were performed on a PC with a processor Intel® Core™ i7-3770 CPU @ 3.40 GHz and RAM: 16 GB. The DABC algorithm was coded in Java and PSO in C++. We use 10 instances from three classes of standard JSSP test problems: instances FT06, FT10, FT20 (FISHER, THOMPSON 1963), instances La02, La19, La21, La27, La30, La40 (LAWRANCE 1984), and SWV11 instance (STORER et al. 1992).

A computational experiment with PSO for JSSP problems

The JSSP test problems are solved by PSO with the number of particles equaling 30, c_1=0.5, c_2=0.3, w=0.5, and 10, 100, 1,000 iterations (SHUA, HSU 2006). The proposed algorithm is tested on 10 job shop scheduling benchmark problems and the outcomes are presented in Table 1.

Table 1

Performance of PSO algorithm (C_{max} value)

Problem size	Performance of PSO (C_{max} value)			
	optimal makespan BKS	Avg (Best) C_{max} 10 iterations	Avg (Best) C_{max} 100 iterations	Avg (Best) C_{max} 1000 iterations
FT6	55	58.7 (57)	58.2 (57)	57.7 (57)
FT10	930	1,129 (1,075)	1,100 (1,075)	1,070 (1,055)
FT20	1,165	1,313 (1,281)	1,258 (1,215)	1,219 (1,170)
La02	655	743 (704)	707 (685)	668 (664)
La19	842	1,000 (973)	971 (948)	951 (922)
La21	1,046	1,334 (1,303)	1,294 (1,258)	1,266 (1,218)
La27	1,235	1,604 (1,523)	1,570 (1,539)	1,531 (1,490)
La30	1,355	1,648 (1,546)	1,637 (1,605)	1,586 (1,567)
La40	1,222	1,559 (1,538)	1,493 (1,469)	1,462 (1,401)
SWV11	2,983	3,763 (3,668)	3,690 (3,632)	3,651 (3,589)

As can be seen from Table 1, the best C_{max} values were obtained with more iterations. It is obvious that with the increase in the number of iterations we get better results of the criterion function, which, however, is associated with a greater amount of calculations. For example, for the SWV 11 problem, the average calculation time for 10 iterations is 2.01 seconds, while for 1000 iterations it increases to 176.15 seconds. Table 1 shows that the best solutions have been found for FT6, FT20 and La02 tasks. Thus, with the growth in the size of the problem, the efficiency of the algorithm worsens.

A computational experiment with DABC for JSSP problems

Due to several parameters and levels of DABC, full factorial experimental design requires high computational resources and is time consuming because of the large number of experimental runs for each replication. The DABC factors and its combinations (design points) in this work are summarized in Table 2. Those factors are the combination of the Source Number (SN), the Maximum Cycle Number (MCN), and Maximum Improvement Trial Number (MITN).

Table 2

Combinations of SN, MCN, and MINT values used with DABC for solve JSSP

Factor	Combinations (design points)				
	1	2	3	4	5
SN	50	200	500	1000	2000
MCN	1,000	4,000	10,000	20,000	40,000
MITN	200	400	600	800	1,000

We want to determine if the factors interact with one another, i.e., whether the effect of one factor in the response depends on the levels of the others. A number of program start-ups were made for various combinations of factor values, each time changing only one of them. For each combination the program was started five times. Results are presented in Figures 3*a* to 3*c*.

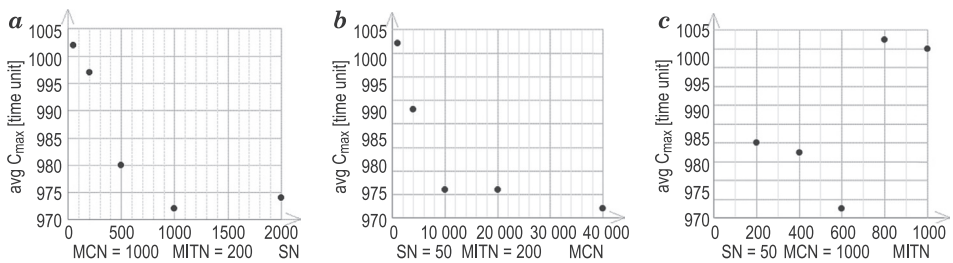

Fig. 3. Influence: *a* – source number (SN), *b* – the maximum cycle number (MCN), and *c* – maximum improvement trial number (MINT) on C_{max} value

Figure 3*a* shows that an increase in the population number (number of food sources – SN) results in achieving a better C_{max} value. With SN =1000, the value reached the lowest average C_{max} value, and no progressive decrease was observed for the average of C_{max} with SN = 2,000 value. Figure 3*b* shows that increasing the maximum cycle number (MCN) results in obtaining a better C_{max} value, and the spread of results decreases with an increase in the population number. We can see an improvement of C_{max} value compared to the previous test point, which is a result of an increase in the MCN value. With MCN = 10,000, the value improvement effect is lower than for previous test points. Figure 3*c* shows that the best C_{max} value was achieved with MITN equaling 60% of MCN value, when the average C_{max} was the lowest.

Figure 4*a* to 4*b* show an influence of other combinations (SN, MCN, and MINT values) on the average and best C_{max} value.

When analyzing Figure 4*a*, we can see that increasing the maximum cycle number (MCN) gives better results (lower C_{max} value) than increasing the source number (SN). For example, for the third test point (optimal C_{max} value

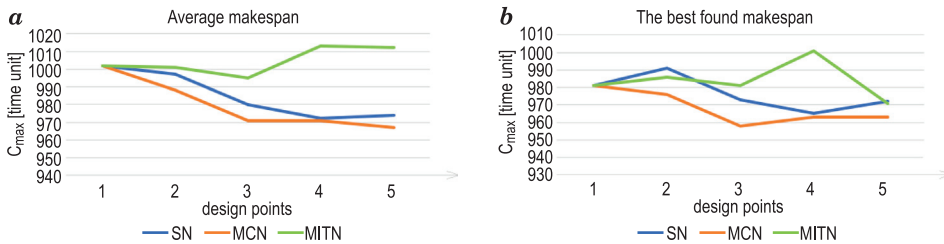

Fig. 4. Influence of other combinations (SN, MCN, and MITN values) on a – the average makespan and b – best makespan (C_{max} value)

for FT10 equals 930), a tenfold increase of the MCN value produced a result better by 9 time units (from 980 to 971), which is an almost 1% improvement compared to the optimal value.

In the experiment, the values of control parameters were adjusted for each problem according with formulas give in (KARABOGA, BASTURK 2007), but "number of operations" is used instead of fixed value "10": SN = $5 \cdot n$; MCN = $n \cdot m \cdot o$; and MITN = $2 \cdot n \cdot m$; where: n – number of jobs, m – number of machines, o – number of operations for a job. The proposed algorithm has been tested on 10 job shop scheduling benchmark problems (with 10 iterations) and the outcomes are presented in Table 3.

Table 3

Performance of DABC algorithm (C_{max} value)

Problem size	Performance of DABC algorithm (C_{max} value)			
	optimal makespan BKS	average found makespan	optimal makespan for DABC	RPI [%]
FT6	55	55	55	0.0
FT10	930	1,005	967	8.0
FT20	1,165	1,275	1,216	10.0
La02	655	676	655	3.0
La19	842	885	863	5.0
La21	1,046	1,152	1,102	10.0
La27	1,235	1,402	1,318	14.0
La30	1,355	1,461	1,404	9.0
La40	1,222	1,367	1,345	12.0
SWV11	2,983	3,944	3,844	32.0

Results comparison for JSSP test problems

KLOUD and KOBLASA (2011) compare SPT, FIFO, and GA taking into account C_{max} values and computational time. Only C_{max} values are compared in this work because of hardware differences. The comparison results are given in Table 4 (C_{max} and RPI values) for GA (KLOUD, KOBLASA 2011), PSO (GRACZYK 2017), DABC (WITKOWSKI et al. 2016), and Teaching-learning-based optimization (WITKOWSKI et al. 2016).

Table 4

C_{max} and RPI values for other algorithms

Problem size	Algorithms					
	GA	PSO	DABC	TLBO	HPSO	DPSO
FT6	57(4.0)	57 (4.0)	55 (0.0)	55 (0.0)	–	–
FT10	974 (5.0)	1,055 (13)	967 (4.0)	980 (5.0)	930 (0.0)	938 (0.8)
FT20	1,198 (3.0)	1,170 (0.5)	1,216 (4.0)	1,225 (5.0)	–	–
La02	668 (2.0)	664 (1.0)	655 (0.0)	686 (5.0)	655 (0.0)	655 (0.0)
La19	876 (4.0)	922 (9.0)	863 (2.0)	894 (6.0)	842 (0.0)	842 (0.0)
La21	1,098 (5.0)	1,218 (16)	1,102 (5.0)	1,145 (9.0)	1,078 (2.0)	1,047 (0.1)
La27	1,350 (9.0)	1,490 (20)	1,318 (7.0)	1,373 (11)	1,257 (3.0)	1,236 (0.1)
La30	1,362 (1.0)	1,567 (15)	1,404 (4.0)	1,411 (4.0)	–	1,355 (0.0)
La40	1,289 (5.0)	1,401(14)	1,345 (10)	1,326 (9.0)	1,224 (0.1)	1,229 (0.6)
SWV11	3,330 (12.0)	3,589 (20)	3,844 (29)	3,472 (16)	–	–

For each algorithm, we use formula RD = 100 (MFM-BKS)/BKS for each instance to calculate the relative deviation RD, where MFM means the minimum C_{max} found and BKS means the best known solution. We use ARD to denote the average value of relative deviations for all the analyzed instances.

For small problems FT06, FT10, FT20 and La02, almost all the algorithms can find good solutions. DABC algorithm shows better C_{max} values than TLBO for GA and PSO with FT10, La02, La19 and La27 problems. PSO algorithm shows better C_{max} values than DABC only for FT20 and SWV11 problems. TLBO algorithm shows better C_{max} values than DABC and PSO and worse than GA for La 40 and SWV11 problems, and GA works very well for solving La30, La40 and SWV11 problems.

Contemporary research on the use of PSO and ABC for solving JSSP problems includes various types of hybrid algorithms resulting from the combination of PSO and ABC with other algorithms. Examples of such applications are SONG (2008) and RAMESHKUMAR and RAJENDRAN (2018), which were used to compare the efficiency of the algorithms. SONG (2008) proposes an idea of a hybrid optimization algorithm HPSO. In order to prevent the algorithm falling

in a local optimization too early, Taboo Search is adopted to realize local parallel search, simultaneously improving the local search ability. In RAMESHKUMAR, RAJENDRAN (2018) the bench-mark JSSP problems are solved by discrete version of the PSO algorithm. DPSO algorithm show the best-known solutions to 3 out of 7 problems (La02, La19 and La30) in this work (Tab. 4). Figure 5 present C_{max} values for job shop scheduling test problems.

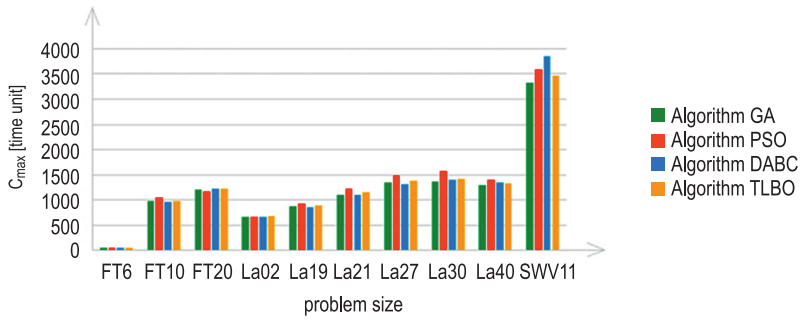

Fig. 5. $C_{max.}$ values for job shop scheduling test problems

A computational experiment with PSO, DABC and other algorithms for a real system

For a real production system the input data include: the matrix of groups of technologically interchangeable machines, the matrix of technological routes, the matrix of operations with an accuracy of group of technologically interchangeable machines, the matrix of processing times t_{ij} i-th of an operation, the matrix of processing times of a setup of machines before proceeding the j-th operation and i-th part. The data set contains 10 parts which need to be processed by 27 machines and 160 operations. The objective is to minimize C_{max} value for the FJSSP problem with a serial type production flow. In a serial production flow an entire batch of parts is processed on one machine and only when all of the parts in the batch have been processed are they sent to the next machine. Table 4 present a comparison of the results (C_{max} value) achieved by the different algorithms under discussion in the two versions of the problem, i.e., the serial flow and the serial-parallel flow (only the GA algorithm). For the real job shop problem with a serial-parallel route, it is not possible to compute C_{max} value analytically.

Analyzing the effectiveness of algorithms is a difficult task. For example, in Table 5 we can see that for the FJSSP problem with serial production flow ANN (WITKOWSKI et al. 2007), PSO (GRACZYK 2017), TLBO and DABC (WITKOWSKI et al. 2016) algorithms give better C_{max} values than the genetic algorithm

(WITKOWSKI 2016). But the GA algorithms were not as thoroughly tested as was the case with PSO, DABC and TLBO. There are specific values for mutation and crossover probability as well as many different types of mutation operators, crossover operators and type of selections for which we can obtain best experiment results. The following are applied in GA: population number = 1,000, generation number = 50, single swap mutation, order-based crossover and roulette wheel selection.

Table 5

C_{max} values for real scheduling problem

Production flow	Algorithms				
	GA	ANN	PSO	DABC	Optimal C_{max} value
Serial flow	57,636.0	50,242.2*	50,242.2*	50,242.2*	50,242.2
Serial-parallel flow	32,084.0	–	–	–	?

Conclusions

This work examined the JSSP problems with the objective of minimizing makespan. Computational results for JSSP problems were compared with some algorithms such as: GA, TLBO (non-hybrid algorithms) and HPSO, DPSO (hybrid algorithms). According to the theorem of No Free Lunch, no intelligent optimization algorithm is better than other intelligent algorithms. That is, every algorithm has its corresponding application circumstances. For small problems (FT6-La21) almost all the algorithms can find good solutions for JSSP problems. For relatively large problems (La30-SWV11), the results of the proposed algorithms DABC and PSO are worse than GA. The computational experiment shows that results given by the DABC and PSO for real job shop scheduling problem generated optimal C_{max} values. In future, we can expect more research to be done on the serial-parallel production flow, where individual items in a batch are sent to the machines as soon as they have been processed on the previous machine.

References

ABU-SRHALM A., AL-HASAN M. 2015. *Hybrid Algorithm using Genetic Algorithm and Cuckoo Search Algorithm for Job Shop Scheduling Problem*. International Journal of Computer Science Issues, 12(2): 288-292.

ADAMS J., BALAS E., ZAWACK D. 1988. *The shifting bottleneck procedure for job shop scheduling*. Management Science, 34(3): 391–401.

Błażewicz J., Ecker K., Pesch E., Schmidt G., Węglarz J. 2007. *Handbook on Scheduling; From Theory to Application*. Springer, Berlin, Heidelberg, New York.

Fisher H., Thompson G. 1963. *Probabilistic Learning combinations of local job shop scheduling rules*. Englewood Cliffs, New York, Prentice-Hall.

Graczyk P. 2017. *Particle swarm optimization for job shop scheduling* (*master thesis*). Warsaw University of Technology, Warsaw.

Krause, J., Cordeiro, J., Parpinelli, R.S., Lopes H.S. 2013. *A Survey of Swarm Algorithms Applied to Discrete Optimization Problems*. In: *Swarm Intelligence and Bio-Inspired Computation*. Eds. X.-S. Yang, Z. Cui, R. Xiao, A.H. Gandomi, M. Karamanoglu. Elsevier Inc., p. 169-191

Karaboga D., Basturk B. 2007. *Artificial Bee Colony (ABC) Optimization Algorithm for Solving Constrained Optimization Problems*. In: *Lecture Notes in Artificial Intelligence*. Eds. P. Melin, O. Castillo, L.T. Aguilar, W. Pedrycz. Springer-Verlag, Berlin, Heidelberg, p. 789–798.

Kloud T., Koblasa F. 2011. *Solving job shop scheduling with the computer simulation*. The International Journal of Transport & Logistics, 3: 7-17.

Lawrence S. 1984. *Resource constrained project scheduling, An experimental investigation of heuristic scheduling techniques*. Technical Report, GSIA, Carnegie Mellon University.

Mesghouni K., Hammadi S., Borne P. 2004. *Evolutionary Algorithms for Job Shop Scheduling*. International Journal of Applied Mathematics and Computer Science, 14(1): 91–103.

Rameshkumar K., Rajendran C. 2018. *A novel discrete PSO algorithm for solving job shop scheduling problem to minimize makespan*. IOP Conference Series: Materials Science and Engineering, 310: 10.

Shua D.Y., Hsu Ch.Y. 2006. *A hybrid particle swarm optimization for job shop scheduling problems*. Computers & Industrial Engineering, 51: 791-808.

Song X., Yang C., Qiu-Hong M. 2008. *Study on particle swarm algorithm for Job Shop Scheduling Problems*. Systems Engineering and Electronics, 30(12): 2398-2401.

Storer R., Wu D., Vaccari R. 1992, *New Search Spaces for Sequencing Problems with Application to Job Shop Scheduling*. Management Science, 38: 1495-1509.

Surekha P., Sumathi S. 2010. *PSO and ACO based approach for solving combinatorial Fuzzy Job Shop Scheduling*. International Journal of Computer Technology and Applications, 2(1): 112-120.

Witkowski T., Strojny G., Antczak P. 2007. *The Application of Neural Networks for Flexible Job Shop Problem*. International Journal of Factory Automation, Robotics and Soft Computing, 2: 116-121.

Witkowski T., Antczak A., Antczak P. 2010. *Comparison of Optimality and Robustness between SA, TS and GRASP Metaheuristics in FJSP Problem*. Lecture Notes in Computer Science, 6215: 319-328.

Witkowski T. 2016. *Scheduling Algorithms for Flexible Job Shop Scheduling*. Wydawnictwo Naukowe PWN, Warszawa.

Witkowski T., Krzyżanowski P., Vasylishyna S. 2016. *Comparison of DABC and TLBO Metaheuristics for Solve Job Shop Scheduling Problem*. 12th International Conference on Natural Computation, Fuzzy Systems and Knowledge Discovery, Changsha, China (poster).

Technical Sciences, 2019, 22(1), 75–86

UNIWERSYTET WARMIŃSKO-MAZURSKI W OLSZTYNIE

Quarterly peer-reviewed scientific journal
ISSN 1505-4675
e-ISSN 2083-4527
TECHNICAL SCIENCES
Homepage: www.uwm.edu.pl/techsci/

THE EFFECT OF THE EXCESS SLUDGE PRETREATMENT ON BIOGAS PRODUCTIVITY

Katarzyna Bernat, Magdalena Zielińska, Dorota Kulikowska, Agnieszka Cydzik-Kwiatkowska, Irena Wojnowska-Baryła, Beata Waszczyłko-Miłkowska, Beata Piotrowicz

Department of Environmental Biotechnology
Faculty of Environmental Sciences
University of Warmia and Mazury

Received 12 January 2018, accepted 4 February 2019, available online 11 February 2019.

Key words: biogas production, sludge pretreatment, activated sludge, aerobic granular sludge, ultrasound disintegration, homogenization.

Abstract

To intensify biogas production during anaerobic stabilization of organic matter in sludge, pretreatment is applied. The effect of pretreatment of excess activated sludge (AS) and excess aerobic granular sludge (GS) on biogas productivity (BP) and composition was investigated. The sludge was pretreated with homogenization (6,500 rpm for 0.5 min ($H_{0.5}$) and 1 min ($H_{1.0}$)) or ultrasound disintegration at 20 kHz (50% amplitude for 2 min ($D_{50\%\_2.0}$) and 4 min ($D_{50\%\_4.0}$), and 100% amplitude for 4 min ($D_{100\%\_4.0}$)). BP of AS of GS without pretreatment was 603.3±5 dm^3/kg TS (793.4±7 dm^3/kg VS); that was 200.6±4 dm^3/kg TS (480.8±6 dm^3/kg VS). With disintegration, the BP of AS increased by 7.8% (650.4±10 dm^3/kg TS) ($D_{50\%\_2.0}$) and 16.1% (700.6±11 dm^3/kg TS) ($D_{100\%\_4.0}$), and that of GS increased by 7.0% (214.0±5 dm^3/kg TS) ($D_{50\%\_2.0}$) and 16.0% (232.8±5 dm^3/kg TS) ($D_{100\%\_4.0}$). With homogenization, BP increased by 2.0-3.0% (AS) and 1.6-3.2% (GS).

Correspondence: Katarzyna Bernat, Katedra Biotechnologii w Ochronie Środowiska, Wydział Nauk o Środowisku, Uniwersytet Warmińsko-Mazurski, ul. Słoneczna 45G, 10-907 Olsztyn, phone: 89 523 41 18, e-mail: bernat@uwm.edu.pl

Introduction

Currently, the majority of wastewater treatment plants are operated with activated sludge, which is in the form of flocs. Recent studies that aimed to improve the process of wastewater treatment by modifying the activated sludge have led to development of aerobic granular sludge technology. Aerobic granular sludge, regarded as one of the most promising biotechnologies for municipal wastewater treatment plants, is a specific type of self-immobilized biomass. Granules are densely packed with heterotrophic and autotrophic microorganisms. They have layers with different substrate and aerobic conditions in their structure, providing a broad range of metabolic processes that can occur simultaneously (Liu, Tay 2004). Such a granule structure allows higher resistance to load fluctuations and makes it possible to abandon multi-chamber reactors and secondary settlers, and allows lower energy consumption (Sławiński 2016). Granules have better settling properties than activated sludge; their sludge volumetric index is about 50 cm^3/g MLSS. Granules can be cultured at loadings ranging from 2.5 to 15.0 kg COD/(m^3·d) (Cydzik-Kwiatkowska, Zielińska 2011).

Other differences between aerobic granules and activated sludge include the much longer sludge age of granules (Beun et al. 1999) in comparison with activated sludge (Cydzik-Kwiatkowska et al. 2012) that results in smaller contribution of organic matter to the dry matter content of biomass. In addition, the operational conditions in reactors with granular biomass cause larger amounts of extracellular polymeric substances (EPS) to be produced by granules than by activated sludge (Rusanowska et al. 2019). These properties could make the granules more difficult to degrade than activated sludge.

Biological aerobic and anaerobic (methane fermentation) stabilization are most often conducted methods of sewage sludge stabilization. In the case of methane fermentation, a measurable effect of the process is the biogas yield. To intensify biogas production, a pretreatment step is used. Proper selection of pretreatment methods has an important effect on the efficiency of fermentation and thus on the composition of the biogas. In general, methods of sludge pretreatment can be classified as mechanical and non-mechanical. Mechanical treatment causes grinding or shearing of the solid particles in substrates, resulting in the release of cellular compounds and enlarging the specific surface area of the substrate (Carrere et al. 2010). The mechanical methods use shear forces or pressure changes, e.g., a mechanical or pressure homogenizer. Non-mechanical treatment can be divided into physical, chemical, biological and mixed methods. Physical methods include, for example, disintegration with ultrasound, thermal treatment using both high (greater than 110°C) and low (lower than 110°C) temperatures or treatment with detergents (Ariunbaatar et al. 2014). Thermal treatment is one of the most studied methods and it is used on an industrial scale. Appropriately high temperatures eliminate pathogens, improve dewatering ability

and reduce digestate viscosity (VAL DEL RIO et al. 2011). Chemical methods are based on the usage of alkaline solutions, acids or preliminary oxidation (e.g. ozone treatment). They are used to improve the rate of hydrolysis (WANG et al. 2011). Biological methods include the use of single enzymes or their mixtures. Mixed methods include, among others, thermo-chemical treatment, thermo-mechanical treatment or steam explosion with the use of pressure (MONTGOMERY, BOCHMANN 2014). Pretreatment releases organic compounds from microbial cells, thereby increasing the concentration of dissolved organic compounds that are accessible to microorganisms.

Although many studies have investigated the biogas productivity of activated sludge and pretreatment methods for improving this productivity, little research has been done on the biogas productivity of aerobic granular sludge. Therefore, the present study compared the biogas productivity of activated sludge (AS) and aerobic granules (GS). In addition, the effect of pretreatment methods (homogenization or ultrasound disintegration) on the productivity and composition of the biogas produced with both kinds of excess sludge was investigated.

Materials and Methods

Substrates used in the experiment

Two kinds of sludges were used in the study: excess activated sludge (AS), and excess aerobic granular sludge (GS). AS was taken from a mechanical-biological municipal wastewater treatment plant (WWTP) with a maximum capacity of 60,000 m^3/d (north-east of Poland). GS was taken from a laboratory reactor (GSBR) fed with municipal wastewater and operated at the Department of Environmental Biotechnology, UWM in Olsztyn (CYDZIK-KWIATKOWSKA et al. 2017). Characteristics of the sludges are given in Table 1.

Table 1

Characteristics of AS, GS and the inoculum

Indicator		AS	GS	Inoculum
Total solids	%	2.24	8.72	1.52
Moisture	%	97.74	91.28	98.48
Volatile solids	%	1.70	3.64	1.05
	% TS	76.04	41.73	69.11
Ash	%	0.54	5.08	0.47
	% TS	23.96	58.27	30.89

Sludge pretreatment

Homogenization and ultrasound disintegration were used as sludge pretreatment methods. Homogenization was carried out with a T 25 basic ULTRA-TURRAX®, IKA® at 6,500 rpm and at a time of 0.5 min ($H_{0.5}$) and 1 min ($H_{1.0}$). Ultrasound disintegration (20 kHz) was carried out with a Sonics Vibra Cell® at 50% amplitude for 2 min ($D_{50\%\_2.0}$) and 4 min ($D_{50\%\_4.0}$), and 100% amplitude for 4 min ($D_{100\%\_4.0}$).

Experimental design (GP_{21})

To analyze the biogas potential with GP_{21} respirometric test, the following samples of the excess sludges (AS, GS) were prepared:

– AS and GS without pretreatment;

– AS and GS after homogenization at $H_{0.5}$ and $H_{1.0}$;

– AS and GS after ultrasound disintegration ($D_{50\%\_2.0}$, $D_{50\%\_4.0}$ and $D_{100\%\_4.0}$).

The biogas production potential of the sludge was determined during 21 days in triplicate (for each sludge sample) in batch assays in glass bottles (OxiTop® Control AN6/AN12), according to HEERENKLANGE and STEGMANN (2005). 100 g of the inoculum was added to each OxiTop bottle along with a sludge sample. As the inoculum, fermented sludge from the closed mesophilic fermentation chambers in above-mentioned WWTP was used (Tab. 1).

To assure a starting load of ca. 5 g VS/dm^3 (kg VS/m^3), the doses of each sewage sample were calculated, taking into account their contents of total solids and volatile solids. This dosage allowed for complete organic matter biodegradation.

Three bottles with the inoculum were incubated under the same conditions to determine its biogas potential. Finally, the biogas production of the inoculum alone was subtracted from the total production of the sludge and inoculum combined. Before starting measurements, each bottle was flushed with N_2 and the lateral connections of the bottles were sealed with rubber stoppers. The contents of the bottles were manually mixed. Each bottle possessed its own head that measured and recorded pressure changes in the bottle during 21 days of fermentation at 36±1°C in a thermostatic incubator. The pressure changes were caused by formation of biogas during fermentation, and were used to calculate the volume of biogas that was produced based on the ideal gas law.

Analytical methods and calculations

The analysis of TS and VS in sludge samples were measured according to APHA (1992). The percentage of CH_4 and CO_2 in the biogas was measured in the head space of the OxiTop bottles using a GA200+ automatic analyzer (Geotechnical Instruments). Biogas production can be assumed to follow pseudo first-order kinetics and can be described with this equation 1.:

$$C_{t;\text{biogas}} = C_{0;\text{biogas}} \cdot \left(1 - e^{k_{\text{biogas}} \cdot t}\right) \quad (1)$$

where:

$C_{t;\text{biogas}}$ [dm^3/kg TS; dm^3/kg VS] – is the cumulative biogas yield at digestion time t (days),

$C_{0;\text{biogas}}$ [dm^3/kg TS; dm^3/kg VS] – is the maximal biogas yield,

k_{biogas} [d^{-1}] – is the kinetic coefficient of biogas production.

The values of $C_{0;\text{biogas}}$, and k_{biogas} were obtained by non-linear regression analysis with Statistica software, version 10.0 (StatSoft). To determine the fit of the model to the data, the coefficient of determination was calculated (R^2).

Differences between samples were tested for significance by using t test, $p < 0.05$ was considered significant.

Results and Discussion

Figure 1 shows changes in biogas productivity from the sludges without pretreatment during 21-day anaerobic respirometric tests. It was shown that biogas production was explained well by a first-order kinetic model (a high degree of fit between the experimental data and the model; R^2 was 0.97-0.99). The biogas production from AS was much higher (statistically significant, $p<0.05$) (603.3±5 dm^3/kg TS; 793.4±7 dm^3/kg VS) than from GS (200.6±4 dm^3/kg TS;

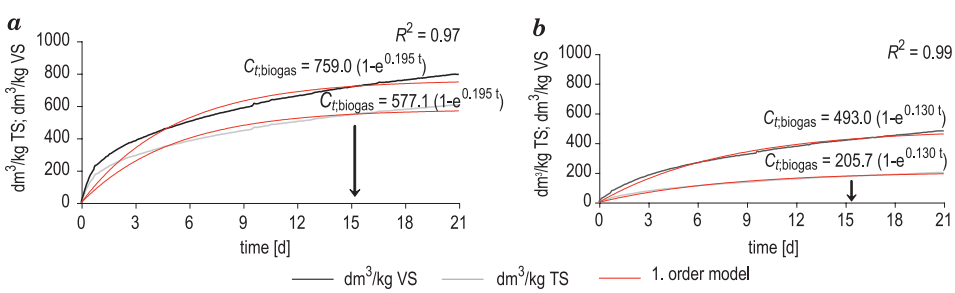

Fig. 1. Biogas productivity of AS (*a*) and GS (*b*) without pretreatment; the arrow shows the time after which 90% of the total amount of biogas was produced

480.8±6 dm^3/kg VS). About 90% of the total biogas production was achieved by the 15-16 day of the measurement. After this time, only a small amount of biogas was produced.

Sewage sludge generated during wastewater treatment with activated sludge is characterized by a high content of organic matter of about 70-80% of TS. Organic matter content in the excess activated sludge used in the present study was ca. 76%, and that of the excess granular sludge was ca. 42%. It is assumed that if the organic substrate has a higher content of organic matter (measured as VS in TS) and a greater biodegradability, it can result in higher biogas production. However, not only the content of organic matter but also its composition (e.g. carbohydrate, lipids, protein or fibre content) affects the effectiveness of anaerobic degradation. BERNAT et al. (2017) compared biogas potential of excess activated sludge (VS/TS ratio of ca. 0.76) and aerobic granular sludge (VS/TS ratio of ca. 0.65). The biogas productivity obtained by the authors were 320-410 dm^3/kg TS (ca. 550 dm^3/kg VS) with the excess granular sludge and ca. 830 dm^3/kg TS (1200 dm^3/kg VS) with the excess activated sludge. VAL DEL RIO et al. (2011, 2013) showed that aerobic granular sludge from a pilot plant with SBR fed with the liquid fraction of pig slurry had biogas productivity of 208±51 dm^3 CH_4/kg VS (ca. 350 dm^3 of biogas/kg VS, with the assumption of 60% of methane content). This biogas productivity with granular sludge was lower than that obtained by BERNAT et al. (2017) and that from the present study.

The composition and characteristics of granular sludge differed from those of activated sludge. BERNAT et al. (2017) found high content of lignocellulosic substances (hard-to-biodegrade lignin comprised ca. 54% of fibrous materials) in GS that may have influenced the potential of biogas production. Detailed characteristics of organic matter in the excess sludge used in the present study was not performed, but it could be assumed that the differences in biogas productivity of AS and GS resulted form different composition of organic matter.

In the next step of the experiment, both kinds of sludge were pretreated with homogenization or ultrasound disintegration before measurements of biogas productivity. Changes in the biogas productivity from the sludges after homogenization during 21-day anaerobic respirometric tests are shown in Figure 2. Biogas productivity with AS after 0.5 min of homogenization was 612.9±5 dm^3/kg TS (806.1±7 dm^3/kg VS), and remained on the similar lever of 617.7±7 dm^3/kg TS (812.3±8 dm^3/kg VS) after 1 min of this pretreatment. In comparison to non-pretreated AS, biogas productivity increased by 1.6% and 2.4% (but statistically insignificant, $p > 0.05$), respectively at $H_{0.5}$ and $H_{1.0}$. Biogas productivity with GS was 205.2±5 dm^3/kg TS (491.7±7 dm^3/kg VS) at $H_{0.5}$, and 207.1±5 dm^3/kg TS (496.2±7 dm^3/kg VS) at $H_{1.0}$. These results were comparable to biogas productivity of GS without pretreatment; an increase of only 2-3% was observed (statistically insignificant, $p > 0.05$).

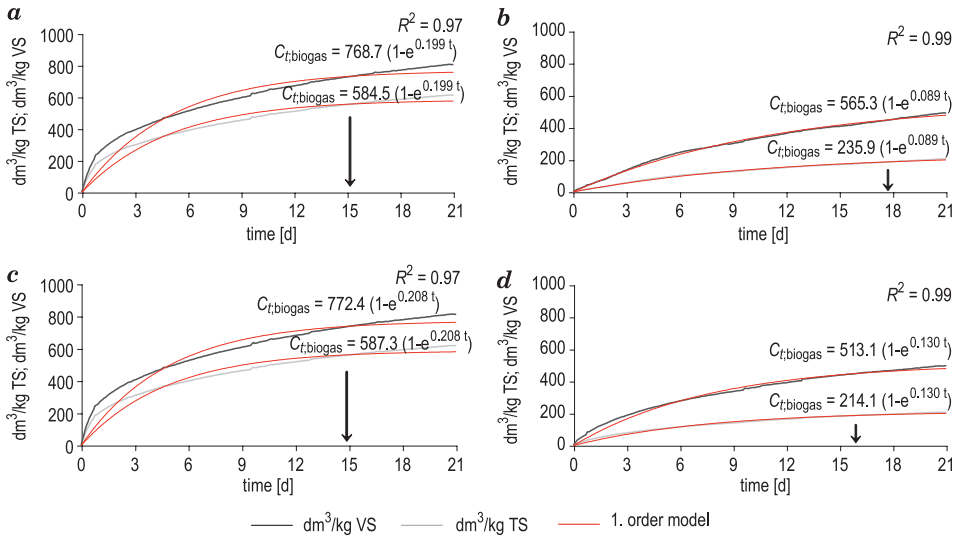

Fig. 2. Biogas productivity of the sludge after homogenization; the arrow shows the time after which 90% of the total amount of biogas was produced: *a* – AS_$H_{0.5}$, *b* – GS_$H_{0,5}$, *c* – AS_$H_{1.0}$, *d* – GS–$H_{1.0}$

After pretreatment with $D_{50\%\_2.0}$, the biogas productivity with AS was 650.4±10 dm^3/kg TS (855.4±12 dm^3/kg VS), and with $D_{50\%\_4.0}$ this productivity increased to 673.1±10 dm^3/kg TS (885.1±12 dm^3/kg VS). With $D_{100\%\_4.0}$, the biogas productivity was the highest – 700.6±11 dm^3/kg TS (921.3±13 dm^3/kg VS). In comparison to AS without pretreatment, there was statistically significant ($p < 0.05$) increase in biogas productivity by 7.8% ($D_{50\%\_2.0}$), 11.6% ($D_{50\%\_4.0}$) and 16.1% ($D_{100\%\_4.0}$). Similar percentage increases (statistically significant ($p < 0.05$) increase in comparison to GS without pretreatment) were obtained when GS was used as a substrate for measurement of biogas productivity, however, the values of biogas productivity were much lower than with AS (214.0±5 dm^3/kg TS; 512.9±7 dm^3/kg VS with $D_{50\%\_2.0}$; 228.2±5 dm^3/kg TS; 546.9±7 dm^3/kg VS with $D_{50\%\_4.0}$ and 232.8±5 dm^3/kg TS; 558.0±7 dm^3/kg VS with $D_{100\%\_4.0}$) (Fig. 3).

Kinetic parameters of the biogas production with both kinds of sludge without pretreatment and after two pretreatment methods are summarized in Table 2 and 3. Kinetic coefficients of biogas production (k_{biogas}) that describe biogas productivity and were determined on the basis of first-model equation were 0.195 d^{-1} and 0.130 d^{-1} for AS and GS, respectively. The rate of biogas productivity (r_{biogas}) with AS was 112.5 dm^3/(kg TS·d) (148.0 dm^3/(kg VS·d)), whereas with GS, r_{biogas} was almost an order of magnitude lower – 26.7 dm^3/(kg TS·d) (64.1 dm^3/(kg VS·d)). In the case of both sludges, homogenization affected neither k_{biogas} nor the methane content in the biogas that was on a similar level as in the case of non-pretreated sludge. Ultrasound disintegration increased

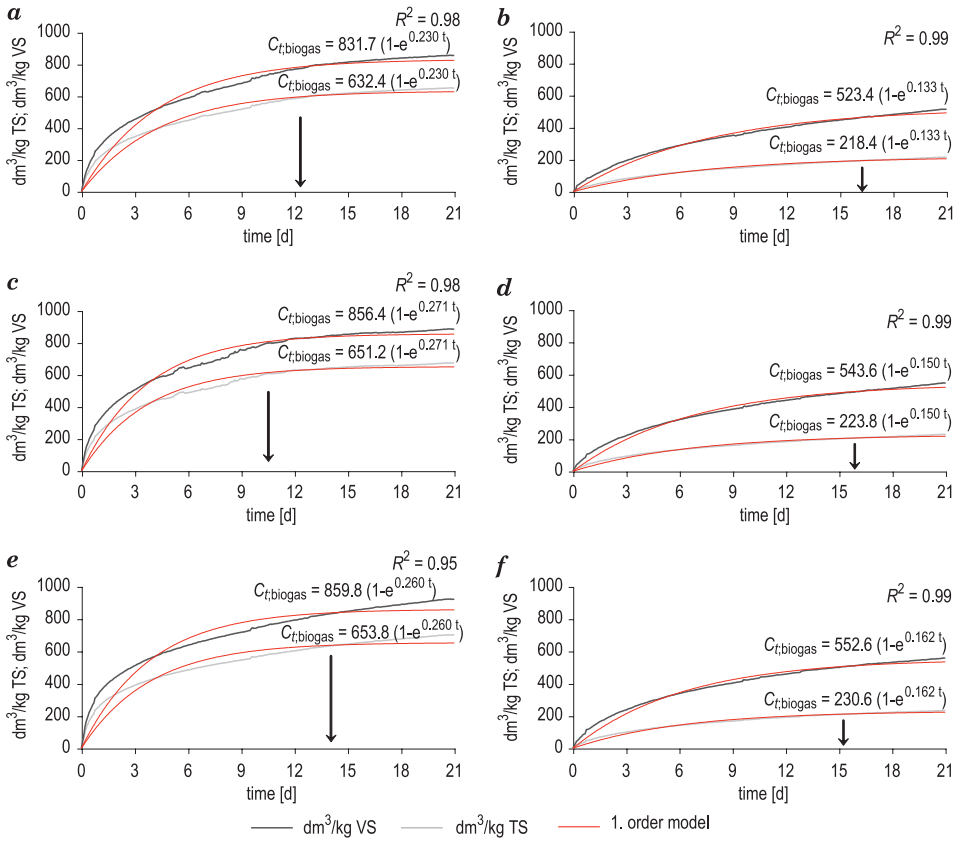

Fig. 3. Biogas productivity of the sludge after disintegration; the arrow shows the time after which 90% of the total amount of biogas was produced: *a* – AS_D$_{50\%_2.0}$, *b* – GS_D$_{50\%_2.0}$, *c* – AS_D$_{50\%_4.0}$, *d* – GS_D$_{50\%_4.0}$, *e* – AS_D$_{100\%_4.0}$, *f* – GS_D$_{100\%_4.0}$

kinetic parameters of the biogas production and methane content more than homogenization. When AS was pretreated by disintegration, k_{biogas} increased in comparison to AS without pretreatment from 0.195 d^{-1} (AS) to 0.230 d^{-1} and to 0.271 d^{-1} (AS after disintegration). Methane content in the biogas also increased and was 64.4% with D$_{50\%_2.0}$, 65.4% with D$_{50\%_4.0}$ and 66.6% with D$_{100\%_4.0}$.

Disintegration of GS caused that k_{biogas} increased in comparison to GS without pretreatment (0.130 d^{-1}), only with D$_{50\%_4.0}$ (0.153 d^{-1}), and with D$_{100\%_4.0}$ (0.162 d^{-1}). Methane content in the biogas increased to ca. 62%.

Many studies have investigated the biogas productivity of activated sludge and the effect of pretreatment step on improving this productivity. For example, BOUGRIER et al. (2007) reported that biogas production of activated sludge was ca. 425 dm^3/kg VS which was lower than the values presented by TCHOBANOGLOUS et al. (2003) (500-750 dm^3/kg VS) and obtained in the study of BERNAT

Table 2

Kinetic parameters of biogas production from AS

Excess activated sludge		*WP	$H_{0.5}$	$H_{1.0}$	$D_{50\%\_2.0}$	$D_{50\%\_4.0}$	$D_{100\%\_4}$
Maximal biogas productivity (experimental data)	dm^3/kg TS	603.3±5	612.9±5	617.7±7	650.4±10	673.1±10	700.6±11
	dm^3/kg VS	793.4±7	806.1±7	812.3±8	855.4±12	885.1±12	921.3±13
$C_{t;\text{biogas}}$	dm^3/kg TS	577.1	584.5	587.3	632.4	651.2	653.8
	dm^3/kg VS	759.0	768.3	772.4	831.7	856.4	859.8
r_{biogas}	dm^3/(kg TS·d)	112.5	116.3	122.2	145.5	176.5	170.0
	dm^3/(kg TS·d)	148.0	152.9	160.7	191.3	232.1	223.5
k_{biogas}	d^{-1}	0.195	0.199	0.208	0.230	0.271	0.260
Increase in the biogas productivity**	%	–	1.6	2.4	7.8	11.6	16.1
Methane content	%	62.3±0.5	61.4±0.5	62.4±0.5	64.4±0.5	65.4±0.5	66.6±0.5

* without pretreatment
** comparing to the value without pretreatment

Table 3

Kinetic parameters of biogas production from GS

Excess granular sludge		* WP	$H_{0.5}$	$H_{1.0}$	$D_{50\%\_2.0}$	$D_{50\%\_4.0}$	$D_{100\%\_4}$
Maximal biogas productivity (experimental data)	dm^3/kg TS	200.6±4	205.2±5	207.1±5	214.0±5	228.2±5	232.8±5
	dm^3/kg VS	480.8±6	491.7±7	496.2±7	512.9±7	546.9±7	558.0±7
$C_{t;\text{biogas}}$	dm^3/kg TS	205.7	235.9	214.1	218.4	226.8	230.6
	dm^3/kg VS	493.0	565.3	513.1	523.4	543.6	552.6
r_{biogas}	dm^3/(kg TS·d)	26.7	21,0	27.8	29.0	34.0	37.4
	dm^3/(kg TS·d)	64.1	50.3	66.7	69.6	81.5	89.5
k_{biogas}	d^{-1}	0.130	0.089	0.130	0.133	0.150	0.162
Increase in biogas productivity**	%	–	2.2	3.2	6.7	13.8	16.0
Methane content	%	58.9±0.5	58.6±0.5	59.2±0.5	61.4±0.5	62.5±0.5	62.6±0.5

* without pretreatment
** comparing to the value without pretreatment

et al. (2017) (738-1176 dm^3/kg VS). These differences confirmed that biogas production may be determined by chemical composition of organic matter in the sludges. This composition varies because sludges are generated during treatment of different kind of wastewater (e.g. municipal, landfill leachate, liquid fraction of pig manure), and in different wastewater systems. TOMCZAK-WANDZEL et al. (2011) tested the effect of ultrasound disintegration (200 W UP 200S, 24 kH) at a time of 5 min on biogas productivity of activated sludge. Total volume of produced biogas after pretreatment was 20% higher than with the sludge

without pretreatment. In addition, the authors indicated that methane content in the biogas increased by 10%, and this was much higher increase than in the present study.

The information on the biogas productivity of aerobic granular sludge are scarce. Little research has been done on pretreatment step on improving the productivity. VAL DEL RIO et al. (2011) studied thermal pretreatment to treat two different aerobic granular sludges, G1 from a reactor fed with pig manure and G2 from a reactor fed with a synthetic medium that simulates municipal wastewater. Biodegradability of the untreated excess aerobic granular sludge (33% for G1 and 49% for G2) was similar to that obtained for an activated sludge (30-50%). The thermal pretreatment of G1 and G2 enhanced anaerobic digestion respectively by 20% and 14% at 60°C and by 88% and 18% at 170°C, in comparison to the untreated sludge. In others study, VAL DEL RIO et al. (2013) also checked the effect of thermal pretreatment (133°C for 20 min) of aerobic granular sludge from pilot plant SBR, fed with the liquid fraction of pig slurry, on biogas potentials. The authors found that biogas production of the granules after pretreatment was more than 30% higher than that of the granules without pretreatment.

Conclusions

The study showed that biogas productivity from excess activated sludge was much higher than from excess granular sludge. The biogas productivity of AS without pretreatment was ca. 603 dm^3/kg TS (ca. 793 dm^3/kg VS); that of GS was ca. 200 dm^3/kg TS (ca. 480 dm^3/kg VS). Ultrasound disintegration increased sludge digestibility more than homogenization. After pretreatment by ultrasound disintegration there was a noticeable increase in biogas productivity and in methane content with both AS and GS. After disintegration of the sludge, the biogas productivity of AS increased by 7.8–16.1%, and that of GS increased by 7.0–16.0% depending on the parameters of disintegration. However, after homogenization, the biogas productivity increased by 2.0-3.0% (AS) and 1.6-3.2% (GS).

Acknowledgements

This work was supported by a Ministry of Science and Higher Education in Poland (Statutory Research, 18.610.006–300).

References

Ariunbaatar J., Panico A., Esposito G., Pirozzi F., Liens P.N.L. 2014. *Pretreatment methods to enhance anaerobic digestion of organic solid waste*. Applied Energy, 123: 143-156.

Bernat K., Cydzik-Kwiatkowska A., Wojnowska-Baryła I., Karczewska M. 2017. *Physico-chemical properties and biogas productivity of aerobic granular sludge and activated sludge*. Biochemical Engineering Journal, 117: 43-51.

Beun J.J., Hendriks A., van Loosdrecht M.C.M., Morgenroth E., Wilderer P.A., Heijnen J.J. 1999. *Aerobic granulation in a sequencing batch reactor*. Water Research, 33(10): 2283-2290.

Bougrier C., Delgenès J.P., Carrère H. 2007. *Impacts of thermal pretreatments on the semi-continuous anaerobic digestion of waste activated sludge*. Biochemical Engineering Journal, 34: 20-27.

Carrere H., Dumas C., Battimelli A., Batsone D.J., Delgenes J.P., Steyer J.P. 2010. *Pretreatment methods to improve sludge anaerobic degradability: a review*. Journal of Hazardous Materials, 183: 1-15.

Cydzik-Kwiatkowska A. 2015. *Bacterial structure of aerobic granules is determined by aeration mode and nitrogen load in the reactor cycle*. Bioresource Technology, 181: 312-320.

Cydzik-Kwiatkowska A., Bernat K., Zielińska M., Bułkowska K., Wojnowska-Baryła I. 2017. *Aerobic granular sludge for bisphenol A (BPA) removal from wastewater*. International Biodeterioration and Biodegradation, 122: 1-11.

Cydzik-Kwiatkowska A., Rusanowska P., Zielińska M., Bernat K., Wojnowska-Baryła I. 2016. *Microbial structure and nitrogen compound conversions in aerobic granular sludge reactors with non-aeration phases and acetate pulse-feeding*. Environmental Science and Pollution Research, 23: 24857-24870.

Cydzik-Kwiatkowska A., Zielińska M. 2011. *Technologia osadu granulowanego w oczyszczaniu ścieków*. In: *Trendy w biotechnologii środowiskowej*. Ed. I. Wojnowska-Baryła. Wydawnictwo Uniwersytetu Warmińsko-Mazurskiego, Olsztyn, p. 63-85.

Cydzik-Kwiatkowska A., Zielińska M., Wojnowska-Baryła I. 2012. *Impact of operational parameters on a bacterial community in a full-scale municipal wastewater treatment plant*. Polish Journal of Microbiology, 61(1): 41-49.

Greenberg A.E., Clesceri L.S., Eaton A.D. 1992. *Standard Methods for the Examination of Water and Wastewater*. 18th edition. American Public Health Association, American Water Works Association, Water Environment Federation, Washington (D.C.).

Heerenklage J., Stegmann R. 2005. *Analytical methods for the determination of the biological stability of waste samples*. Tenth International Waste Management and Landfill Symposium, S. Margherita di Pula, Cagliari, Italy.

Liu Y., Tay J.H. 2004. *State of the art of biogranulation technology for wastewater treatment*. Biotechnology Advanced, 22: 533-563.

Montgomery L.F.R., Bochmann G. 2014. *Pretreatment of feedstock for enhanced biogas production*. IEA Bioenergy.

Rusanowska P., Cydzik-Kwiatkowska A., Świątczak P., Wojnowska-Baryła I. 2019. *Changes in extracellular polymeric substances (EPS) content and composition in aerobic granule size-fractions during reactor cycles at different organic loads*. Bioresource Technology, 272: 188-193.

Sławiński J.W. 2016. *Tlenowy granulowany osad czynny: nowy standard dla energooszczędnego, niskonakładowego i zrównoważonego oczyszczania ścieków*. Forum Eksploatatora, 82: 32-36.

Tchobanoglous G., Burto F.L., Stensel H.D. 2003. *Wastewater Engineering: Treatment and Reuse*. 4th ed. Metcalf and Eddy Inc., McGraw-Hill, New York.

Tomczak-Wandzel R., Ofverstrom S., Dauknys R., Mędrzycka K. 2011. *Effect of disintegration pretreatment of sewage sludge for enhanced anaerobic digestion*. In Environmental Engineering, The 8th International Conference, Vilnius Gediminas Technical University.

VAL DEL RIO A., MORALES N., ISANTA E., MOSQUERA-CORRAL A., CAMPOS J.L., STEYER J.P., CARRÈRE H. 2011. *Thermal pre-treatment of aerobic granular sludge: impact on anaerobic biodegradability*. Water Research, 45(18): 6011-6020.

VAL DEL RIO A., PALMEIRO-SANCHEZ T., FIGUEROA M., MOSQUERA-CORRAL A., CAMPOS J.L., MÉNDEZ R. 2013. *Anaerobic digestion of aerobic granular biomass: effects of thermal pre-treatment and addition of primary sludge*. Journal of Chemical Technology and Biotechnology, 89: 690-697.

WANG L., MATTSSON M., RUNDSTEDT J., KARLSSON N. 2011. *Different pretreatments to enhance biogas production*. Master of Science Thesis, Halmstad University, Halmstad.

Technical Sciences, 2019, 22(1), 87–98

UNIWERSYTET WARMIŃSKO-MAZURSKI W OLSZTYNIE

Quarterly peer-reviewed scientific journal
ISSN 1505-4675
e-ISSN 2083-4527
TECHNICAL SCIENCES
Homepage: www.uwm.edu.pl/techsci/

MODIFICATION OF ACTIVATED CARBONS FOR APPLICATION IN ADSORPTION COOLING SYSTEMS

Eliza Wolak, Elżbieta Vogt, Jakub Szczurowski

Faculty of Energy and Fuels
AGH University of Science and Technology in Cracow

Received 1 August 2018, accepted 12 December 2019, available online 8 January 2019.

K e y w o r d s: activated carbon, hydrophobization, modification, heat of wetting.

A b s t r a c t

In this paper commercially available activated WD-extra carbon (Gryfskand) which is applied for water treatment was used. Activated carbon was modified by the following chemical agents: H_2O_2, HNO_3 and HCl. Chemical modifications significantly affect the chemical, structural and surface properties of activated carbons. Hydrophobization with ethereal stearic acid was performed on the raw material and samples after chemical modification. Hydrophobic properties of the samples were specified. The relationship of the chemical modification agents with hydrophobization degree was indicated. The thermal effects of wetting by methanol was measured. The heat of wetting was calculated. The purpose of the work was to modify the WD carbon properties to obtain an adsorbent for cooling systems characterized by both good thermal capacity and moisture resistance. The modifying chemical substances applied accounted for an increase in the concentration of the acid functional groups. The hydrophobized and HCl-modified WD(HCl) carbon has the best hydrophobized properties. The results of studies describing such modifications allow to conclude that the use of hydrophobic materials may lead to the production of sorbents with new functions facilitating their storage and use.

Correspondence: Eliza Wolak, Katedra Chemii Węgla i Nauk o Środowisku, Wydział Energetyki i Paliw, Akademia Górniczo-Hutnicza im. Stanisława Staszica, al. Mickiewicza 30, 30-059 Kraków, e-mail: eklimows@agh.edu.pl

Introduction

Activated carbons are known to be excellent adsorbents and are therefore used to remove a broad spectrum of dissolved organic and inorganic species from both the gas phase and he liquid phase. Coals applications are also known and widely used, but the specific properties of this material may be useful in other areas as well. Theoretical and experimental work has done that the application of carbon adsorbents for heat storage in adsorptive cooling systems/adsorptive refrigerators is useful (MEUNIER 2001). The most interesting system may be methyl alcohol pair and microporous carbon materials (LEITE et al. 2005). Carbon is a good solid adsorbent for storage of mass and energy because of its good internal porosity and large specific surface area. (MARSH, RODRIGUEZ--REINOSO 2006). It is worth to add that are much cheaper than systems with the use of zeolites. Additionally methanol is a very good adsorbate because it can work at temperatures considerably lower than 0°C (WANG et al. 2003). Carbons effectiveness in such applications primarily depends on structural properties and chemical properties of the surface. Techniques to modify and characterize the surface chemical properties of activated carbons constituted the subject of interest for many scientists (MENENDEZ et al. 1996).

The chemical modifications may be carried out by various agents, the most common of which include the following: a strong oxidizing nitric acid (EL-HENDAWY 2003), inorganic acids: hydrochloric acid (HCl) and hydrofluoric acid (HF) (BAGREEV et al. 2001). Operation of the carbon-oxidizing agents causes the introduction of the activated carbon surfaces into a variety of oxygen-containing surface groups (carboxyl, lactone, phenol, ketone, quinone and ethereal groups). Many properties of carbon adsorbents are definitely influenced by chemisorbed oxygen, which can be bound in the form of various functional groups (KALIJADIS et al. 2011). The modifying surface carbon may change the nature of hydrophobic to hydrophilic what is not always beneficial when they are used. So, it is very important what kind of modification rewords treatment-enhancing properties (structural and surface parameters) of carbon sorbents are used (REPELEWICZ et al. 2009, BUCZEK, WOLAK 2008).

The change of the hydrophobic properties of the carbon materials, which is applied during production filters for removing oil and organic pollutants (LEE et al. 2011) or in the purification processes used frying oils, is possible (BUCZEK, CHWIAŁKOWSKI 2005). Hydrophobization is a beneficial process from the economic point of view since, as it is commonly known, hydrophobic materials are sensitive to the harmful effect of humidity to a much lower degree than solids with similar applications but not possessing this characteristic. The results of studies describing such modifications allow to conclude that the use of the hydrophobized materials can lead to production of less amount of the solid waste during the industrial purification process, moreover new features of the sorbents

make its storage and dosage easier. The topic of the hydrofobization different material is actual and such researches could have a potential to contribute to improvements of waste purification processes.

The kind of material which is useful for the specific application results directly from its properties. The activated carbons used for the removal of pollution from solutions are characterized by high water absorption. It may be unfavorable during the regeneration process. In the case of cooling systems, the damp material will have a lower thermal capacity. Therefore in this application also an important feature of carbons may be resistance to the water. Water resistance of carbons can be changed by means of the hydrophobization process (DUONG DO 1998, THOMAS, CRITTENDEN 1998, YANG 2003, KERRY 2006).

Experimental part

Sample preparation

During the preparation of this paper a commercially available WD-extra activated carbon (Gryfskand) which is applied for water treatment was used. It was obtained from coal dust and binder and it was used as a raw material (WD). Activated carbon (WD) was modified by the following chemical agents: HCl (1 M – with a molar concentration 1 mol/dm^3), HNO_3 (1:1 – 65% acid diluted with 1:1 distilled water) and H_2O_2 (30% – with a percentage concentration). The 10 g sample of adsorbent was poured with 300 cm^3 of the oxidizing agent and this led to boiling. Modification was carried out at the boiling point during 3 hours. Subsequently the samples were filtered, washed with distilled water to a constant pH and dried. The modified carbon was obtained which is denoted by WD(HCl), WD(HNO_3) and WD(H_2O_2), respectively. pH values were measured for all modifying substances. The values of pH for the raw materials were the following: WD – 9.6, WD(HCl) – 5.2, WD(HNO_3) – 4.7, WD(H_2O_2) – 7.8. The modification of activated carbon with chemical agents exerted a strong influence on the chemical character of its surface. The alkaline raw material after modification with strong HCl and HNO_3 becomes an acidic adsorbent. The modification of the alkaline adsorbent by H_2O_2 was obtained but the values of pH from 9.6 to 7.8 was decreased.

Structural properties

The standard parameters of the porous structure were calculated by means of low-temperature (77 K) nitrogen adsorption isotherms. Porous texture parameters were determined by means of an apparatus for precise measurement

of physical adsorption and chemisorption – AUTOSORB-1-C (Quantachrome Instruments, USA). Before measurement, the samples were degassed at 200°C for 12 hours using a vacuum degasser system equipped with a turbomolecular pump.

The surface areas (S_{BET}) were obtained from physical adsorption isotherms data using the BET equation. The BET equation presents a formula (1).

$$a = \frac{a_m \cdot c \cdot x}{(1-x) \cdot [1 + (c-1)] \cdot x} \tag{1}$$

where:

a – equilibrium adsorption with a relative pressure $x = p/p_0$ [mole],
a_m – adsorption capacity of the monolayer [mole],
c – constant dependent on the adsorption heat.

The total volume pores (V_t) were read from the isotherms for the relative pressure equal to 0.995. The micropore volume (W_o), adsorption energy (E_o) and micropore surface area (S_{mic}) were calculated using the Dubinin-Radushkevich (DR) equation. The mesopore volumes (V_{BJH}), surface area of mesopore (S_{BJH}) were determined using the standard Barreta, Joynera, Halendy method (BJH). All structural parameters are summarized in Table 1.

Table 1

Structural of activated carbon samples

Adsorbent	S_{BET} [m^2g^{-1}]	V_t [cm^3g^{-1}]	W_o [cm^3g^{-1}]	E_o [$kJ \cdot mol^{-1}$]	S_{mic} [m^2g^{-1}]	V_{BJH} [cm^3g^{-1}]	S_{BJH} [m^2g^{-1}]
WD	1,583	0.845	0.591	18.37	1,662	0.302	289
WD(HCl)	1,235	0.627	0.448	20.96	1,259	0.162	126
WD(HNO_3)	652	0.299	0.204	21.87	575	0.098	91
WD(H_2O_2)	1,129	0.574	0.406	21.50	1,142	0.159	138

As a result of the chemical modification, the obtained materials were characterized by a less developed microporous structure. This is evidenced by lower values of the specific surface area and the volume of micropores. The smallest specific surface area of S_{BET} was obtained for activeted carbon modified with strong acid HNO_3.

Chemical surface characterization

The chemical properties of the surface were estimated by Boehm's method which is a general procedure used to determine the distribution of the surface functional groups (BOEHM 2002). The Boehm titration method gives both

qualitative and quantitative information only about basic and acidic groups (in the form of carboxyl, lactone and phenol). These groups differ in their acidities and can be distinguished by neutralization with different solutions: HCl (for basic groups) and $NaHCO_3$, Na_2CO_3 and NaOH (for acidic groups). The total numbers of the groups of basic character were determined by titration of the NaOH solution, the excess of unreacted HCl. The amount and the type of surface oxygen groups by Boehm titration was examined. The obtained results are given in Table 2.

Table 2

Concentration of oxygen functional groups

Adsorbent	Basic groups [mmol·g^{-1}]	Acidic groups [mmol·g^{-1}]			
		Carboxyl	Lactone	Phenol	Total
WD	2.210	0.125	0.124	0.359	0.608
WD(HCl)	0.246	0.373	0.371	1.594	2.338
WD(HNO_3)	0.123	2.455	2.984	4.745	10.184
WD(H_2O_2)	2.094	0.123	0.125	0.374	0.622

Hydrophobization process

During the hydrophobization process a commercial modifier – stearic acid – was used. The method of carbon hydrophobization with the use of stearic acid was carried out with the use of ether stearic acid solution. The concentration of the ether solution was chosen in such a way that after evaporation of the solvent, the content of stearic acid in a solid material was equal to 1%. Hydrophobization was carried out by mixing stearic acid solution with the carbon in a laboratory evaporator, at an increased temperature. The detailed descriptions of the conducted hydrophobization processes can be found in the author's earlier works (VOGT 2008).

Evaluation of the hydrophobization degree by "floating on water" test. In this work a relative evaluation of the hydrophobization degree of the analysed materials was based on a simple experiment – the so-called "floating on water" test (VOGT 2012). The experiment consisted in placing a small amount of material on the surface of water in a beaker. The hydrophobization degree of materials modified in the work was evaluated on the basis of the material amount floating on the water surface for a specified period of time. Figure 1 presents the photographs of the "floating on water" test for the materials, obtained immediately after placing the samples on the water surface.

Evaluation of the water absorption. Water absorption was determined by means of a modified method based on the EN 1097-6:2013 standard (EN 1097-6: 2013 standard). Water absorption is the amount of water that is retained

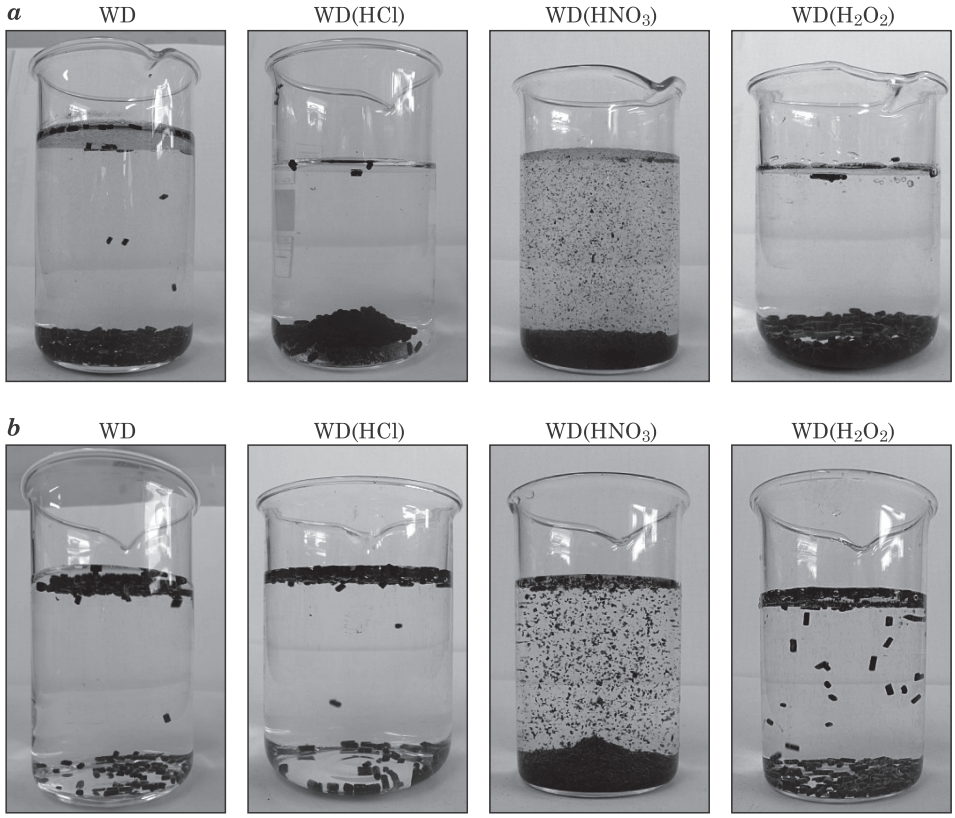

Fig. 1. The photographs of the "floating on water" test: *a* – not hydrophobized, *b* – hydrophobized

in the entire volume of the test sample immersed in the water. The test portion of material was placed in a beaker and completely immersed in the water. After that the test portion was placed in the wire basket. The sample remained in the basket for a certain time until the water has stopped dripping. In our test absorbent clothes have not been used for draining excess water.

The amount of water determined during a test carried out in this manner is adequate to the amount of water retained in the bed of activated carbon which will be generated in industrial conditions.

The mass m_1 of the saturated test portion of material was obtained. The water absorption (*WA*) was calculated from the formula (2):

$$WA = \frac{m_1 - m_2}{m_2} \cdot 100\% \tag{2}$$

where:

m_1 – mass of the saturated test portion [g],

m_2 – mass of the oven-dried at 105°C, test portion [g].

The obtained results are presented in Table 3.

Carbons lose their natural hydrophobic properties after acid modification. Water adsorption results obtained for acid-modified carbons are higher than for raw material WD (Tab. 3). The hydrophobization process allows both the reproduction of this natural hydrophobicity and, in the case of WD(HCl)–H material even decreases the water adsorption value as compared to the raw material of WD.

Table 3

Water absorption

Water absorption [%]			
WD	WD(HCl)	WD(HNO_3)	WD(H_2O_2)
164	211	292	167
WD–H	WD(HCl)–H	WD(HNO_3)–H	WD(H_2O_2)–H
142	124	206	164

Heat effects

For the estimation of the energetic effects characterizing the investigated carbons, the heat of their wetting by methanol has been determined. The heat of wetting, evolved as a result of the mutual interaction of the molecules of the wetting liquid and the adsorbent surface, is a valuable source of information. The heat of wetting can be used to determine the relative surface area of carbon, heat of adsorption, as well as for the determination of its hydrophilicity and the degree of the oxidation of the adsorbent surface (LÓPEZ-RAMÓN et al. 2000, SZYMAŃSKI et al. 2002).

The measurements of the heat of wetting were carried out in the original apparatus, which was presented in (BUCZEK, WOLAK 2009). At first, the activated carbon samples were heated at 105°C for about 3 hours. The investigated adsorbents were measured in the amount of 2 g samples. As the wetting liquid 10 cm^3 of methyl alcohol was used. The temperature in the apparatus was measured with an accuracy of 0.1°C. During the whole measurement procedure the electronic system registered the changes of temperature in time. The measurement was stopped when successive temperature measurements showed a decrease. Temperature changes as a function of time is presented in Figure 2.

Analyzing the course of temperature changes over time, it was noticed that for all hydrophobic coals thermal effects of wetting with methanol are slightly lower than for non-hydrophobic coals. The function is similar for all samples tested. Such values allow to conclude that the hydrophobization process does not significantly reduce the thermal effects during the adsorption of methanol

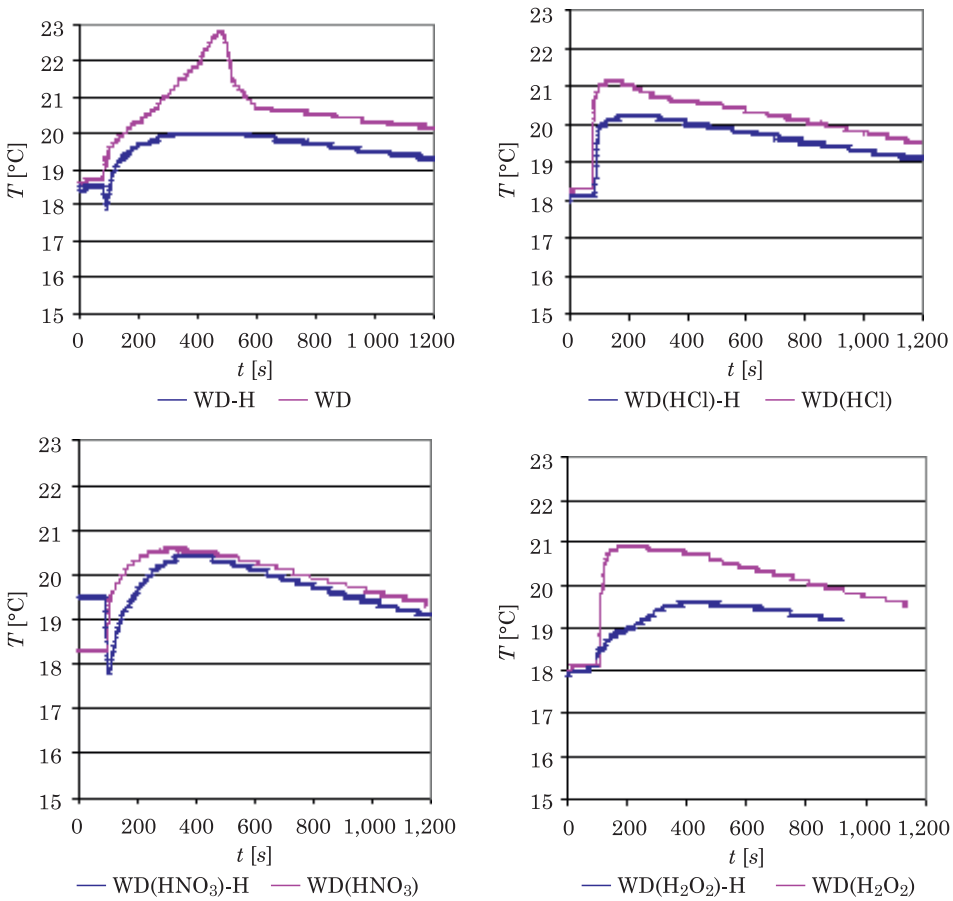

Fig. 2. Temperature variation in time

vapors. This effect is profitable when using hydrophobized carbons in cooling systems. What's more, the hydrophobic carbons will not get wet with ambient water during storage or use. Thus, their efficiency as a sorbent used in cooling systems will be higher.

On the basis of the measurements carried out, the heat of wetting with methanol was calculated with Equation (3).

$$q = (C_{wA} V_A d_A + C_{wC} m_C) \Delta T \tag{3}$$

where:

C_{wA} – specific heat of methanol [J·g^{-1}],
V_A – volume of methanol [cm^3],
d_A – density of methanol [g·cm^{-3}],
C_{wC} – specific heat of carbon, constant for all samples [J·g^{-1}],

m_C – mass of activated carbon [g],
ΔT – temperature rise from steady state to maximum.

The values of the heat effect (ΔT) and the heat of wetting (q [J] and Q [J/g]), are collected in Table 4.

Table. 4

Heat effect and heat of weeting of activated carbon samples

Adsorbent	ΔT	q [J]	Q [J·g^{-1}]
WD	4.2	88.0	44.8
WD-H	1.6	33.5	17.1
WD(HCl)	2.9	61.0	30.1
WD(HCl)–H	2.2	46.1	23.5
WD(HNO_3)	2.3	48.3	24.2
WD(HNO_3)–H	0.9	19.0	9.1
WD(H_2O_2)	2.9	61.2	29.3
WD(H_2O_2)–H	1.6	33.4	17.5

For the modified HCl coal WD(HCl) after the hydrophobization process WD(HCl)-H, the smallest reduction in thermal effects was determined. It can be concluded that such a procedure for modifying WD carbon to obtain a hydrophobic material is most advantageous for obtaining a sorbent for a cooling system (WD carbon-methanol). What's more, such hydrophobic coal will not take water from surrounding during storage or use. Thus, its efficiency as a sorbent used in cooling systems may be higher in the case of high humidity.

Results and discussion

The proposed method of the modification of WD-extra activated carbon influenced its surface and structural properties. The greatest impact on the structure of the porous activated carbon was particularly distinct when use was made of nitric acid at the boiling point. It was demonstrated that the modifying substance (WD(HNO_3)) reduced surface area by almost 60% compared to the raw material. Both the micropore volume (0.204 cm^3/g) and particularly the mesopore volume (0.098 cm^3/g) is reduced. Nitric acid causes too much destruction of pore structure so it isn't good modification for obtaining new sorbent for cooling systems. Modification with non-oxidant hydrochloric acid and hydrogen peroxide also influenced the pore structure of the carbon, but they were not quite as big.

The modifying substances applied accounted for an increase in the concentration of the acid functional groups (Tab. 2). The raw carbon contained predominantly the groups of basic character and a negligible amount of acidic

groups. The greatest increase of the acidic groups was observed in the case of nitric acid, which is consistent with the literature (PRADHAN, SANDLE 1999, REPELEWICZ et al. 2009). Also the increase of concentration of acidic groups was particularly distinct when HCl was used. The WD(H_2O_2) modifying material remained as the only alkaline carbon.

In adsorptive cooling systems, better sorbents are materials with a developed microporous surface, greater adsorptive capacity with respect to methanol and better thermal conductivity. The introduction of acidic/basic groups onto the carbon surface can increase the adsorption efficiency of polar methanol molecules.

On the basis of the results obtained from the "floating on water" test (immediately after placing the samples on the water surface) it was stated (Fig. 1) that the hydrophobization process changed the water resistance of carbons. Non-hydrophobized materials became immediately moist and fell onto the beaker bottom. In the case of hydrophobized materials raw (WD) or HCl modified coals WD(HCl) almost the complete portion of the materials remained on the water surface. In the case of hydrophobized and H_2O_2 modified materials WD(H_2O_2) more than half of the sample fell to the bottom of the beaker. The worst hydrophobic properties were obtained by carbon modified with nitric acid WD(HNO_3) – almost the whole quantity of the material fell to the bottom of the beaker. The material on the water surface was observed for another 2 hours. After that only hydrophobized and HCl-modified WD(HCl) carbon remained on the water surface. This material has the best hydrophobized properties. It floated on the water also on the next day as the only one of all the modified materials.

Conclusion

The aim of the work was to modify the WD carbon properties to obtain an adsorbent for cooling systems characterized by both good thermal capacity and moisture resistance.

The water absorption measurements confirm the hydrophobization process changed the water resistance of carbons. In the case of hydrophobized and HCl modified carbon WD(HCl) the water absorption was the smallest from the values obtained for all samples. The obtained values of water absorption enable us not only to compare the hydrophobic properties of hydrophobized carbons but also tell us how much of water is absorbed. In the case of hydrophobized and HCl-modified, WD(HCl)-H carbon this value is almost less than half the value for non-hydrophobized material.

Such hydrophobic carbon WD(HCl)-H will not take water from surrounding during storage or usage. Thus, its efficiency as a sorbent used in cooling systems may be higher in the case of high humidity. The procedure of obtaining a sorbent for a cooling system (WD carbon – methanol) consisting on connecting

activation process by HCl (WD(HCl)) and hydrofobization process (WD(HCl)-H)) it seems to be the best of the used methods.

It was found that the types of chemical modification of carbons that are used affect the hydrophobization ability of the material. The results of studies describing such modifications allow to conclude that the use of hydrophobic materials may lead to the production of sorbents with new functions facilitating their storage and use.

The work was carried out within the research to keep the research potential AGH (11.11.210.374).

References

BAGREEV A., BANDOSZ T.J., LOCKE D.C. 2001. *Pore structure and surface chemistry of adsorbents obtained by pyrolysis of sewage sludge-derived fertilizer*. Carbon, 39: 13.

BOEHM H.P. 2002. *Surface oxides on carbon and their analysis: a critical assessment*. Carbon, 40: 145.

BUCZEK B., CHWIAŁKOWSKI W. 2005. *Wpływ modyfikacji powierzchni węgla aktywnego na jego zdolność do oczyszczania zużytego oleju smażalniczego*. Żywność. Nauka. Technologia. Jakość, 4: 45.

BUCZEK B., WOLAK E. 2008. *Potassium hydroxide modified active carbon for adsorptive refrigerators*. Adsorption, 14 : 283-287.

BUCZEK B., WOLAK E. 2009. *Nanostructural active carbons from vegetable precursors for heat storage system*. Chemical and Process Engineering, 30: 173-180.

DUONG DO D. 1998. *Adsorption analysis: Equilibria and kinetics*. Imperial College Press.

EL-HENDAWY A.N.A. 2003. *Influence of HNO_3 oxidation on the structure and adsorptive properties of corncob-based activated carbon*. Carbon, 41: 4.

EN 1097-6:2013 standard. *Tests for mechanical and physical properties of aggregates*. Part 6: *Determination of particle density and water absorption*.

KALIJADIS A.M., VUKCEVIC M.M., JOVANOVIC Z.M., LAUSEVIC Z.V., LAUSEVIC M.D. 2011. *Characterization of surface oxygen groups on different carbon materials by the Boehm method and temperature programmed desorption*. Journal of the Serbian Chemical Society, 76 : 5.

KERRY F.G. 2006, *Industrial gas handbook: gas separation and purification*. Taylor & Francis Group, LLC.

LEE C.H., JOHNSON N., DRELICH J., YAP Y.K. 2011. *The performance of superhydrophobic and superoleophilic carbon nanotube meshes in water – oil filtration*. Carbon, 49: 669.

LEITE A.P.F., GRILO M.B., ANDRADE R.R.D., BELO F.A., MEUNIER F. 2005. *Experimental evaluation of a multi-tubular adsorber operating with activated carbon-methanol*. Adsorption, 11: 543–548.

LÓPEZ-RAMÓN M.V., STOECKLI F., MORENO-CASTILLA C., CARRASCO-MARÍN F. 2000. *Specific and non-specific interactions of water molecules with carbon surfaces from immersion calorimetry*. Carbon, 38: 825-829.

MARSH H., RODRIGUEZ-REINOSO F. 2006. *Activated carbon*. Elsevier, Amsterdam.

MENENDEZ J.A., PHILLIPS J., XIA B., RADOVIC L.R. 1996. *On the Modification and Characterization of Chemical Surface Properties of Activated Carbon: In the Search of Carbons with Stable Basic Propertiesi*. Langmuir, 12(18): 4404-4410.

MEUNIER F. 2001. *Adsorptive cooling: a clan technology*. Clean Production Process, 3: 8–20.

NAMASIVAYA, C., SANGEETHA, D., GUNASEKARAN, R. 2007. *Trans IChemE*. Part B. Process Safety and Environmental Protection, 85(B2): 181.

NTIM S.A., MITRA S. 2012. *Adsorption of arsenic on multiwall carbon nanotube–zirconia nanohybrid for potential drinking water purification*. Journal of Colloid and Interface Science, 375: 154.

PRADHAN B.K., SANDLE N.K. 1999. *Effect of different oxidizing agent treatments on the surface properties of activated carbons*. Carbon, 37: 8.

REPELEWICZ M., JEDYNAK K., CHOMA J. 2009. *Struktura porowata i chemia powierzchni węgli aktywnych modyfikowanych kwasami nieorganicznymi*. Ochrona Środowiska, 31(3) : 45-50.

SZYMAŃSKI G.S., BINIAK S., RYCHLICKI G. 2002. *Carbon surface polarity from immersion calorimetry*. Fuel Processing Technology, 79: 217-223.

THOMAS W.J., CRITTENDEN B. 1998. *Adsorption Technology and Design*. Elsevier Science & Technology Books.

VOGT E. 2008. *Hydrophobization of fine solids presented on the example of limestone powder*. Polish Journal of Chemical Technology, 10: 1.

VOGT E. 2012. *Zastosowanie przemysłowych domieszek do hydrofobizacji mączki wapiennej*. Cement Lime Concrete, 3: 160.

WANG L.W., WU J.Y., WANG R.Z., XU Y.X., WANG S.G. 2003. *Experimental study of a solidified activated carbon-methanol adsorption ice maker*. Applied Thermal Engineering, 23: 1453–1462.

YANG R.T. 2003. *Adsorbents: Fundamentals and application*. John Wiley & Sons, New York.

Guide for Autors

Introduction

Technical Sciences is a peer-reviewed research Journal published in English by thePublishing House of the University of Warmia and Mazury in Olsztyn (Poland). Journal is published continually since 1998. Until 2010 Journal was published as a yearbook, in 2011 and 2012 it was published semiyearly. From 2013, the Journal is published quarterly in the spring, summer, fall, and winter.

The Journal covers basic and applied researches in the field of engineering and the physical sciences that represent advances in understanding or modeling of the performance of technical and/or biological systems. The Journal covers most branches of engineering science including biosystems engineering, civil engineering, environmental engineering, food engineering, geodesy and cartography, information technology, mechanical engineering, materials science, production engineering etc.

Papers may report the results of experiments, theoretical analyses, design of machines and mechanization systems, processes or processing methods, new materials, new measurements methods or new ideas in information technology.

The submitted manuscripts should have clear science content in methodology, results and discussion. Appropriate scientific and statistically sound experimental designs must be included in methodology and statistics must be employed in analyzing data to discuss the impact of test variables. Moreover there should be clear evidence provided on how the given results advance the area of engineering science. Mere confirmation of existing published data is not acceptable. Manuscripts should present results of completed works.

There are three types of papers: a) research papers (full length articles); b) short communications; c) review papers.

The Journal is published in the printed and electronic version. The electronic version is published on the website ahead of printed version of Technical Sciences.

Technical Sciences does not charge submission or page fees.

Types of paper

The following articles are accepted for publication:

Reviews

Reviews should present a focused aspect on a topic of current interest in the area of biosystems engineering, civil engineering, environmental engineering, food engineering, geodesy and cartography, information technology, mechanical engineering, materials science, production engineering etc. They should include all major findings and bring together reports from a number of sources. These critical reviews should draw out comparisons and conflicts between work, and provide an overview of the 'state of the art'. They should give objective assessments of the topic by citing relevant published work, and not merely present the opinions of individual authors or summarize only work carried out by the authors or by those with whom the authors agree. Undue speculations should also be avoided. Reviews generally should not exceed 6,000 words.

Research Papers

Research Papers are reports of complete, scientifically sound, original research which contributes new knowledge to its field. Papers should not exceed 5,000 words, including figures and tables.

Short Communications

Short Communications are research papers constituting a concise description of a limited investigation. They should be completely documented, both by reference list, and description of the experimental procedures. Short Communications should not occupy more than 2,000 words, including figures and tables.

Letters to the Editor

Letters to the Editor should concern with issues raised by articles recently published in scientific journals or by recent developments in the engineering area.

Contact details for submission

The paper should be sent to the Editorial Office, as a Microsoft Word file, by e-mail: techsci@uwm.edu.pl

Referees

Author/authors should suggest, the names, addresses and e-mail addresses of at least three potential referees. The editor retains the sole right to decide whether or not the suggested reviewers are used.

Submission declaration

After final acceptance of the manuscript, the corresponding author should send to the Editorial Office the author's declaration. Submission of an article implies that the work has not been published previously (except in the form of an abstract or as part of a published lecture or academic thesis or as an electronic preprint), that it is not under consideration for publication elsewhere, that publication is approved by all authors and tacitly or explicitly by the responsible authorities where the work was carried out, and that, if accepted, it will not be published elsewhere in the same form, in English or in any other language.

To prevent cases of ghostwriting and guest authorship, the author/authors of manuscripts is/are obliged to: (i) disclose the input of each author to the text (specifying their affiliations and contributions, i.e. who is the author of the concept, assumptions, methods, protocol, etc. used during the preparation of the text); (ii) disclose information about the funding sources for the article, the contribution of research institutions, associations and other entities.

Language

Authors should prepare the full manuscript i.e. title, abstract and the main text in English (American or British usage is accepted). Polish version of the manuscript is not required.

The file type

Text should be prepared in a word processor and saved in doc or docx file (MS Office).

Article structure

Suggested structure of the manuscript is as follows:

Title
Authors and affiliations
Corresponding author
Abstract
Keywords
Introduction
Material and Methods
Results and Discussion
Conclusions

Acknowledgements (optional)
References
Tables
Figures

Subdivision – numbered sections

Text should be organized into clearly defined and numbered sections and subsections (optionally). Sections and subsections should be numbered as 1. 2. 3. then 1.1 1.2 1.3 (then 1.1.1, 1.1.2, …). The abstract should not be included in numbering section. A brief heading may be given to any subsection. Each heading should appear on its own separate line. A single line should separate paragraphs. Indentation should be used in each paragraph.

Font guidelines are as follows:

– Title: 14 pt. Times New Roman, bold, centered, with caps
– Author names and affiliations:12 pt. Times New Roman, bold, centered, italic, two blank line above
– Abstract: 10 pt. Times New Roman, full justified, one and a half space. Abstract should begin with the word Abstract immediately following the title block with one blank line in between. The word Abstract: 10 pt. Times New Roman, centered, indentation should be used
– Section Headings: Not numbered, 12 pt. Times New Roman, bold, centered; one blank line above
– Section Sub-headings: Numbered, 12 pt. Times New Roman, bold, italic, centered; one blank line above
– Regular text: 12 pt. Times New Roman, one and a half space,full justified, indentation should be used in each paragraph

Title page information

The following information should be placed at the first page:

Title

Concise and informative. If possible, authors should not use abbreviations and formulae.

Authors and affiliations

Author/authors' names should be presented below the title. The authors' affiliation addresses (department or college; university or company; city, state and zip code, country) should be placed below the names. Authors with the same affiliation must be grouped together on the same line with affiliation information following in a single block. Authors should indicate all affiliations with a lower-case superscript letter immediately after the author's name and in front of the appropriate address.

Corresponding author

It should be clearly indicated who will handle correspondence at all stages of refereeing and publication, also post-publication process. The e-mail address should be provided (footer, first page). Contact details must be kept up to date by the corresponding author.

Abstract

The abstract should have up to 100-150 words in length. A concise abstract is required. The abstract should state briefly the aim of the research, the principal results and major conclusions. Abstract must be able to stand alone. Only abbreviations firmly established in the field may be eligible. Non-standard or uncommon abbreviations should be avoided, but if essential they must be defined at their first mention in the abstract itself.

Keywords

Immediately after the abstract, author/authors should provide a maximum of 6 keywords avoiding general, plural terms and multiple concepts (avoid, for example, 'and', 'of'). Author/authors should be sparing with abbreviations: only abbreviations firmly established in the field may be eligible.

Abbreviations

Author/authors should define abbreviations that are not standard in this field. Abbreviations must be defined at their first mention there. Author/authors should ensure consistency of abbreviations throughout the article.

Units

All units used in the paper should be consistent with the SI system of measurement. If other units are mentioned, author/authors should give their equivalent in SI.

Introduction

Literature sources should be appropriately selected and cited. A literature review should discuss published information in a particular subject area. Introduction should identify, describe and analyze related research that has already been done and summarize the state of art in the topic area. Author/authors should state clearly the objectives of the work and provide an adequate background.

Material and Methods

Author/authors should provide sufficient details to allow the work to be reproduced by other researchers. Methods already published should be indicated by a reference. A theory should extend, not repeat, the background to the article already dealt within the Introduction and lay the foundation for further work. Calculations should represent a practical development from a theoretical basis.

Results and Discussion

Results should be clear and concise. Discussion should explore the significance of the results of the work, not repeat them. A combined Results and Discussion section is often appropriate.

Conclusions

The main conclusions of the study may be presented in a Conclusions section, which may stand alone or form a subsection of a Results and Discussion section.

Acknowledgements

Author/authors should include acknowledgements in a separate section at the end of the manuscript before the references. Author/authors should not include them on the title page, as a footnote to the title or otherwise. Individuals who provided help during the research study should be listed in this section.

Artwork

General points

– Make sure you use uniform lettering and sizing of your original artwork
– Embed the used fonts if the application provides that option
– Aim to use the following fonts in your illustrations: Arial, Courier, Times New Roman, Symbol
– Number equations, tables and figures according to their sequence in the text
– Size the illustrations close to the desired dimensions of the printed version

Formats

If your electronic artwork is created in a Microsoft Office application (Word, PowerPoint, Excel) then please supply 'as is' in the native document format

Regardless of the application used other than Microsoft Office, when your electronic artwork is finalized, please 'Save as' or convert the images to one of the following formats (note the resolution requirements given below):

EPS (or PDF): Vector drawings, embed all used fonts

JPEG: Color or grayscale photographs (halftones), keep to a minimum of 300 dpi

JPEG: Bitmapped (pure black & white pixels) line drawings, keep to a minimum of 1000 dpi or combinations bitmapped line/half-tone (color or grayscale), keep to a minimum of 500 dpi

Please do not:

– Supply files that are optimized for screen use (e.g., GIF, BMP, PICT, WPG); these typically have a low number of pixels and limited set of colors
– Supply files that are too low in resolution
– Submit graphics that are disproportionately large for the content

Color artwork

Author/authors should make sure that artwork files are in an acceptable format (JPEG, EPS PDF, or MS Office files) and with the correct resolution. If, together with manuscript, author/authors submit color figures then Technical Sciences will ensure that these figures will appear in color on the web as well as in the printed version at no additional charge.

Tables, figures, and equations

Tables, figures, and equations/formulae should be identified and numbered consecutively in accordance with their appearance in the text.

Equations/mathematical and physical formulae should be presented in the main text, while tables and figures should be presented at the end of file (after References section). Mathematical and physical formulae should be presented in the MS Word formula editor.

All types of figures can be black/white or color. Author/authors should ensure that each figure is numbered and has a caption. A caption should be placed below the figure. Figure must be able to stand alone (explanation of all symbols and abbreviations used in figure is required). Units must be always included. It is noted that figure and table numbering should be independent.

Tables should be numbered consecutively in accordance with their appearance in the text. Table caption should be placed above the table. Footnotes to tables should be placed below the table body and indicated with superscript lowercase letters. Vertical rules should be avoided. Author/authors should ensure that the data presented in tables do not duplicate results described in figures, diagrams, schemes, etc. Table must be able to stand alone (explanation of all symbols and abbreviations used in table is required). Units must be always included. As above, figure and table numbering should be independent.

References

References: All publications cited in the text should be presented in a list of references following the text of the manuscript. The manuscript should be carefully checked to ensure that the spelling of authors' names and dates of publications are exactly the same in the text as in the reference list. Authors should ensure that each reference cited in the text is also present in the reference list (and vice versa).

Citations may be made directly (or parenthetically). All citations in the text should refer to:

1. Single author

The author's name (without initials, with caps, unless there is ambiguity) and the year of publication should appear in the text

2. Two authors

Both authors' names (without initials, with caps) and the year of publication should appear in the text

3. Three or more authors

First author's name followed by et al. and the year of publication should appear in the text

Groups of references should be listed first alphabetically, then chronologically.

Examples:

"... have been reported recently (ALLAN, 1996a, 1996b, 1999; ALLAN and JONES, 1995). KRAMER et al. (2000) have recently shown..."

The list of references should be arranged alphabetically by authors' names, then further sorted chronologically if necessary. More than once reference from the same author(s) in the same year must be identified by the letters "a", "b", "c" etc., placed after the year of publication.

References should be given in the following form:

KUMBHAR B.K., AGARVAL R.S., DAS K. 1981. Thermal properties of fresh and frozen fish. International Journal of Refrigeration, 4(3), 143–146.

MACHADO M.F., OLIVEIRA F.A.R., GEKAS V. 1997. Modelling water uptake and soluble solids losses by puffed breakfast cereal immersed in water or milk. In Proceedings of the Seventh International Congress on Engineering and Food, Brighton, UK.

NETER J., KUTNER M.H., NACHTSCHEIM C.J., WASSERMAN W. 1966. Applied linear statistical models (4th ed., pp. 1289–1293). Irwin, Chicago.

THOMSON F.M. 1984. Storage of particulate solids. In M. E. Fayed, L. Otten (Eds.), Handbook of Powder Science and Technology (pp. 365–463). Van Nostrand Reinhold, New York.

Citation of a reference as 'in press' implies that the item has been accepted for publication.

Note that the full names of Journals should appear in reference list.

Submission checklist

The following list will be useful during the final checking of an article prior to the submission. Before sending the manuscript to the Journal for review, author/authors should ensure that the following items are present:

– Text is prepared with a word processor and saved in DOC or DOCX file (MS Office). One author has been designated as the corresponding author with contact details: e-mail address
– Manuscript has been 'spell-checked' and 'grammar-checked'
– References are in the correct format for this Journal
– All references mentioned in the Reference list are cited in the text, and vice versa
– Author/authors does/do not supply files that are too low in resolution
– Author/authors does/do not submit graphics that are disproportionately large for the content